Theoretical and numerical modelling of electronic transport in nanostructures

Dominik Szczesniak Szczęśniak

Theoretical and numerical modelling of electronic transport in nanostructures

Modélisation théorique et numérique du transport électronique dans les nanostructures

a thesis presented by

Dominik Szczęśniak

to

the Laboratory for Molecules and Materials
CNRS UMR 6283
at the University du Maine of Le Mans
in France

and

the Institute of Physics
at the Jan Długosz University of Częstochowa
in Poland

in partial fulfillment of the requirements for the degree of
Doctor of Philosophy
in the subject of
Physics

Supervisors:
Prof. Antoine Khater
University du Maine of Le Mans, France
and
Prof. Zygmunt Bąk
Jan Długosz University of Częstochowa, Poland

Le Mans\Częstochowa, December 2012

List of publications

Parts of this thesis have been previously published in:

1. **Quantum conductance of silicon-doped carbon wire nanojunctions**

   D. Szczęśniak, A. Khater, Z. Bąk, R. Szczęśniak, M. Abou Ghantous

   Nanoscale Res. Lett. **7** (2012) 616

2. **Electronic conductance via atomic wires: a phase field matching theory approach**

   D. Szczęśniak, A. Khater

   Eur. Phys. J. B **85** (2012) 174

3. **A simple analytical model for electronic conductance in a one dimensional atomic chain across a defect**

   A. Khater, D. Szczęśniak

   J. Phys.: Conf. Ser. **289** (2011) 012013

Author of this thesis is also a co-author of other papers:

1. **Superconducting state in the atomic metallic hydrogen just above the pressure of the molecular dissociation**

   R. Szczęśniak, D. Szczęśniak, E.A. Drzazga

   Solid State Commun. **152** (2012) 2023-2026

2. **Characterization of the high-pressure superconductivity in the *Pnma* phase of calcium**

   R. Szczęśniak, D. Szczęśniak

   Phys. Status Solidi B **249** (2012) 2194-2201

3. **Thermodynamic investigations of high-pressure superconducting state in $CaLi_2$ at 45 GPa**

   R. Szczęśniak, D. Szczęśniak

   Solid State Commun. **152** (2012) 779-783

4. **Superconductivity in the presence of a pseudogap induced by local charge density waves**

   R. Szczęśniak, D. Szczęśniak

   Chem. Met. Alloys **4** (2011) 50-57

5. **The thermodynamic critical field of YNi_2B_2C superconductor**

   M.W. Jarosik, R. Szczęśniak, D. Szczęśniak

   Acta Phys. Pol. A **118** (2010) 1031-1033

6. **Pressure-induced superconductivity in the *fcc* phase of lithium: strong-coupling approach**

   R. Szczęśniak, M.W. Jarosik, D. Szczęśniak

   Physica B **405** (2010) 4897-4902

To my Parents

I want to thank my thesis directors, Prof. Antoine Khater (University du Maine, France) and Prof. Zygmunt Bak (Jan Dlugosz University, Poland), who have shown me support, kindness, and provided me with permanent motivation. I would also like to sincerely thank Prof. Antoine Khater who made it possible for me to travel to France and conduct this research work in his group at the Institute for Molecules and Materials du Mans UMR 6283 CNRS in the University du Maine in France. I want to thank him particularly for his research guidance and valuable scientific insight throughout this period, which enabled me to develop my research work.

I present my sincere thanks to my CST committee members, Prof. Hong Guo (McGill University, Canada) and Prof. Jacek Kasperczyk (Jan Dlugosz University, Poland), for their refereeing of my annual thesis reports; their constructive comments surely improved this work.

I want to particularly thank both Prof. Makowska-Janusik Malgorzata and DR CNRS Philippe Dollfus, for kindly accepting to referee this thesis, and to thank Prof. Florent Calvayrac equally for accepting to be a member of my doctorate Panel.

I acknowledge with gratitude the French Ministry of Foreign Affairs doctorate grant (CNOUS 2009-2374) for the three years. A recent part of this work has also been financed by the research grant of the Polish National Science Center (DEC-2011/01/N/ST3/04492), for which I am equally grateful. Further, I would like to acknowledge the administrative support of the 3MPL Graduate School of the University du Maine and of the Jan Dlugosz University, for their efforts that allowed me to carry out my doctorate studies under the cotutelle program. This turned out to be a great research and training experience, and it certainly strengthened my character.

I am also very thankful to the people whom I have met and interacted with during my thesis studies, from whom I was lucky to learn a great deal at the University du Maine and the Jan Dlugosz University, notably M Doried Ghader and M Rabah Chadli.

Last but not least, very special and thanks go to my parents for their support in all personal areas of life. I dedicate this work to them, and to my father who died before the end of this work.

Résumé

Les besoins technologiques, aussi bien actuels que futurs, nécessitent de plus en plus une recherche scientifique intensive sur les propriétés des matériaux à l'échelle nanoscopique. L'un des domaines les plus importants à l-heure actuelle concerne la nanoélectronique dans ses diverses applications. Le grand intérêt de ce domaine, introduit dans les chapitres 1 et 2, découle de la possible réduction de taille des composants des circuits, en conservant leur qualité et fonctionnalité, et tout en visant des meilleurs rendements, une augmentation des capacités de stockage et une baisse des coûts pour les composants des dispositifs physiques correspondants.

L'objectif de cette thèse dans le domaine de la nanoélectronique est de présenter une contribution à l'analyse des phénomènes de transport électronique qui se produisent au niveau quantique dans les nanostructures. Pour ce faire, nous développons spécifiquement la théorie de raccordement des champs de phase (PFMT - Phase Field Matching Theory), une méthode algébrique de différences finies, en conformité avec le formalisme de Landauer-Büttiker. Cette technique peut être considérée comme une alternative aux nombreuses techniques basées sur la fonction de Green. En particulier, notre méthode repose sur un choix pertinent du raccordement de phase entre les états électroniques des électrodes aux contacts idéaux avec les nanojonctions, d'une part, et les états électroniques localisés dans la zone des nanojonctions, d'autre part. Dans cette approche, les propriétés électroniques du système sont décrites dans le cadre de la méthode des liaisons fortes.

Notre travail dans le chapitre 3 présente formellement pour la première fois la dérivation complète et la discussion de la méthode PFMT pour un système nanoélectronique arbitraire entre deux contacts électriques. Le formalisme PFMT peut être considéré comme un outil compact et efficace pour l'étude du transport quantique électronique, pour un large éventail de matériaux nanostructurés. Il offre un compromis entre le rendement de calcul et la capacité prédictive par rapport aux méthodes plus lentes basées sur les principes premiers, et il pourrait potentiellement traiter les propriétés de conductance électronique des nanojonctions moléculaires complexes.

La méthode PFMT est appliquée dans ce travail de thèse pour la modélisation théorique et numérique du transport électronique quantique cohérent à travers un certain nombre de systèmes de nanojonctions. En particulier, ceux-ci sont préparés à partir de nanomatériaux à une ou plusieurs orbitales de valence.

Les résultats de cette modélisation sont présentés au chapitre 4 pour déterminer la conductance quantique électronique de nanojonctions à fils finis monovalents entre des électrodes, le système de la nanojonction étant à zéro potentielle externe. Nous appliquons nos calculs pour des fils monoatomiques linéaires de sodium (Na) en suspension

entre les électrodes du même élément, et pour de fils diatomiques de cuivre-cobalt (Cu-Co) entre des électrodes de cuivre sur un substrat de cuivre. Les calculs pour les systèmes Na confirment la justesse et la fonctionnalité de notre méthode PFMT. Nous présentons les spectres de transmission pour ces systèmes, et montrons que leurs propriétés de transport présentent des oscillations de conductance pour les fils à nombre d'atomes pairs et impairs, en accord avec les résultats rapportés précédemment par des méthodes de principes premiers. Les calculs numériques pour les nanojonctions de fil Cu-Co sont motivés par la stabilité de ces systèmes à basse température. Nos résultats pour les spectres de transmission des électrons σ présentent pour ce système, à son énergie de Fermi, une décroissance exponentielle de la conductance avec l'augmentation de la longueur du fil Cu-Co. Il s'agit d'un effet cumulatif qui est discuté en détail et peut s'avérer utile pour les applications dans les nano-circuits.

La modélisation de la conductance électronique quantique à travers les nanojonctions faites de nanofils de carbone dopés au silicium (Si-C), entre des électrodes de carbone, est présentée dans le chapitre 5. Cela se fait par une généralisation appropriée de la méthode PFMT pour les processus de multidiffusion des excitations électroniques aux nanojonctions. Nos calculs des structures de bandes électroniques des chaines atomiques de carbone et de silicium, et des chaines diatomiques de carbure de silicium, sont comparés avec les résultats de la théorie fonctionnelle de la densité (DFT - Density Functional Theory) correspondante afin d'optimiser les paramètres de la méthode des liaisons fortes. Les atomes de silicium et de carbone sont traités à égalité en caractérisant chacun de ces éléments avec leurs orbitales multivalentes correspondantes. Plusieurs types de structures de nanojonctions sont analysés afin de calibrer leur comportement sous différentes configurations atomiques. Nous calculons pour chaque nanojonction les contributions individuelles à la conductance des électrons σ, π, et $\sigma*$ incidents des électrodes de carbone. Par souci d'exhaustivité, nous présentons aussi dans le chapitre 5 les calculs de notre modélisation pour déterminer la conductance électronique quantique des nanojonctions de fil atomique fini d'arséniure de gallium (Ga-As) multivalent entre des électrodes de gallium (Ga). Les résultats calculés pour les systèmes Si-C et Ga-As présentent un nombre de caractéristiques remarquables qui comprennent l'influence des configurations périodiques ordonnées des paires atomiques et la suppression de la conductance quantique due à un désordre de substitution et à une symétrie artificiellement organisée.

Dans le chapitre 6 de la thèse, nous présentons brièvement nos conclusions et les perspectives pour les futures investigations sur le transport électronique quantique à travers des nano-jonctions à base de graphene.

Resume

Current and future technological needs increasingly motivate the intensive scientific research of the properties of materials at the nano scale. One of the most important domains in this respect at present concerns nanoelectronics in its diverse applications. The great interest in this domain, introduced in chapter 1 and 2, arises from the potential reduction of the size of the circuit components, maintaining their quality and functionality, and aiming at greater efficiency, economy, and storage characteristics for the corresponding physical devices.

The aim of this thesis in the nanoelectronics domain is to present a contribution to the analysis of the electronic transport phenomena that occur at the quantum level in nanostructures. For this purpose, we specifically develop the phase field matching theory (PFMT), a finite-difference algebraic method, in accordance with the Landauer-Büttiker formalism. It can be considered as an alternative to the available range of the Green's function-based techniques. In particular, our method is based on appropriate phase matching of the Bloch electronic states of the ideal leads to the local electronic states in the scattering region on nanojunction structures. In this approach, the electronic properties of the system are described in the framework of the tight-binding formalism.

Our work in chapter 3, formally presents for the first time the complete derivation and discussion of the PFMT method for an arbitrary nanoelectronic system between two electric leads. The PFMT formalism can be considered as a compact and efficient tool for the study of the electronic quantum transport for a wide range of material nanostructures. It provides a trade-off in computational efficiency and predictive capability as compared to slower first-principle based methods, and has the potential to treat the conductance properties of complex molecular nanojunctions.

The PFMT method is applied in the thesis work to the theoretical and numerical modeling of the quantum coherent electronic transport across a number of nanojunction structures of interest. In particular these are prepared from the mono- and multi-orbital valence nanomaterials.

Model calculations are presented in chapter 4 to determine the quantum electronic conductance of mono-valence finite atomic wire nanojunctions between electric leads at zero bias limit. We apply our calculations for freely suspended monatomic linear sodium wires (Na) between leads of the same element, and for the diatomic copper-cobalt wires (Cu-Co) between copper leads on a copper substrate. Calculations for the Na systems confirm the correctness and functionality of our PFMT method. We present novel transmission spectra for this system, and show that its transport properties exhibit the conductance oscillations for the odd- and even-number atomic wires in agreement with pre-

viously reported first-principle results. The numerical calculations for the Cu-Co wire nanojunctions are motivated by the stability of these systems at low temperatures. Our results for the transmission spectra of the σ electrons yield for this system, at its Fermi energy, a monotonic exponential decay of the conductance with increasing wire length of the Cu-Co pairs. This is a cumulative effect which is discussed in detail and may prove useful for applications in nano circuits.

The unknown quantum electronic conductance across nanojunctions made of silicon-doped carbon wires (Si-C) between carbon leads is investigated in chapter 5. This is done by an appropriate generalization of the PFMT for the multi-scattering processes of the electronic excitations at the nanojunction, and the use of the tight-binding method. Our calculations of the electronic band structures for carbon, silicon and for diatomic silicon carbide, are matched with the available corresponding density functional theory (DFT) results to optimize the required tight-binding parameters. The silicon and carbon atoms are treated on the same footing by characterizing each with their corresponding multi-valence orbitals. Several structural types of nanojunctions are analyzed to sample their behavior under different atomic configurations. We calculate for each nanojunction the individual contributions to the conductance from the σ, π, and $\sigma*$ electrons incident from the carbon leads. For completeness, we present model calculations in chapter 5 to determine the quantum electronic conductance of the multi-valence gallium-arsenide (Ga-As) finite atomic wire nanojunctions between gallium (Ga) leads. The calculated results for the Si-C and Ga-As systems show a number of remarkable features which include the influence of the ordered periodic configurations of atomic pairs and the suppression of quantum conductance due to minimum substitutional disorder and artificially organized symmetry.

In chapter 6 of the thesis we briefly present our conclusions and the perspectives for future investigations on the quantum electronic transport across graphene-based nanojunctions.

Contents

List of Figures

List of Tables

Chapter 1

Introduction

The development of science during last few decades is marked by an international drive for miniaturization of technology and devices. This can be traced back to the atomic theory which was established in chemistry at the beginning of the nineteenth century, to be next developed in other areas such as physics and biology [Dupas *et al.* 2007].

From the beginning of the 1980s onwards, several new domains associated with the prefix *nano* appeared. Nowadays terms such as nanoscience, nanotechnology *etc.* pop up in almost every sector of modern science. They describe areas where the size of the *object of interest* is, in at least one dimension, in the range from 0.1 nm to 100 nm, or in other words from 1 Å to 0.1 μm [Dupas *et al.* 2007], [Wolf 2003]. It should be pointed out that rather than a new scientific offshoot field of science, nanoscience is a new approach to material science at a scale which brings to the forth new and unknown effects and equally new technological applications due to the scale itself. The importance and popularity of this area of science lies in its multidisciplinarity, which based on fruitful integrations between physics, chemistry and life sciences [Dupas *et al.* 2007], [Borisenko & Ossicini 2008].

The idea of the limiting size of the objects is interesting due to the numerous applications that this may have in industry, and in fact determine the importance and usefulness of a new concepts in nanoscience. Currently the most important advantages of making devices smaller, can be seen notably in modern semiconductor electronics [Wolf 2003].

In the near future the so-called *nanotechnology* should allow complete manipulation of matter on the scale of nanometers. One of the most important applications of nanotechnology can be found *e.g.* in biology where molecular scale machines could be engineered to solve biological problems, like correcting defects in cells, killing dangerous cells (such as cancer cells), or even repairing cell damage presented after thawing of biological tissue, frozen as a means of preservation [Wolf 2003], [Scott *et al.* 2002].

On the account of potential and wide application of electronic devices these days,

one of the most important areas of nanoscience is *nanoelectronics*. In general, nanoelectronics correspond to the field that takes into account the studies and applications of nanosize electronic devices as well as fabrication of these components. Such novel nanoelectronic devices could improve, enhance and maybe even substitute present microelectronics [Mitin *et al.* 2008]. Nanoelectronics refers especially to electronic components like transistors. However transistors in nanotechnology meaning are significantly different from traditional ones, where the most important dissimilarity lies in the operational principle of nanoelectronic components which is determined by the quantum effects. These novel nanoelectronic devices are built on the basis of single atoms, quantum dots, nanotubes or molecules [Mozos *et al.* 1998] (please see an example of graphene based field emission transistor as depicted on figures 1.1).

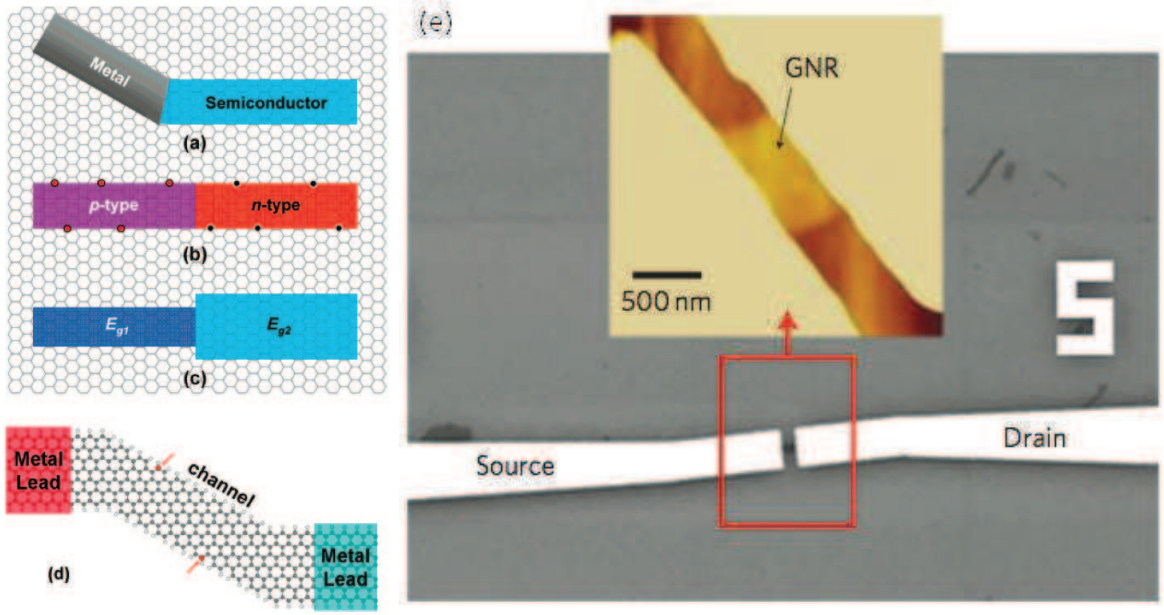

Figure 1.1: Three basic nanodevice building blocks: (a) a metal-semiconductor junction, (b) a *p*-*n* junction, and (c) a heterojunction, which can be made by carving out of graphene appropriate strips (the so-called *graphene nanoribbons*, GNR), along different direction, with different edge doping, and with different width, respectively. Various devices can be constructed from such blocks. For example, a field emission transistor (FET) can be made by two metal-semiconductor junctions, as presented in (d) [Yan *et al.* 2007]. The experimental realization of such idea is already possible as depicted in (e) where a FET fabricated using a nanoribbon end-bonded by two metal electrodes, is presented [Shimizu *et al.* 2010].

Among the various physical components which constitute the nanoelectronic devices, the nanojunctions therein are of crucial importance and will become increasingly so in the future [Nitzan & Ratner 2003], [Lamba 2009]. Such low-dimensional elements, which

can act *e.g.* as switches or gates [Nitzan & Ratner 2003], are considered to be key circuit components connecting the larger nanostructures. At present they are experimentally prepared and investigated by means of several techniques, such as the mechanically controllable break junction methods [Agraït *et al.* 2003], [Valkering *et al.* 2005], feedback-stabilized break junction technique [Smith *et al.* 2010], scanning tunneling microscopy [Agraït *et al.* 2003], [Kröger *et al.* 2009], atomic force microscopy [Agraït *et al.* 2003], as well as transmission electron microscopy [Jin *et al.* 2009], [Bettini *et al.* 2006] (please see an example high-resolution transmission electron microscopy of carbon wire nanojunction obtained by [Jin *et al.* 2009] as in figures 1.2).

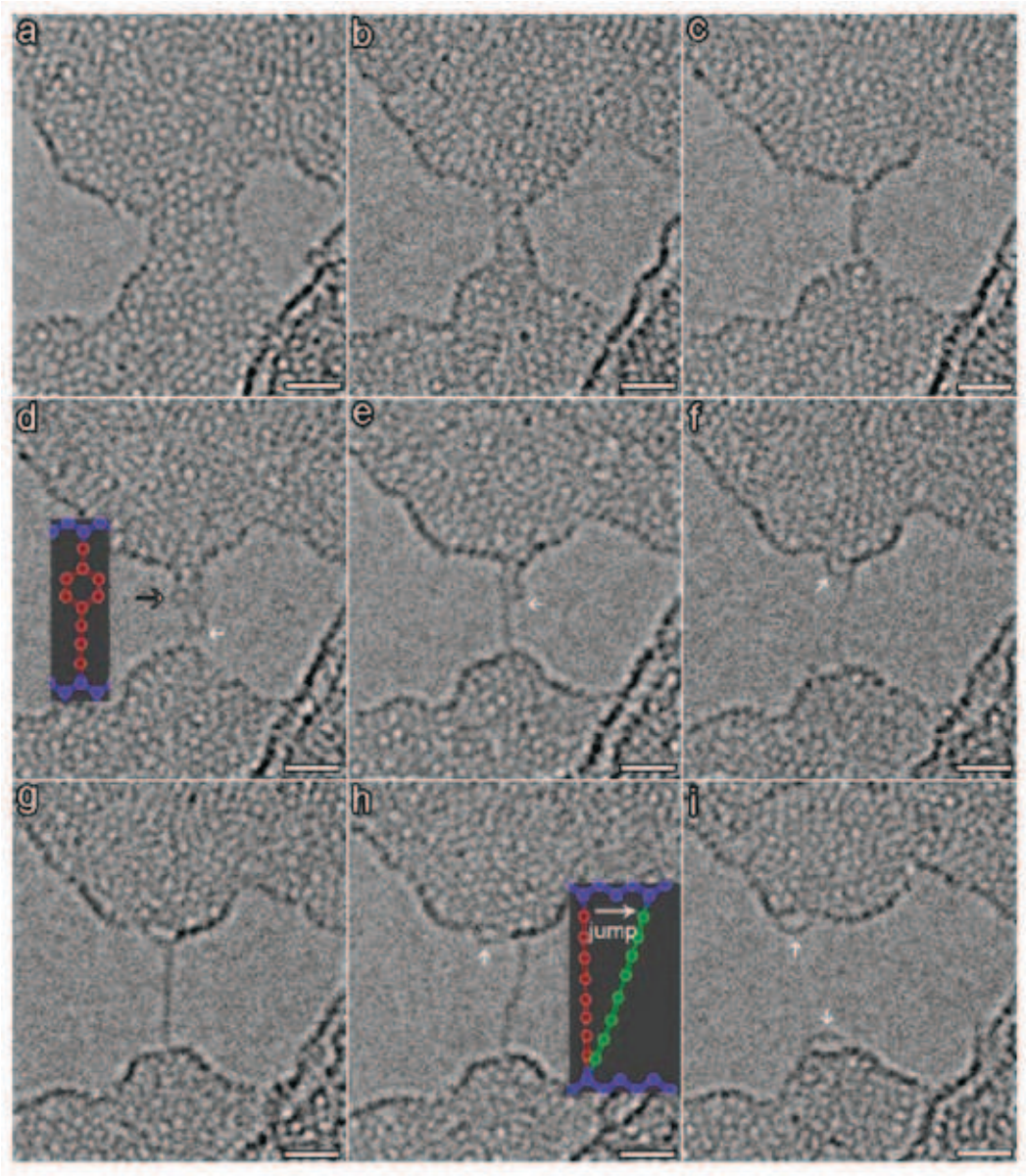

Figure 1.2: Consecutive high-resolution transmission electron microscopy images showing the formation (A-H) from graphene and finally breakage (I) of freestanding carbon nanojunction wire by continuous electron beam irradiation [Jin *et al.* 2009].

Atomic wires represent a particular class of such nanojunctions in nanoelectronic circuits. The conductance properties of atomic wires are the most interesting features of these systems, they depend on the materials used to fabricate them and on their structural properties. For example, the conductance of the monatomic wire nanojunctions does not stay constant or decrease when the length of the wire increases, rather it oscillates as a function of the number of the wire atoms. The periodicity of the oscillations may vary depending on the type of the atomic wire. It has been shown that, in the monovalent wire nanojunctions composed of alkali (Na and Cs) or noble metals (Ag, Au and Cu), the conductance oscillations exhibit the two-atom periodicity [Lang & Avouris 1998], [Smit *et al.* 2003], [Lee *et al.* 2008], [Khomyakov & Brocks 2006]. In contrast the Al wire nanojunctions present the oscillations with a period of four or six atoms, depending on the considered interatomic distances between consecutive sites [Thygesen & Jacobsen 2003], [Xu *et al.* 1992]. As well as in Al wires, the conductance oscillations have been observed in other multivalence wire nanojuctions, as platinum and iridium [de la Vega *et al.* 2004], carbon [Lang & Avouris 1998], [Shen *et al.* 2010], and silicon systems [Mozos *et al.* 1997], [Zhou *et al.* 2008].

Understanding the electronic transport properties of such nanojunctions is hence of particular importance. The electrons which contribute to the transport via nanojunctions present characteristic wavelengths comparable to the size of these components, leading to quantum coherent effects. The properties of the nanoelectronic device and its functionality may be then greatly affected or even built on such nanojunction quantum effects [Ke *et al.* 2008], and cannot be described in the framework of the classical regime [Havu *et al.* 2006]. The efficient and exact determination of the scattering transmission and reflection probabilities for the electrons as quantum particles in nanostructures is consequently a key concern.

In the present thesis the above issues are addressed, starting with the brief discussion as regards the theory of conductance as it appears in macro- and microscopic regimes (chapter 2). Next, the general form of the algebraic phase field matching theory (PFMT) that allows the calculations of the Landauer-Buttiker scattering probabilities is developed, in comparison with other mathematical formalisms. This PMFT method has the potential to treat the conductance properties of even complex molecular nanojunctions (chapter 3). Then the model calculations are developed and numerically applied to a spectrum of wire nanojunction systems of interest (chapters 4 and 5). Finally the pertinent conclusions and perspectives for future research are given in chapter 6.

Chapter 2

Theory of conductance

2.1 From macroscopic to microscopic regime

In the present work the electronic transport will be consequently characterized in the terms of electronic conductance (G), by arguing the fact that conductance is the most natural observable measured for the transport of electrons.

In general, proper description of the electronic transport that determine the electronic conductance in solids concerns about the nature of motion of electrical current carriers in matter. However, as already mentioned in chapter 1, when a dimensions of the given material decreases the general behavior of the electrons may change. The type of electron transport will then depend on whether or not one of the characteristic lengths known as the *mean-free path of electrons* ($\mathscr{L}$) (which is a length between two successive collisions of electrons with impurities or phonons) is comparable to the dimension of the material *i.e.* its diameter and length.

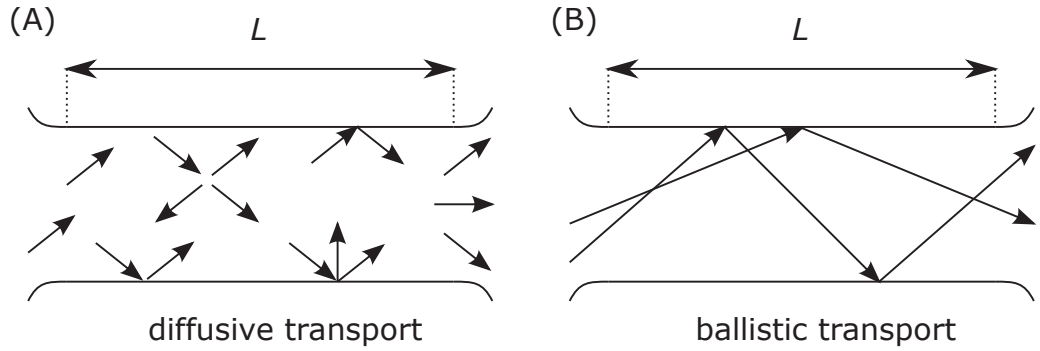

Figure 2.1: Schematical representation of the diffusive (figure 2.1 (A)) and ballistic (figure 2.1 (B)) electronic transport across given object of interest with length L.

When dealing with very small objects in its diameter scale, the electronic transport can be then classified only on the basis of the their length (L). Due to this fact the

electronic transport can divided into two general types (or regimes), namely *diffusive* or *ballistic* one.

When $L \gg \mathscr{L}$ (see figure 2.1 (A)), conductance depends on L, and is defined by the classical expression:

$$G \equiv \frac{\sigma S}{L}, \tag{2.1}$$

where S is a cross-section area of given object. In this case transport is known as diffusive. On the other hand when $L < \mathscr{L}$ (see figure 2.1 (B)), conductance becomes quantized:

$$G \equiv \frac{2e^2}{h}, \tag{2.2}$$

where e is the charge of electron, h is Planck's constant and conductance is independent on the length of the object. In this regime transport is known as ballistic[1] [Ventra 2008].

Based on above classification the electronic transport in nanodevices have to be then considered in the quantum regime. Since in nanostructures only elastic scattering can occur, the transport characteristics are usually described employing the scattering theory for electronic excitations [Newton 2002]. The relationship between quantum scattering and the electronic conductance is then initially provided by the work of Landauer [Landauer 1957], together with its generalization to the case of multiple scattering as developed by Büttiker [Büttiker 1986].

2.2 Landauer-Büttiker approach

In the Landauer-Büttiker formalism the object of interest, at which the scattering occurs, is modeled by quantum barrier and is connected to two reservoirs via perfect conducting wires (see figure 2.2), where *reservoirs* take a role of electric leads[2]. In what follows one of the leads is responsible for injecting electrons in the state defined by reservoir electrochemical potential μ and the second one for absorbing arriving electrons. Since reservoirs act as electric leads, a potential difference is applied across them in order to impose flow of the current via system. Hence, ideal conducting wires which are connected to the reservoirs can adiabatically transmit electrons into the sample. However, the electric current flowing through such system should be small to avoid variations of the transmission and the density of states, over considered energy range. In extreme limit (the *zero bias limit*) the applied potential can be assumed to be infinitesimally small in order to simplify discussion.

[1] Please note, that both Eq. (2.1) and (2.2) are written for one-dimensional system in its diameter scale, in order to clarify the discussion.

[2] Such sheme is know as two-terminal system, and represents initial formulation of the Landauer-Büttiker formalism. However, if needed, additional leads can be connected as presented by [Büttiker 1986].

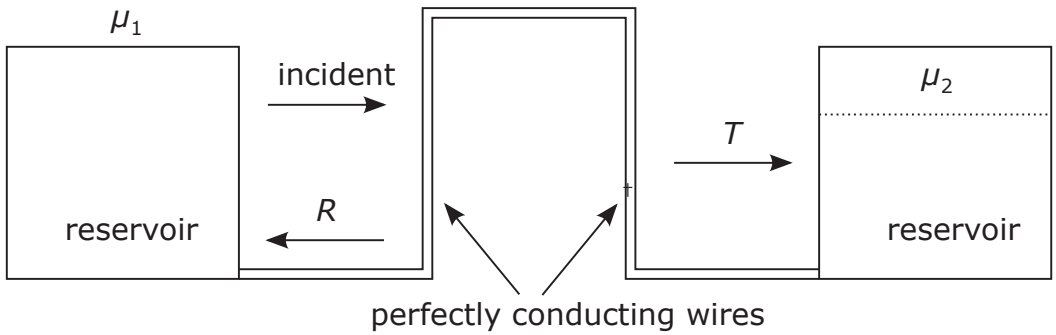

Figure 2.2: Scheme representation of the ballistic transport in the framework of Landauer-Büttiker approach for sample between two reservoirs.

I order to derive expressions for electronic conductance in the framework of the Landauer-Büttiker approach, let us consider the simplest one-dimensional case. In what follows the number of *conduction channels*, which are the modes of propagation characterized by the quantization of the wave vector, is limited only to a single one in one-dimensional case.

On the basis on figure 2.2 it can be noticed that consideration of the electron states below μ_2, either for first or second reservoir is redundant since resultant current is equal zero for such energies. This situation occurs due to the fact that below μ_2 values of currents flowing across the system from right to left reservoir or inversely are equal. From this point of view, only energies above the μ_2 level are significant for the transport problem. In this range of energies between μ_1 and μ_2, the $2\,(\mu_1 - \mu_2)\,\partial N/\partial E$ available states electronic states wil exist, where $\partial N/\partial E$ is the *the density of states* in one-dimension for N allowed states at energy E.

The total current for one-dimensional system in the framework of the Landauer-Büttiker approach is then given by following formula:

$$I_t = ev_f\,(\mu_1 - \mu_2)\,T\frac{\partial N}{\partial E}, \tag{2.3}$$

where v_f is the velocity of particles at the Fermi level. Equation (2.3) may be further simplified due to the assumed one-dimensional limit as:

$$\frac{\partial N}{\partial k} = \frac{\partial N}{\partial E}\frac{\partial E}{\partial k} = \frac{1}{\pi}, \tag{2.4}$$

where k is the wave number, and,

$$\frac{\partial N}{\partial E} = \frac{2}{hv_f}, \tag{2.5}$$

giving in a result the total electric current in the following form:

$$I_t = ev\,(\mu_1 - \mu_2)\,T\frac{2e}{h}. \tag{2.6}$$

Next the expression for the conductance and resistivity can be derived. Assuming that voltage V is measured directly at the terminals of the reservoirs injecting the current ($eV = \mu_1 - \mu_2$), the conductance is given by the formula:

$$G = \frac{I_t}{V} = \frac{2e^2}{h}T, \tag{2.7}$$

and the resistance by:

$$R = \frac{1}{G} = \frac{h}{2e^2}\frac{1}{T}. \tag{2.8}$$

Generalization to the multichannel case is then a very simple task, and can be done in following way. Let us assume *the scattering matrix*, which will be a $2\Gamma \times 2\Gamma$ matrix, where Γ denotes number of available conducting channels. Matrix elements $T_{\gamma,\gamma'}$ are the probability amplitudes of electrons which are transmitted from left channel γ into the right channel γ'. The generalized formula for the total electronic conductance is then written as:

$$G = \frac{I_t}{V} = \frac{2e^2}{h}\sum_{\gamma} T_\gamma, \tag{2.9}$$

where T_γ are the total transmission amplitudes for the available channels. If a perfect sample is applied, for which the transmission is equal to unity in all channels, the conductance will be then given by following expression:

$$G = \frac{Ne^2}{h}. \tag{2.10}$$

Chapter 3

Finite-difference approach to the electronic transport calculations

3.1 The electronic band structure of solids

3.1.1 Initial formulation of the tight-binding approximation

In order to proceed with the description of the scattering processes at the nanosystems the way to describe the electronic states in solids have to be chosen. To fully benefit from the theoretical method presented in section 3.2, our model dynamics are described in the framework of the theory appropriate for modeling realistic band structures of solids in a single-particle regime, known as the tight-binding approximation (TBA) in chemistry referred also as a linear combination of the atomic orbitals (LCAO).

From the historical point of view the first contribution to the development of TBA theory was given by Felix Bloch in his doctoral thesis from 1929 [Bloch 1929]. To trace back the initial formulation of the TBA theory let us begin with the secular single-particle equation:

$$H\Psi(\mathbf{r},\mathbf{k}) = E(\mathbf{k})\Psi(\mathbf{r},\mathbf{k}), \tag{3.1}$$

where H is the single-particle Hamiltonian, $\Psi(\mathbf{r},\mathbf{k})$ denotes the crystal wavefunction, and E stands for the electron eigenvalues. By multiplying the equation 3.1 by the $\Psi^*(\mathbf{r},\mathbf{k})$ and then integrating over the range of values where $\Psi(\mathbf{r},\mathbf{k})$ is defined, one can arrive with the following relation:

$$E(\mathbf{k}) = \frac{\int d\mathbf{r}\Psi^*(\mathbf{r},\mathbf{k})H\Psi(\mathbf{r},\mathbf{k})}{\int d\mathbf{r}\Psi^*(\mathbf{r},\mathbf{k})\Psi(\mathbf{r},\mathbf{k})}. \tag{3.2}$$

As it can be seen, the direct calculation of the energy levels of given crystal with a use of explicit forms of the wave functions $\Psi(\mathbf{r},\mathbf{k})$ is complicated. To simplify this, the true form of the wavefunction $\Psi(\mathbf{r},\mathbf{k})$ is expressed within TBA by the linear combination of

the appropriate trial functions $\Phi_l(\mathbf{r}-\mathbf{r}_n,\mathbf{k})$:

$$\Psi(\mathbf{r},\mathbf{k}) = \sum_{l,n} c_l(\mathbf{r}_n,\mathbf{k})\Phi_l(\mathbf{r}-\mathbf{r}_n,\mathbf{k}), \tag{3.3}$$

where $\mathbf{r}_n$ stands for the vector that marks the nth position of the atom in the crystal lattice, and l takes the values of the angular momentum character *i.e.* denotes type of the atomic orbitals (s, p, d etc.). The wavefunction coefficients $c_l(\mathbf{r}_n,\mathbf{k})$ represents the weight contribution which comes form a l-type atomic orbitals at lattice sites n. The basis states $\Phi_l(\mathbf{r}-\mathbf{r}_n,\mathbf{k})$ are then described by the sum of the $\phi_l(\mathbf{r}-\mathbf{r}_n-\mathbf{R}_N,\mathbf{k})$ functions as:

$$\Phi_l(\mathbf{r}-\mathbf{r}_n,\mathbf{k}) = \frac{1}{\sqrt{N_N}}\sum_N z\phi_l(\mathbf{r}-\mathbf{r}_n-\mathbf{R}_N,\mathbf{k}), \tag{3.4}$$

for all N_N unit cells at positions described by the corresponding $\mathbf{R}_N$ vectors. The $\phi_l(\mathbf{r}-\mathbf{r}_n-\mathbf{R}_N,\mathbf{k})$ functions are chosen to have the same symmetry properties as the atomic orbitals, and hence to be *tightly bound* to the atoms. The correctness of the this assumption can be qualitatively explained by arguing the fact that core electrons of the atoms which create the crystal mostly retain some of the properties from the free atoms, here its strong localization. Further, in equation 3.4, the quantity $z = e^{\pm i\mathbf{k}\mathbf{R}_N}$ is the Bloch phase factor, which describes wave propagating to the right (+) or left (-). Due to this, functions $\Phi_l(\mathbf{r}-\mathbf{r}_n,\mathbf{k})$ obey the Bloch-Floquet theorem in the following way:

$$\begin{aligned}
\Phi_l(\mathbf{r}-\mathbf{r}_n+\mathbf{R}_N,\mathbf{k}) &= \frac{1}{\sqrt{N_N}}\sum_{N'} e^{i\mathbf{k}(\mathbf{R}_{N'}-\mathbf{R}_N)}e^{i\mathbf{k}\mathbf{R}}\phi_l(\mathbf{r}-\mathbf{r}_n-\mathbf{R}_{N'}+\mathbf{R}_N,\mathbf{k}) \\
&= e^{i\mathbf{k}\mathbf{R}}\frac{1}{\sqrt{N_N}}\sum_{N'} e^{i\mathbf{k}(\mathbf{R}_{N'}-\mathbf{R}_N)}\phi_l(\mathbf{r}-\mathbf{r}_n-(\mathbf{R}_{N'}-\mathbf{R}_N),\mathbf{k}) \\
&= e^{i\mathbf{k}\mathbf{R}}\frac{1}{\sqrt{N_N}}\sum_{N''} e^{i\mathbf{k}\mathbf{R}_{N''}}\phi_l(\mathbf{r}-\mathbf{r}_n-\mathbf{R}_{N''},\mathbf{k}) \\
&= e^{i\mathbf{k}\mathbf{R}}\Phi_l(\mathbf{r}-\mathbf{r}_n,\mathbf{k}),
\end{aligned} \tag{3.5}$$

what signify that such functions in different unit cells are related by the Bloch-type phase factors, assuming $\mathbf{R}_{N''} = \mathbf{R}_{N'} - \mathbf{R}_N$ as another lattice vector.

The calculation of the energy levels can now be made, by substituting the trials functions $\Phi_l(\mathbf{r}-\mathbf{r}_n,\mathbf{k})$ into the equation 3.1 and arrive with the following form of the secular equation:

$$\begin{aligned}
&\sum_{l,n}\left[\int d\mathbf{r}\Phi^*_{l'}(\mathbf{r}-\mathbf{r}_{n'},\mathbf{k})H\Phi_l(\mathbf{r}-\mathbf{r}_n,\mathbf{k}) - E(\mathbf{k})\int d\mathbf{r}\Phi^*_{l'}(\mathbf{r}-\mathbf{r}_{n'},\mathbf{k})\Phi_l(\mathbf{r}-\mathbf{r}_n,\mathbf{k})\right] \\
&\times c_l(\mathbf{r}_n,\mathbf{k}) = 0.
\end{aligned} \tag{3.6}$$

Above relation represents linear system of equations of size equal to the product of the total number of distinctive atoms per unit cell and the total number of distinctive atomic

orbitals per each atom. This product gives us then the number of total energy levels at each $\mathbf{k}$ point in the Brillouin zone. In this manner, equation 3.6 is then essentially the discretized Schrödinger equation [Boykin & Klimeck 2004], [Boykin & Klimeck 2005].

In order to solve equation 3.6, the integrals inside this equation are evaluated in the following way:

$$\begin{aligned}\int d\mathbf{r}\Phi^*_{l'}(\mathbf{r}-\mathbf{r}_{n'},\mathbf{k})\Phi_l(\mathbf{r}-\mathbf{r}_n,\mathbf{k}) &= \frac{1}{N_N}\sum_{N',N''} e^{i\mathbf{k}(\mathbf{R}_{N'}-\mathbf{R}_{N''})} \\ &\times \int d\mathbf{r}\phi'_l(\mathbf{r}-\mathbf{r}_{n'}-\mathbf{R}_{N''},\mathbf{k})\phi_l(\mathbf{r}-\mathbf{r}_n-\mathbf{R}_{N'},\mathbf{k}) \\ &= \frac{1}{N_N}\sum_{N,N'} e^{i\mathbf{k}\mathbf{R}_N} \\ &\times \int d\mathbf{r}\phi_{l'}(\mathbf{r}-\mathbf{r}_{n'},\mathbf{k})\phi_l(\mathbf{r}-\mathbf{r}_n-\mathbf{R}_N,\mathbf{k}) \\ &= \sum_N e^{i\mathbf{k}\mathbf{R}_N} \\ &\times \int d\mathbf{r}\phi_{l'}(\mathbf{r}-\mathbf{r}_{n'},\mathbf{k})\phi_l(\mathbf{r}-\mathbf{r}_n-\mathbf{R}_N,\mathbf{k}), \qquad (3.7)\end{aligned}$$

and by analogy to the above:

$$\begin{aligned}\int d\mathbf{r}\Phi^*_{l'}(\mathbf{r}-\mathbf{r}_{n'},\mathbf{k})H\Phi_l(\mathbf{r}-\mathbf{r}_n,\mathbf{k}) &= \sum_N e^{i\mathbf{k}\mathbf{R}_N} \\ &\times \int d\mathbf{r}\phi_{l'}(\mathbf{r}-\mathbf{r}_{n'},\mathbf{k})H\phi_l(\mathbf{r}-\mathbf{r}_n-\mathbf{R}_N,\mathbf{k}). \qquad (3.8)\end{aligned}$$

In equation 3.7 the integrals $\int d\mathbf{r}\phi_{l'}(\mathbf{r}-\mathbf{r}_{n'},\mathbf{k})\phi_l(\mathbf{r}-\mathbf{r}_n-\mathbf{R}_N,\mathbf{k})$ are know as the *overlap integrals*, whereas the $\int d\mathbf{r}\phi_{l'}(\mathbf{r}-\mathbf{r}_{n'},\mathbf{k})H\phi_l(\mathbf{r}-\mathbf{r}_n-\mathbf{R}_N,\mathbf{k})$ ones of equation 3.8 as the *Hamiltonian integrals*. Both of these integrals are the crucial quantities in the TBA approach, since they are responsible for description of the atomic orbitals assumed in calculations and the interactions between them.

However, at the time when the TBA model was initially introduced it was almost impossible to compute all of these integrals. The most important simplification to the initial form of the TB approximation was given by John Clarke Slater and George Fred Koster in their milestone work entitled *Simplified LCAO method for the periodic potential problem* [Slater & Koster 1954]. In the Slater-Koster tight-binding approach (SK-TBA) the problematic integrals has been replaced by the adjustable constants, which can be fitted to the results of the more accurate but slower methods like those based on the first-principle calculations (such TBA model is often referred as the semi-empirical) or directly to the experimental data (the empirical TBA approach). The full set of the original SK-TBA parameters incorporates the binding energies ε_l of a certain atomic orbital at given lattice site, defined as:

$$\int d\mathbf{r}\phi_{l'}(\mathbf{r}-\mathbf{r}_{n'},\mathbf{k})H\phi_l(\mathbf{r}-\mathbf{r}_n-\mathbf{R}_N,\mathbf{k}) = \delta_{l,l'}\delta_{n,n'}\delta_{0,N}\varepsilon_l, \qquad (3.9)$$

as well as the parameters $h_{l,l'}$ which describe the interactions between two orbitals at different sites:

$$\int d\mathbf{r}\phi_{l'}(\mathbf{r}-\mathbf{r}_{n'},\mathbf{k})H\phi_l(\mathbf{r}-\mathbf{r}_n-\mathbf{R}_N,\mathbf{k}) = \delta_{n,n+\nu}h_{l,l'}, \tag{3.10}$$

where ν denotes the order of the nearest-neighbors included in the calculations, *e.g.* $\nu = 1$ for the first-nearest-neighbor regime (in chemistry known as Hückel approximation [Hückel 1931]). In the SK-TBA approach the $h_{l,l'}$ parameters are also known as a two-center integrals, what means that, the single particle potential is located at the same site as one of the atomic wave functions, whereas remaining atomic wave function is located at different lattice position. In this manner the atomic wave functions are considered to be orthogonal, what from the physical point of view is not acceptable since it neglects the overlap between two neighboring atomic wave functions *i.e.*:

$$\int d\mathbf{r}\phi_{l'}(\mathbf{r}-\mathbf{r}_{n'},\mathbf{k})\phi_l(\mathbf{r}-\mathbf{r}_n-\mathbf{R}_N,\mathbf{k}) = \delta_{l,l'}\delta_{n,n'}\delta_{0,N}, \tag{3.11}$$

and prevents any interactions between these functions. However, Slater and Koster show that using this approach the atomic orbitals should be treated more like Lödwin functions [Lödwin 1950] then typical atomic wave functions. Even if such simplifications may seems to be too radical, the Lödwin functions still have the same symmetry properties as the atomic orbitals. In fact the electronic calculations which based on the original SK-TB formulation usually give qualitatively good results, however sometimes allows to obtain even quantitative description of the electronic properties. In order to raise the accuracy of the SK-TB model, the non-orhogonality can be introduced into the minimal basis of the atomic wave functions as presented by Mattheiss [Mattheiss 1972a], [Mattheiss 1972b]. Using the non-orthogonal minimal basis of the atomic orbitals one has to extend the SK-TBA parameters set by the additional overlap integrals $s_{l,l'}$:

$$\int d\mathbf{r}\phi_{l'}(\mathbf{r}-\mathbf{r}_{n'},\mathbf{k})\phi_l(\mathbf{r}-\mathbf{r}_n-\mathbf{R}_N,\mathbf{k}) = \delta_{n,n+\nu}s_{l,l'}. \tag{3.12}$$

In this form the tight-binding method is much more accurate when comparing to the SK-TB formulations, however it is also slower because of the additional overlap terms.

3.1.2 Tight-binding approximation in modern physics

Despite the long history of the tight-binding approximation approach, and the fact that modern computers already allow to carry calculations in the frameworks of more sophisticated methods (like the density functional theory) within reasonable time limits, the TBA is still widely exploited for numerous electronic properties computations. At present, the application of the TBA covers the calculations of the basic electronic

properties like total energies, band structures or the density of states [Harrison 2004], [Papaconstantopoulos & Mehl 2003], [Harrison 2002]. Furthermore this formalism can be used for more complex tasks like simulating the scanning tunneling microscope images of nanostructures [Delga *et al.* 2011], [Hands *et al.* 2010] or by integrating its approach with methods for electronic transport calculations [Szczęśniak & Khater 2012], [Szczęśniak *et al.* 2012], [Wu & Childs 2011], [Kobayashi 2011]. The fact that TBA is indeed a interesting alternative to other models that allow the electronic properties calculations, is moreover reinforced by its following advantages:

- relatively simple mathematical formulation,
- correct band mixing description,
- direct interpretation of the atomic details,
- low computational costs,
- fully real-space mathematical formulation.

In order to handle described applications of the TBA model, various implementations of this method has been presented in past years which have common objective in its initial formulation presented in previous subsection. On the basis of discussion provided in subsection 3.1.1, the general concern in using the TBA is the correct determination of all integrals (often referred as *tight-binding parameters*) that enter the secular equation, both for onthonormal or non-orthogonal interactions. As already mentioned, these integrals can be fitted directly to the experimental data or to the results of more accurate methods. Nevertheless, if such fitting procedure is carried only for a specific system of interst and gives even quantitative agreement with other results, the obtained integrals are not *transferable*. This is a major disadvantage of such attempt since, it forbids any comparisons on the same footing between different materials. The solution to this problem is to use one of the wide range of transferable parametrization methods. At present the following popular ones can be listed:

- Harrison tight-binding theory (HTBT) [Harrison 2004] - one of the first universal schemes for the tight-binding calculations that provides a simple way to calculate the tight-binding parameters in the orthonormal regime. Within this method the orbital type dependent onsite energies (ε_l) are predetermined and their values are relative to the energy of the ground state of hydrogen. On the other hand the coupling parameters ($h_{l,l'}$), consistent with the Slater-Koster convention

[Slater & Koster 1954], are distance dependent and calculated on the basis of the following expression:

$$h_{l,l',m}^{n,n',\beta} = \eta_{l,l',m} \frac{\hbar^2}{m_e d_\beta^2}, \tag{3.13}$$

where $\eta_{l,l',m}$ are the dimensionless and already predefined Harrison coefficients, m_e the electron mass in vacuum, and d_β the interatomic distance for interacting neighbors. Please note that above form of the onsite and coupling parameters is presented as it appears in its classical form for simple compounds [Harrison 2004]. This formulation gives mostly qualitative description of the electronic bands, but can be simply re-parametrized for specific applications when quantitative agreement with more accurate results is required. An specific extensions for *e.g.* semiconductors or transition metals are available [Harrison 2004]. Even the non-orthogonal formulation of the HTBT is present, however the universality of this implementation is restricted to the transition, alkaline earth, and noble metals [Shi & Papaconstantopoulos 2004].

The HTBT method is chosen due to its transparency and intuitive form as a basic parametrization method for numerical calculations presented in this thesis, except the calculations carried for diatomic copper-cobalt nanojunctions presented in section 4.2, which based on the parameters fitted to the experimental results.

- Cohen *et al.* theory [Cohen *et al.* 1994] - is the fully non-orthogonal universal TBA model. Within this approach the binding energies are environmentally dependent terms expressed using the Birch-like equations. This model incorporates both the tight-binding coupling terms ($h_{l,l'}$) as well as the overlap parameters ($s_{l,l'}$).

- Density-functional tight-binding theory (DFTB) [Porezag *et al.* 1995] - a model which is parametrized directly using density functional theory, and despite the fact it still cannot be considered as an *ab initio* method because of its TBA origins, it is rooted in first principles deeper than other parametrization methods. This conjunction of the TBA and DFT approaches into one results in high accuracy and reasonable transferability of the model. In general this theory based on the second-order expansion of the Kohn-Sham total energy in DFT, taking into account the charge density fluctuations. In this manner the zeroth order approach is equivalent to a classical tight-binding scheme. An interesting introduction to the DFTB method can be found in [Koskinen & Mäkinen 2009].

3.2 The phase field matching theory approach

3.2.1 The general formulation of the phase field matching theory

Let us next develop the appropriate method for description of the scattering processes at the nanosystems. In this section we present the complete derivation and discussion of the finite-difference algebraic method namely the *phases field matching theory* (PFMT) as presented in [Szczęśniak & Khater 2012] and [Szczęśniak *et al.* 2012], which was originally and intensively developed for the scattering and transport of phonon and magnon excitations in nanostructures [Khater *et al.* 2011a], [Khater *et al.* 2011b], [Tigrine *et al.* 2008], [Virlouvet *et al.* 1999], [Fellay *et al.* 1997]. While at first sight, the formulation of the PFMT may be expected to be formally similar for different types of excitations, *i.e.* replacing here the dynamical equation for phonons or magnons by the Schrödinger equation, there are however significant technical dissimilarities which play an important role. For example, we can refer to the fact that in the electron scattering problem one has to consider allowed symmetries of the atomic orbitals, which is not the case for phonon and magnon excitations.

The schematic representation of the system under study with an arbitrary nanojunction region is presented in Figure 3.1. With reference to the Landauer-Büttiker theory for the analysis of the electronic scattering processes [Landauer 1957], [Büttiker 1986], this system is divided into three main parts, namely the finite nanojunction region (red color), and two other regions to the right and left of the nanojunction which are semi-infinite quasi one-dimensional carbon leads (blue color). Each color block, red and blue, represents primitive unit cell[1]. Moreover, for the purpose of the quantum conductance calculations, the so-called irreducible region and the matching domains are depicted. Figure 3.1 is used throughout section 3.2.1 as a graphical reference for the analytical discussion.

The system presented in Figure 3.1 is described by the general tight-binding Hamil-

[1]Note that in order to keep transparent theoretical discussion, we treat in this section an equivalent number of atoms for all unit cells in the system, *i.e.* in the leads and on the nanojunction. However, the PFMT method allows us in general to consider systems with unit cells of different dimensions and shapes.

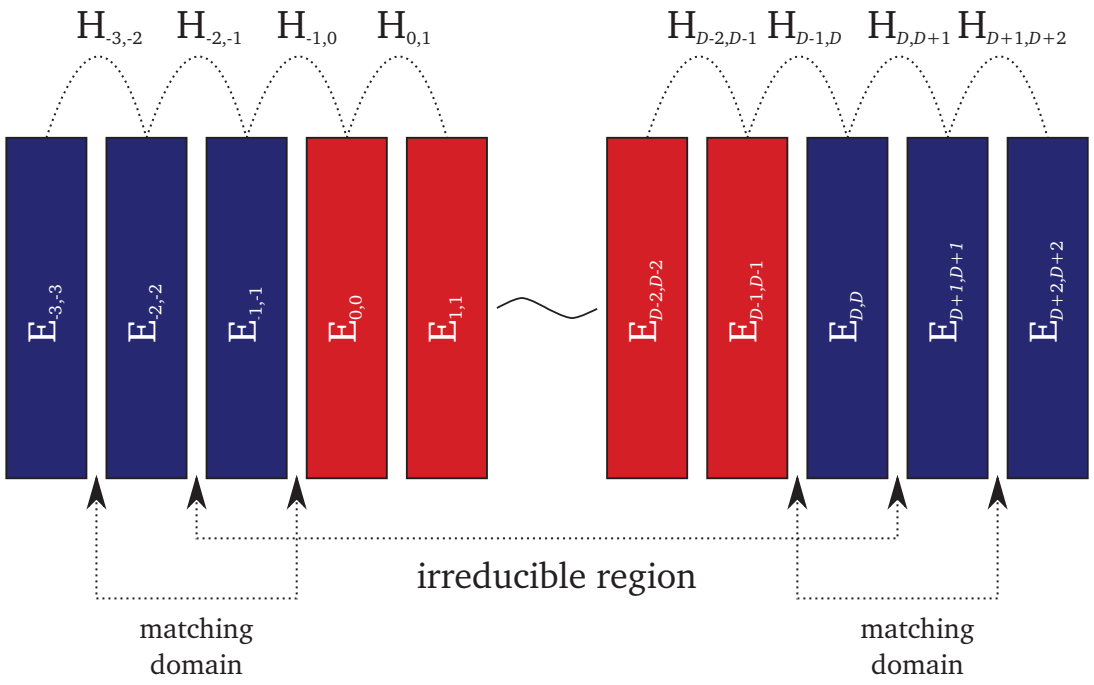

Figure 3.1: Schematic planar projection in the direction of propagation of an arbitrary three-dimensional Landauer-Büttiker-type system. The unit cells of the nanojunction ($N \in [0, D-1]$) and two semi-infinite leads ($N \in [-\infty, -1]$ and $N \in [D, \infty]$) are denoted by red and blue colors, respectively. The corresponding Hamiltonian on- and off-diagonal sub-matrices are also depicted. Note that in order to keep the figure simple we show the Hamiltonian sub-matrices for interactions between different unit cells only for $i < j$.

tonian block matrix

$$\mathbf{H} = \begin{bmatrix} \ddots & \cdots & 0 & 0 & \\ \vdots & \mathbf{E}_{N-1,N-1} & \mathbf{H}^{\dagger}_{N,N-1} & 0 & 0 \\ 0 & \mathbf{H}_{N,N-1} & \mathbf{E}_{N,N} & \mathbf{H}^{\dagger}_{N+1,N} & 0 \\ 0 & 0 & \mathbf{H}_{N+1,N} & \mathbf{E}_{N+1,N+1} & \vdots \\ & 0 & 0 & \cdots & \ddots \end{bmatrix}. \tag{3.14}$$

This is defined in general for a system of N_x inequivalent atoms per unit cell, where N_l denotes the number of the basis orbitals per atomic site, assuming spin degeneracy. In equation (3.14), $\mathbf{E}_{i,j}$ denote the on-diagonal matrices composed of both diagonal $\varepsilon_l^{n,\alpha}$ and off-diagonal $h_{l,l',m}^{n,n',\beta}$ elements for a selected unit cell. In contrast the $\mathbf{H}_{i,j}$ matrices contain only off-diagonal elements for the interactions between different unit cells. Each diagonal element is characterized by the index α that identifies the atom type on the nth site in a unit cell and the lower index l for the angular momentum state. The off-diagonal elements $h_{l,l',m}^{n,n',\beta}$ describe the m-type bond between l and l' nearest-neighbor states.

In our calculations the single-particle electronic wave functions are expanded in the orthonormal basis of local atomic wave functions $\phi_l(\mathbf{r})$ as follows

$$\Psi(\mathbf{r},\mathbf{k}) = \sum_{l,n,N} c_l(\mathbf{r}_n - \mathbf{R}_N, \mathbf{k})\phi_l(\mathbf{r} - \mathbf{R}_N, \mathbf{k}). \tag{3.15}$$

In equation (3.15), $\mathbf{k}$ is the real wave vector, $\mathbf{R}_N$ the position vector of the selected unit cell, and $\mathbf{r}_n$ the position vector of the nth atom in the selected unit cell. For the ideal leads, the wavefunction coefficients $c_l(\mathbf{r}_n - \mathbf{R}_N, \mathbf{k})$ are characterized under the Bloch-Floquet theorem in consecutive unit cells by the following phase relation

$$c_l(\mathbf{r}_n - \mathbf{R}_{N+1}, \mathbf{k}) = z c_l(\mathbf{r}_n - \mathbf{R}_N, \mathbf{k}), \tag{3.16}$$

where z is the phase factor

$$z_\pm = e^{\pm i\mathbf{k}\mathbf{R}_N}, \tag{3.17}$$

which correspond here to waves propagating to the right (+) or to the left (-).

Note at this point that the choice of the orthonormal basis is made only to simplify our notation in further part of this section and to make our discussion more transparent to the reader. In general, any kind of the minimal basis can be chosen, depending on the considered structure and assumed approximations.

The electronic equations of motion for a leads unit cell, independent of N, may be expressed in square matrix form, with an orthonormal minimal basis set of local wavefunctions, as

$$(E\mathbf{I} - \mathbf{M}_d) \times \mathbf{c}(\mathbf{k}, E) = 0. \tag{3.18}$$

E stands for the electron eigenvalues, $\mathbf{I}$ is the identity matrix, while the dynamical matrix $\mathbf{M}_d$ contains the Hamiltonian matrix elements and the z phase factors. The $\mathbf{c}(\mathbf{k}, E)$ is the $N_x \times N_l$ size vector defined as

$$\mathbf{c}(\mathbf{k}, E) = \begin{bmatrix} c_s(\mathbf{r}_1, \mathbf{k}, E) \\ c_{p_x}(\mathbf{r}_1, \mathbf{k}, E) \\ \vdots \\ c_{l-1}(\mathbf{r}_n, \mathbf{k}, E) \\ c_l(\mathbf{r}_n, \mathbf{k}, E) \end{bmatrix} \equiv \begin{bmatrix} \mathbf{c}_l(\mathbf{r}_1, \mathbf{k}, E) \\ \vdots \\ \mathbf{c}_l(\mathbf{r}_n, \mathbf{k}, E) \end{bmatrix}. \tag{3.19}$$

Equation (3.18) gives the $N_x \times N_l$ eigenvalues with corresponding eigenvectors which determine the electronic structure of the lead system, where l under the vector $\mathbf{c}_l$ corresponds to the total N_l different orbitals assumed in the calculations.

The complete description of the electronic states on the ideal leads requires a full understanding of the propagating and of the evanescent electronic states on the leads. This arises because the nanojunction (red color blocks in Figure 3.1) breaks the perfect

periodicity of the infinite leads (blue color blocks in Figure 3.1), and forbids a formulation of the problem only in terms of the pure Bloch states as given in equation (3.17). Depending on the complexity of a given electronic state, it follows that the evanescent waves may be defined by the phase factors for a purely imaginary wave vectors $\mathbf{k} = i\boldsymbol{\kappa}$ such that

$$z = z_{\pm} = e^{\mp \boldsymbol{\kappa} \mathbf{r}_n}, \tag{3.20}$$

or for complex wave vectors $\mathbf{k} = \boldsymbol{\kappa}_1 + i\boldsymbol{\kappa}_2$ such that

$$z = z_{\pm} = e^{\mp (i\boldsymbol{\kappa}_1 - \boldsymbol{\kappa}_2) \mathbf{r}_n}. \tag{3.21}$$

The phase factors of equations (3.20) and (3.21) correspond to pairs of hermitian evanescent and divergent solutions on the leads. Only the evanescent states are physically considered, where the spatial evanescence occurs to the right and left away from the nanojunction localized states. Note that the l-type evanescent state corresponds to energies beyond the propagating band structure for this state.

The functional behavior of $z(E)$ for the propagating and evanescent states on the leads may be obtained by various techniques. An elegant method presented previously for phonon and magnon excitations [Fellay *et al.* 1997], is adapted here for the electrons. It is described on the basis of equations (3.16) and (3.18) by the generalized eigenvalue problem for z

$$\left[\left[\begin{array}{cc} E\mathbf{I} - \mathbf{E}_{N,N} & \mathbf{H}_{N,N-1} \\ \mathbf{I} & 0 \end{array} \right] - z \left[\begin{array}{cc} -\mathbf{H}^{\dagger}_{N,N-1} & 0 \\ 0 & \mathbf{I} \end{array} \right] \right] \times \left[\begin{array}{c} \mathbf{c}(\mathbf{R}_N, z, E) \\ \mathbf{c}(\mathbf{R}_{N-1}, z, E) \end{array} \right] = 0. \tag{3.22}$$

Equation (3.22) gives the $2N_xN_l$ eigenvalues as an ensemble of N_xN_l pairs of z and z^{-1}. Only solutions with $|z| = 1$ (propagating waves) and $|z| < 1$ (evanescent waves) are retained as a physical ones. In equation (3.22) $\mathbf{k}$ is then replaced by the appropriate energy E variable. Furthermore, for systems with more than one atom per unit cell, the matrices $\mathbf{H}_{N,N-1}$ and $\mathbf{H}^{\dagger}_{N,N-1}$ in this procedure are singular. In order to obtain the physical solutions, the eigenvalue problem of equation (3.22) is reduced from the $2N_xN_l$ size problem to the appropriate $2N_l$ one, by using the partitioning technique (please see Appendix B).

Consider next the scattering problem at the nanojunction. An electron incident along the leads has a given energy E and wave vector $\mathbf{k}$, where $E = E_{\gamma}(\mathbf{k})$ denotes the available dispersion curves for the $\gamma = 1, 2, ..., \Gamma$ propagating eigenmodes, where Γ corresponds to the total number of allowed solutions for the eigenvalue problem of phase factors in equation (3.22). In any given energy interval, however, these may be evanescent or

propagating eignemodes, and together constitute a complete set of available channels necessary for the scattering analysis.

The irreducible domain of atomic sites for the scattering problem includes the nanojunction domain itself, ($N \in [0, D-1]$), and the atomic sites on the left and right leads which interact with the nanojunction, as in Figure 3.1. This constitutes a necessary and sufficient region for our considerations, *i.e.* any supplementary atoms from the leads included in the calculations do not change the final results. The scattering at the boundary yields then the coherent reflected and transmitted fields, and in order to calculate these, we establish the *system* of equations of motion for the atomic sites ($N \in [-1, D]$) of the irreducible nanojunction domain. This procedure leads to the general matrix equation

$$\mathbf{M}_{nano} \times \mathbf{V} = 0. \tag{3.23}$$

$\mathbf{M}_{nano}$ is a $(D+2) \times (D+4)$ matrix composed of the block matrices $(E\mathbf{I} - \mathbf{E}_{N,N} - \mathbf{H}_{N,N-1} - \mathbf{H}^{\dagger}_{N,N-1})$, and the state vector $\mathbf{V}$ of dimension $D+4$ is given as

$$\mathbf{V} = \begin{bmatrix} \mathbf{c}_l(\mathbf{r}_1 - \mathbf{R}_{-2}, E) \\ \vdots \\ \mathbf{c}_l(\mathbf{r}_n - \mathbf{R}_{-2}, E) \\ \vdots \\ \vdots \\ \mathbf{c}_l(\mathbf{r}_1 - \mathbf{R}_{D+1}, E) \\ \vdots \\ \mathbf{c}_l(\mathbf{r}_n - \mathbf{R}_{D+1}, E) \end{bmatrix}. \tag{3.24}$$

Since the number of unknown coefficients in equation (3.23) is always greater than the number of equations, such a set of equations cannot be solved directly.

Assuming that the incoming electron wave propagates from left to right in the eigenmode γ over the interval of energies $E = E_\gamma$, the field coefficients on the left and right sides of the irreducible nanojunction domain may be written as

$$\begin{aligned} \mathbf{c}^L_l(\mathbf{r}_n - \mathbf{R}_N, z_\gamma, E_\gamma) &= \mathbf{c}_l(\mathbf{r}_n, z_\gamma, E_\gamma) z_\gamma^{-N} \\ &+ \sum_{\gamma'}^{\Gamma} \mathbf{c}_l(\mathbf{r}_n, z_{\gamma'}, E_\gamma) z_{\gamma'}^{N} r_{\gamma,\gamma'}(E_\gamma) \text{ for } N \leqslant -1, \end{aligned} \tag{3.25}$$

$$\mathbf{c}^R_l(\mathbf{r}_n - \mathbf{R}_N, z_\gamma, E_\gamma) = \sum_{\gamma'}^{\Gamma} \mathbf{c}_l(\mathbf{r}_n, z_{\gamma'}, E_\gamma) z_{\gamma'}^{N} t_{\gamma,\gamma'}(E_\gamma) \text{ for } N \geqslant D, \tag{3.26}$$

where $\gamma' \in \Gamma$ is an arbitrary channel into which the incident electron wave scatters, and $\mathbf{c}_l(\mathbf{r}_n, z_\gamma, E_\gamma)$ denotes the the eigenvector of the lead dynamical matrix of equation

(3.18) for the inequivalent site n, at z_γ and E_γ. The terms $r_{\gamma,\gamma'}$ and $t_{\gamma,\gamma'}$ denote the scattering amplitudes for respectively backscattering and transmission from the γ into the γ' eigenmodes, and constitute the basis of the Hilbert space which describes the reflection and transmission processes.

Equations (3.25) and (3.26) are next used to transform the $(D+2)\times(D+4)$ matrix of the system of equations of motion, equation (3.23), into an inhomogeneous $(D+2)\times(D+2)$ matrix for the scattering problem. This procedure leads to the new form of the vector

$$\mathbf{V} = \begin{bmatrix} z^2 & 0 & \cdots & \cdots & \cdots & \cdots & 0 \\ z & 0 & & & & & \vdots \\ 0 & 1 & & & & & \vdots \\ \vdots & & \ddots & & & & \vdots \\ \vdots & & & 1 & & & \vdots \\ \vdots & & & & \ddots & & \vdots \\ \vdots & & & & & 1 & 0 \\ \vdots & & & & & 0 & z \\ 0 & \cdots & \cdots & \cdots & \cdots & 0 & z^2 \end{bmatrix} \times \begin{bmatrix} \mathbf{r}_{\gamma,\gamma'} \\ \mathbf{c}_l(\mathbf{r}_1 - \mathbf{R}_0, E_\gamma) \\ \vdots \\ \mathbf{c}_l(\mathbf{r}_n - \mathbf{R}_0, E_\gamma) \\ \vdots \\ \vdots \\ \mathbf{c}_l(\mathbf{r}_1 - \mathbf{R}_{D-1}, E_\gamma) \\ \vdots \\ \mathbf{c}_l(\mathbf{r}_n - \mathbf{R}_{D-1}, E_\gamma) \\ \mathbf{t}_{\gamma,\gamma'} \end{bmatrix} + \begin{bmatrix} \mathbf{c}_l(\mathbf{r}_1, z_\gamma, E_\gamma) z_\gamma^{-2} \\ \vdots \\ \mathbf{c}_l(\mathbf{r}_n, z_\gamma, E_\gamma) z_\gamma^{-2} \\ \mathbf{c}_l(\mathbf{r}_1, z_\gamma, E_\gamma) z_\gamma^{-1} \\ \vdots \\ \mathbf{c}_l(\mathbf{r}_n, z_\gamma, E_\gamma) z_\gamma^{-1} \\ 0 \\ \vdots \\ 0 \end{bmatrix}. \tag{3.27}$$

The rectangular sparse matrix in equation (3.27) has $(D+4)\times(D+2)$ size. The vectors $\mathbf{r}_{\gamma,\gamma'}$ and $\mathbf{t}_{\gamma,\gamma'}$ are column vectors of the backscattering and transmission Hilbert basis.

Substituting equation (3.27) into equation (3.23) yields an inhomogenous system of

equations as follows

$$\mathbf{M} \times \begin{bmatrix} \mathbf{r}_{\gamma,\gamma'} \\ \mathbf{c}_l(\mathbf{r}_1 - \mathbf{R}_0, E_\gamma) \\ \vdots \\ \mathbf{c}_l(\mathbf{r}_n - \mathbf{R}_0, E_\gamma) \\ \vdots \\ \vdots \\ \mathbf{c}_l(\mathbf{r}_1 - \mathbf{R}_{D-1}, E_\gamma) \\ \vdots \\ \mathbf{c}_l(\mathbf{r}_n - \mathbf{R}_{D-1}, E_\gamma) \\ \mathbf{t}_{\gamma,\gamma'} \end{bmatrix} = - \begin{bmatrix} \mathbf{M}_1^{in} \\ \mathbf{M}_2^{in} \\ 0 \\ \vdots \\ 0 \end{bmatrix} \tag{3.28}$$

In equation 3.28, $\mathbf{M}$ is the *matched* $(D+2) \times (D+2)$ square matrix, and the vector of dimension $(D+2)$ which incorporates the $\mathbf{M}_1^{in}$ and $\mathbf{M}_2^{in}$ elements, regroups the inhomogeneous terms of the incident wave. The explicit forms of the $\mathbf{M}$ matrix elements and and $\mathbf{M}_N^{in}$ vectors are presented in Appendix C.

In practice, equation (3.28) can be solved using standard numerical procedures, over the entire range of available electronic energies, yielding the coefficients $\mathbf{c}_l$ for the atomic sites on the nanojunction domain itself, and also the Γ reflection $r_{\gamma,\gamma'}(E)$ and the Γ transmission $t_{\gamma,\gamma'}(E)$ coefficients. However for simple systems it is possible to calculate explicit analytical expressions for the transmission and reflection coefficients as it has been shown in [Khater & Szczęśniak 2011].

The reflection and transmission coefficients give respectively the reflection $R_{\gamma,\gamma'}(E)$ and transmission $T_{\gamma,\gamma'}(E)$ probabilities, by normalizing with respect to their group velocities v_γ in order to obtain the unitarity of the scattering matrix, as

$$R_{\gamma,\gamma'}(E) = \frac{v_{\gamma'}}{v_\gamma} \left| r_{\gamma,\gamma'}(E) \right|^2 , \tag{3.29}$$

$$T_{\gamma,\gamma'}(E) = \frac{v_{\gamma'}}{v_\gamma} \left| t_{\gamma,\gamma'}(E) \right|^2 , \tag{3.30}$$

where $v_\gamma \equiv v_\gamma(E)$ denotes the group velocity of the incident electron wave in the eigenmode γ. The group velocities are calculated by a straightforward procedure as in Appendix D. For the evanescent eigenmodes $v_{\gamma'} = 0$. Although the evanescent eigenmodes do not contribute to the electronic transport, they are required for the complete description of the scattering processes.

Furthermore, using equations (3.29) and (3.30), the overall reflection probability, $R_\gamma(E)$, for an electron incident in the γ eigenmode, and the total electronic reflection

probability, $R(E)$, from all the eignemodes may be expressed respectively as

$$R_\gamma(E) = \sum_{\gamma'}^{\Gamma} R_{\gamma,\gamma'}(E) \text{ and } R(E) = \sum_{\gamma}^{\Gamma} R_\gamma(E). \tag{3.31}$$

Similarly, for the transmission probabilities, we may write the equivalent equations as

$$T_\gamma(E) = \sum_{\gamma'}^{\Gamma} T_{\gamma,\gamma'}(E) \text{ and } T(E) = \sum_{\gamma}^{\Gamma} T_\gamma(E). \tag{3.32}$$

The $T_\gamma(E)$ and $T(E)$ probabilities are very important for the electronic scattering processes since they correspond directly to the experimentally measurable observables. Likewise, the total transmission $T(E_\gamma)$ allows to calculate the overall electronic conductance. In this work we assume the zero bias limit and write the total conductance in the following way

$$G(E_F) = G_0 T(E_F). \tag{3.33}$$

In equation (3.33), G_0 is the conductance quantum and equals $2e^2/h$. Due to the Fermi-Dirac distribution the $G(E_F)$ is calculated at the Fermi level of the perfect leads band structure, since electrons only at this level give the important contribution to the electronic conductance. The Fermi energy can be determined using various methods, where in the present work E_F is calculated the basis of the density of states calculations.

3.2.2 Remarks on other available techniques

Despite developed in this thesis phase field matching theory, the scattering probabilities for the transport of electrons can be determined thanks to other theoretical methods which have a common objective in the framework of the Landauer-Büttiker formalism [Landauer 1957], [Büttiker 1986], and can be employed by integrating in their approach, the density functional theory [Egami *et al.* 2010], [Tsukamoto *et al.* 2009] or the tight-binding model [Kobayashi 2011], [Nozaki *et al.* 2010], [Zhang *et al.* 2011a].

The most popular alternatives to the PFMT approach are the matrix Green's function method by Ando [Ando 1991] or the non-equilibrium Green's function formalism (NEGF), also known as the Keldysh formalism[2]. However, there has been a debate whether the Ando's formalism is complete [Krstić *et al.* 2002], and in spite of the fact that usual combination of the Keldysh formalism and DFT is still very often computationally demanding [Havu *et al.* 2006], [Zhang *et al.* 2011a] motivating intensive research for solutions to this difficulty, the NGEF is the most relevant alternative to the PFMT.

[2]For discussion of the non-equlibrium Green's function formalism (originally formulated by L.V. Keldysh in [Keldysh 1965]) for a electronic transport simulations we refer to [Datta 1995].

Please note that an interesting discussion of different types of the optimization techniques for NGEF formalism in the case of electronic transport calculations may be found in [Deretzis & Magna 2011], [Egami *et al.* 2010] and [Tsukamoto *et al.* 2009].

The main differences between PFMT and NEGF methods arise mainly from the fact that PFMT technique leads to the transparent matrix structures which are numerically solvable in a direct manner, in contrast with the characteristic NEGF calculations which require special numerical optimization methods [Deretzis & Magna 2011]. It should be also noted that, contrary to the Green's function methods, the PFMT equation (3.28) allows us to solve the scattering problem directly for real energies, providing at once not only the overall transmission spectra but also the component spectras for each of the available transmission channels [Szczęśniak *et al.* 2012]. The latter problem can be somehow avoided in the NEGF formalism, but it requires the calculation of the overall transmission first and afterwards, by applying appropriate procedure, decoupling it into component contributions [Krstić *et al.* 2002]. Hence, such procedure is much less intuitive. Moreover, the boundary terms of **M** matrix in equation (3.28), known as a self-energies in the Green's function formalism, are not only real but also energy independent in the PFMT method when the interactions between neighbor atoms in the leads are symmetric [Szczęśniak & Khater 2012]. This leads to the simpler mathematical notation for certain cases when compared to the NEGF.

The agreement between results for electronic transport calculations obtained within PFMT and NEGF formalism is fullfiled. For example our numerical calculations presented in next chapter for monatomic sodium wires agrees qualitatively with the results given by the NEGF first principle computations. It has been also shown that for magnon excitations, the *matching*-based techniques gives the same results as NEGF, when both are applied for exactly the same systems [Zhang *et al.* 2008].

In this manner our PFMT formalism can be considered as a compact and efficient tool for the study of the electronic quantum transport for a wide range of nanomaterial systems. It provides a trade-off in computational efficiency and predictive capability as compared to slower first-principle based methods, and has the potential to treat the conductance properties of complex molecular nanojunctions.

Chapter 4

Quantum electronic transport in mono-valence nanosystems

4.1 Monatomic sodium nanojunctions

The PFMT model calculation is first applied numerically for the monatomic linear sodium wire nanojunctions (MLNaW) between sodium leads as presented in Fig.4.1. Our numerical results are determined for wires of various lengths, in particular they are presented typically here for $D \in [1, 6]$.

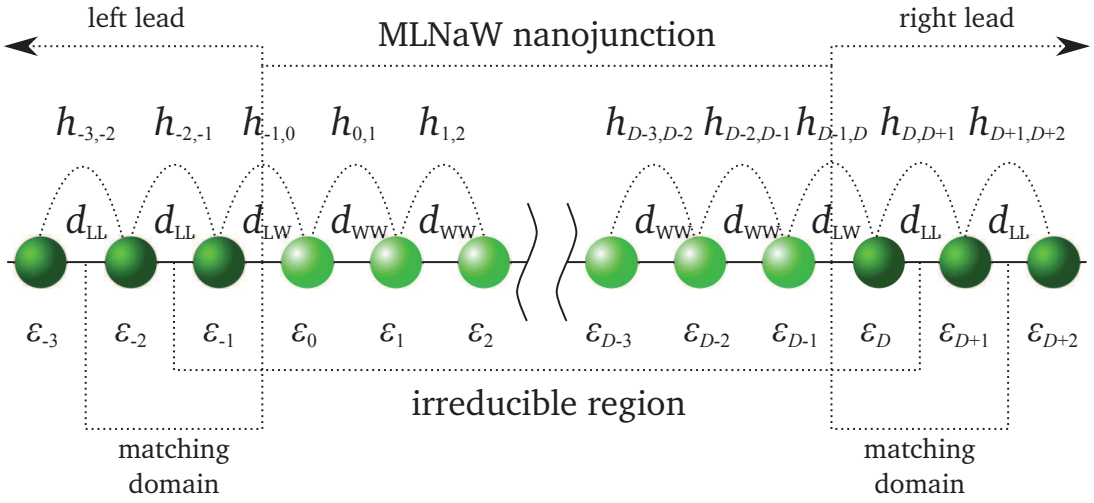

Figure 4.1: Schematic representations of the D-atomic linear nanojunction made of sodium atoms (light green color) between sodium leads (dark green color). The corresponding binding energies ε_n for sites n, and the nearest-neighbor couplings $h_{n,n'}$ between sites n and n' are depicted. Note that in order to keep the figures simple we show the nearest-neighbor coupling terms only for $n < n'$. Additionally, three different interatomic spacings are considered: d_{WW} for the nanojunction wire, d_{LL} in the leads, and d_{WL} at the contact.

These calculations are motivated by the fact that the MLNaW nanojunctions, which have been investigated previously using other theoretical methods [Egami *et al.* 2010], [Li & Kosov 2006], [Khomyakov & Brocks 2006], [Lee *et al.* 2004], are known as good benchmark systems for electronic conductance calculations [Zugarramurdi *et al.* 2011], [Havu *et al.* 2006]. This initial analysis is hence carried out in order to demonstrate the correctness and functionality of the PFMT method by comparing with previous results.

The assumed binding energies of Na atoms are constant and equal -4.96 eV, while the distance dependent coupling terms are modeled using HTBT approach [Harrison 2004]. The interatomic distance on the Na leads $d_{\mathrm{LL}} = 3.64$Å is considered to correspond to the bulk Na nearest-neighbor distance. However, the interatomic distances on the MLNaW nanojunction take on a value of $d_{\mathrm{WW}} = 3.39$Å which is the average interatomic distance for the finite Na wires [Khomyakov & Brocks 2006]. In contrast, the lead-nanojunction spacing is considered for two numerical values, d_{WL} which is equal to 3.99Å and 3.29 Å. These numbers correspond to a choice range of approximately 20% weaker (WC) and stronger (SC) lead-nanojunction couplings, respectively, compared to the intrinsic lead coupling. This is a physically reasonable range to test. Taking into account the above values of the interatomic distances, we note that the D=1 case is equivalent to the situation of the infinite chain with the two bond defects, however this is not true for the remaining wire lengths due to the fact that $d_{\mathrm{LL}} \neq d_{\mathrm{WW}}$.

In Fig.4.2, the overall transmission $T(E)$ and reflection $R(E)$ probabilities are presented as a function of the incident electronic energy E, for various wire lengths N, and for the two different lead-chain coupling values SC and WC defined above. For each sub-figure of Fig.4.2, $T(E)$ and $R(E)$ are calculated independently, and the unitarity requirement for the scattering processes is checked by the sum $T(E) + R(E)$. Note that E_F is set as a zero energy reference in these figures.

The positions of the transmission spectral resonances vary as a function of the lead-nanojunction couplings, as expected and as may be seen from Fig.4.2. Due to the mirror symmetry and assumed local charge neutrality in the considered MLNaW systems, all energy levels, excluding the central peak for odd D, are distributed symmetrically with respect to the referential E_F, for both even and odd D. Analyzing the transmission spectra, the number of the resonances is always equal to the number of the atoms in the considered MLNaW wire up to $D = 3$. This equality is also conserved for $D = 4$ for the strong SC couplings, but reduced to $D - 2$ for the weak WC couplings. The $D - 2$ states are also observed for the five odd- and the six even-numbered wires for both SC and WC cases. The displacement of the resonances to outside the transmission spectra for any D is directly related to the lead-nanojunction couplings for the considered system. This displacement happens when the resonance goes to a localized state

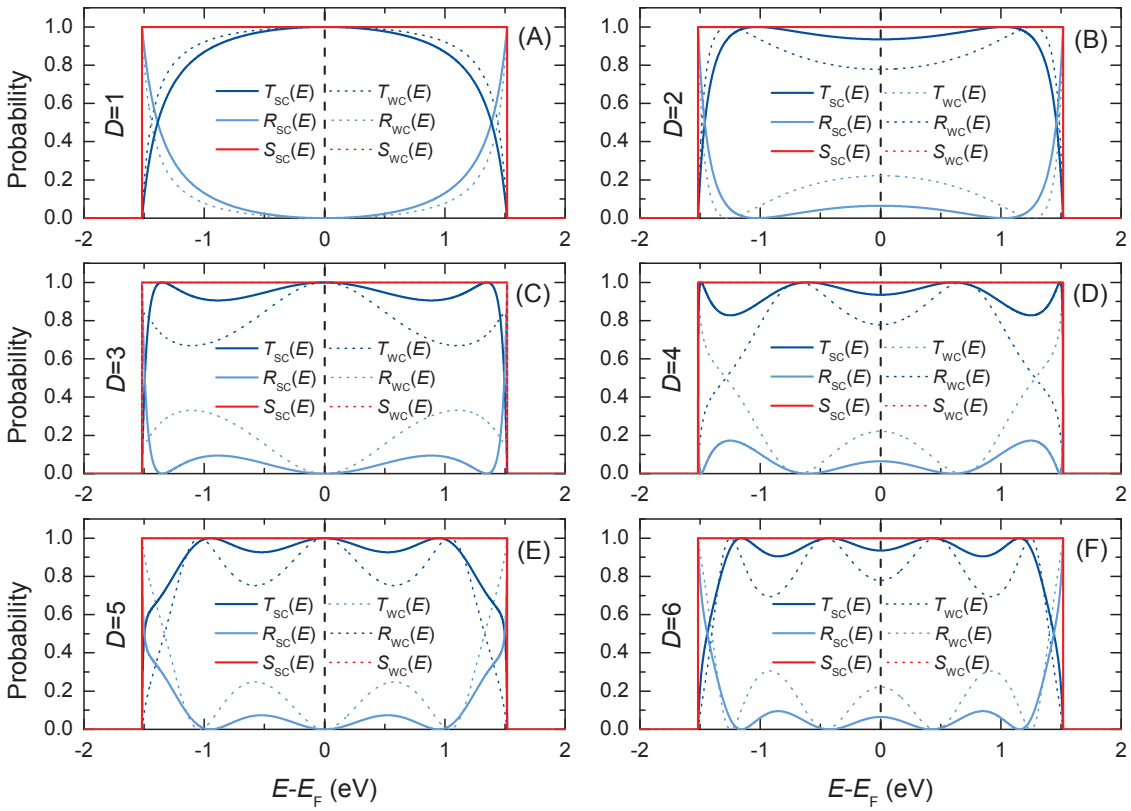

Figure 4.2: The overall transmission $T(E)$ and reflection $R(E)$ probabilities as a function of energy for the MLNaW wire nanojunctions composed of D atoms, with strong (SC) or weak (WC) lead-wire couplings. Subfigures (A), (C) and (E) correspond to the odd-number D, (B), (D) and (F) to the even-number. E_F is set as a zero energy reference, and the unitarity condition is represented by the sum $S(E)$.

outside the leads monovalent s-type conduction band. This effect is equally observed for resonances and localized vibration states on atomic nanojunctions [Khater *et al.* 2011a], [Virlouvet *et al.* 1999], [Fellay *et al.* 1997]. Further, when the MLNaW wire increases in length this displacement is quicker for the WC connected wires than for the SC ones.

As mentioned previously, the only significant contribution to the overall conductance comes from electronic states in the neighborhood of the Fermi level E_F. It is hence noticeable that for the odd-number wires, one of the resonant maxima appears systematically at E_F, which yields as a consequence a conductance maximum for the corresponding systems. In contrast, the even-numbered wires do not present any maxima at E_F, which outcome results in successive minima for the conductance of these systems.

The total conductance $G(N, E_F)$ for the considered MLNaW wires is presented in Fig.4.3, as a function of the wire length D, reflecting the maxima and minima of the transmission spectra at E_F, and exhibiting the usual conductance oscillations, here with a two-atom period. This situation relates directly to the interaction of the free electrons

in the lead band with the electronic states of the nanojunction wire. In particular, since the σ state for a sodium atom can take two electrons by the Pauli principle, one notes that there are half-empty states available for the odd-number wires while non available for the even-number wires. Since the Fermi energy E_F is equal to the binding energy of the Na atoms, the odd-number wires present a greater local density of states LDOS accessible at the Fermi level, compared to that for the even-number wires. This ensures that the hopping mobility is unimpeded for the odd-number wires, whereas this is not the case for the even-number wires. The corresponding electronic transport is consequently a maximum at $\sim G_0$ for the odd-number MLNaW wire nanojunctions, for both the weak WC and the strong SC couplings. The electronic conductance decreases for the even-number wires, and this decrease varies with the lead-nanojunction couplings, it is $\sim 0.065G_0$ for SC and $\sim 0.221G_0$ for WC, respectively. Furthermore, one observes that the conductance of the even-number MLNaW wire nanojunctions increases slightly but monotonically with the increase of the wire length. This situation may be explained qualitatively by arguing that the electric leads have a bigger influence on the LDOS at the Fermi level for the short wires than for the longer ones. An interesting discussion on the problem of how the different types of leads may influence the overall electronic conductance can be found in [Khomyakov & Brocks 2006].

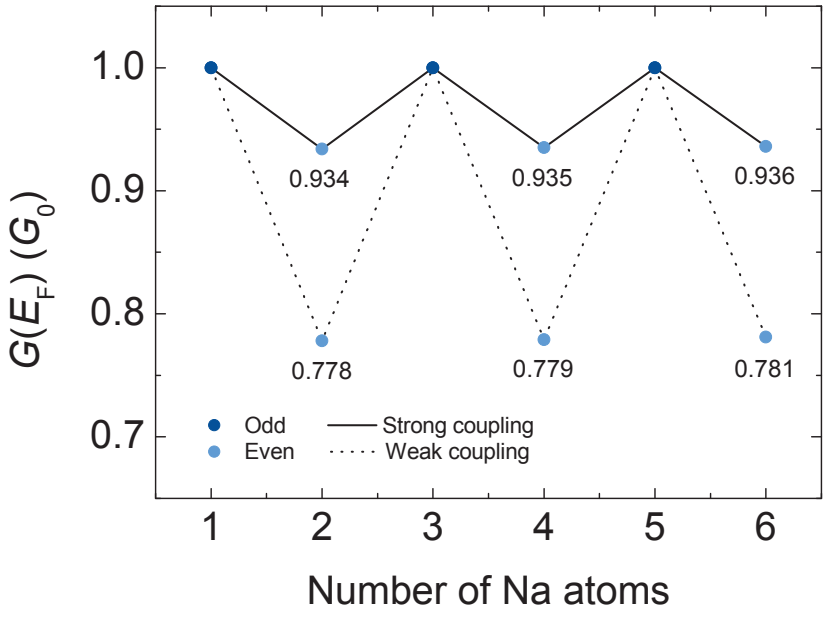

Figure 4.3: The total electronic conductance $G(N, E_F)$ at the Fermi level as a function of the number of atoms on the MLNaW wire nanojunction, in units of G_0.

In summary, the electronic conductance determined in this subsection presents hitherto unknown detailed transmission spectra, and confirms the well known even-odd conductance oscillation effect [Yamaguchi *et al.* 1997], which is previously reported for the

MLNaW nanojunctions [Lang 1997], as well as for other wire systems [Lee *et al.* 2004], [Thygesen & Jacobsen 2003], [Lang & Avouris 1998]. We also note that our results are in agreement with those obtained on the basis of the first-principle calculations in other model calculations [Lee *et al.* 2004], [Egami *et al.* 2010], [Egami *et al.* 2005]. This clearly confirms the validity of the PFMT approach. The minor quantitative differences between our results for the conductance and those previously reported, for the same D-number MLNaW wire systems, appear mainly due to the assumed structures of the electric leads.

4.2 Diatomic copper-cobalt nanojunctions

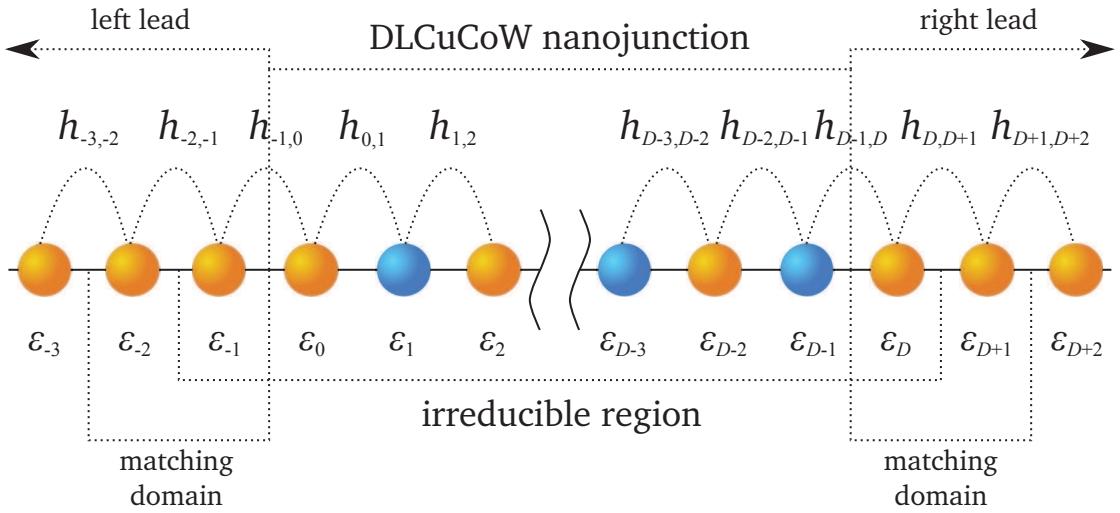

Figure 4.4: Schematic representations of the D-atomic linear nanojunction made of pairs of copper (orange color) and cobalt (blue color) atoms between copper leads. The corresponding binding energies ε_n for sites n, and the nearest-neighbor couplings $h_{n,n'}$ between sites n and n' are depicted. Note that in order to keep the figures simple we show the nearest-neighbor coupling terms only for $n < n'$.

The second considered system in this work concerns the supported diatomic linear copper cobalt wire nanojunctions (DLCuCoW) as presented in figure 4.4. Finite - Cu - Co - wire systems have been experimentally prepared previously as grouped adatoms on the flat Cu(111) surface by Lagoute *et al.* [Lagoute *et al.* 2007], with the use of the low-temperature scanning tunneling microscope technique. Initially, these systems have been developed as magnetic/nonmagnetic finite atomic wires for the investigation of their potential magnetic properties. Subjects concerning their spin dynamics [Saubanère *et al.* 2010], their storage potential [Brovko *et al.* 2011], and the observation of the Kondo effect in their structure [Néel *et al.* 2011], have been indeed addressed recently. However, their electronic transport properties have not been considered previously,

despite their intrinsic interest under a DLCuCoW configuration, and their mechanical and thermodynamical stability at low temperatures. Note in this respect the increasing interest in the stability of such supported wire systems [Oncel 2008] for arbitrary ranges of temperature.

In principle, the electron dynamics of the supported DLCuCoW nanojunctions can be discussed within the *s*-like single band effective tight-binding model proposed in [Lagoute *et al.* 2007]. This possibility arises from the existence of unoccupied confined quantum states formed along the Cu-Co wire nanojunctions by linking the orbitals of sp_z character. Such confined states have been observed in other supported wire systems like the monatomic Cu [Fölsch *et al.* 2004] and Au [Nilius *et al.* 2002], the diatomic Au-Pd nanojunction systems [Wallis *et al.* 2005], and Fe nano-islands [Delga *et al.* 2011].

In this context the possibility of using semiconductor surfaces which present a band gap is equally interesting as a support for the atomic wires. These surfaces may electronically decouple from the supported wire orbitals in certain cases, allowing one to study the electronics of stable one-dimensional wire systems [Oncel 2008].

From our point of view the diatomic nanojunction wires may be used to control the value of the overall electronic conductance in low-dimensional nanoelectronic circuits. In particular, the foreign cobalt atoms injected directly into the monatomic copper wire, act as controllable chemical defects which modify the initial system and its electronic properties as a consequence. Furthermore, the substrate supported configurations of the lead - DLCuCoW wire nanojunctions - lead, suggest a greater mechanical and thermodynamic stability than for the freely suspended wires, which is one of the most important features required for future nanoelectronic devices.

Our model calculations for the electronic quantum conductance of the DLCuCoW systems are presented for wires composed of different numbers of periodically arranged Cu-Co atomic pairs, as in Figure 4.4. The length of the DLCuCoW wire may characterized by the number D_{CuCo} of such pairs, and the results in this subsection are hence presented in terms of this latter variable for a given DLCuCoW nanojunction.

In the case of the DLCuCoW nanojunctions, we assume the Hamiltonian elements of Eq.(**??**) to have the values proposed in [Lagoute *et al.* 2007]. Following these studies, the binding energy 3.31 eV is considered to be the same for all the copper atoms, whereas for cobalt it is 2.96 eV. The coupling terms between copper nearest-neighbors on the leads, and between copper and cobalt nearest-neighbors on the wire nanojunction, are close to each other with values of -0.95 eV and -0.94 eV, respectively.

It is important to note that the $D_{\mathrm{CuCo}} = 1$ nanojunction wire is a very particular case since it has quite a different symmetry from all other lengths and is open to different structural definitions; we have calculated the total conductance for this particular case

to be $0.9658G_0$, but will not use it in our discussion of the properties of the conductance $G(D_{\mathrm{CuCo}}, E_F)$ for a general wire length.

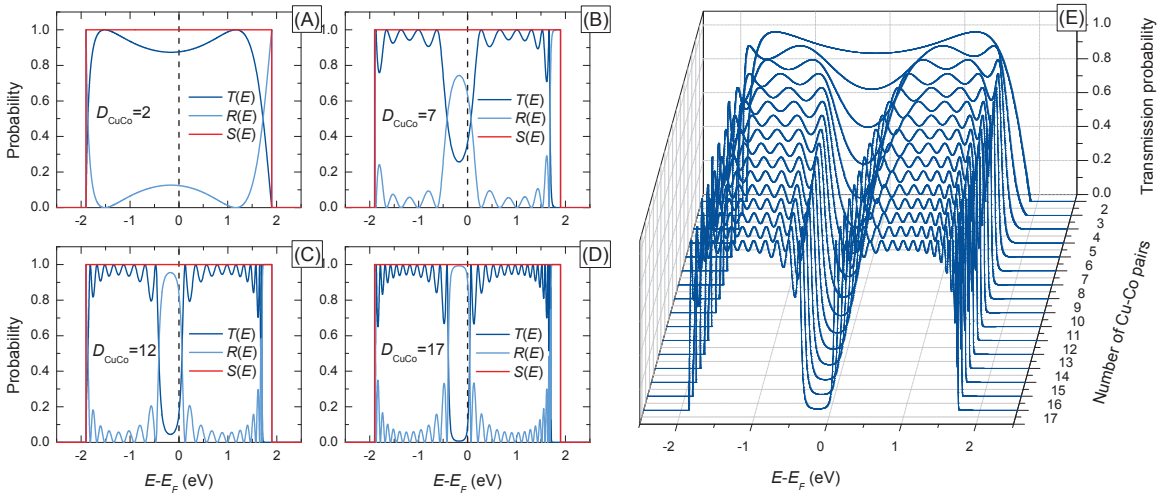

Figure 4.5: (A) - (D): The selected spectra of the transmission $T(E)$ and reflection $R(E)$ probabilities for respectively 2, 7, 12 and 17 copper-cobalt atomic pairs in the DLCuCoW scattering region. The unitarity condition is represented by the sum $S(E)$. (E): Surface plot of the transmission probabilities as a function of energy and number of the Cu-Co atomic pairs in the DLCuCoW scattering region. For all subfigures the E_F is set at zero of energy.

In Figure 4.5 (A)-(D) we present the detailed transmission $T(E)$ and reflection $R(E)$ spectra of the DLCuCoW nanojunction, for the selected values of $D_{\mathrm{CuCo}} = 2$, 7, 12, and 17. The resonance maxima and minima can be observed as for the MLNaW wires, where E_F is again set as a zero energy reference. However, the transmission and reflection spectra are not symmetric with respect to this reference, due the slight difference between the cobalt and copper binding energies. The most important conclusion concerns the value of the transmission probabilities close to E_F. The transmission spectra in Fig.4.5 (A)-(D) show strong resonant minima for both the even- and the odd-number wires. In particular, we observe that the value of the transmission at the Fermi level decreases when the length of the effective nanojunction increases. This trend is summarized in Fig.4.5 (E) for the ensemble of the transmission spectra for D_{CuCo} values ranging from 2 to 17. At the upper limit the conductance goes to $G(D_{\mathrm{CuCo}} = 17, E_F) \sim 10^{-1}G_0$ which is sufficient for the purpose of the present calculation.

The overall electronic conductance $G(D_{\mathrm{CuCo}}, E_F)$ as a function of the DLCuCoW wire length in terms of Cu-Co atomic pairs, is presented in Figure 4.6, along with a fitting

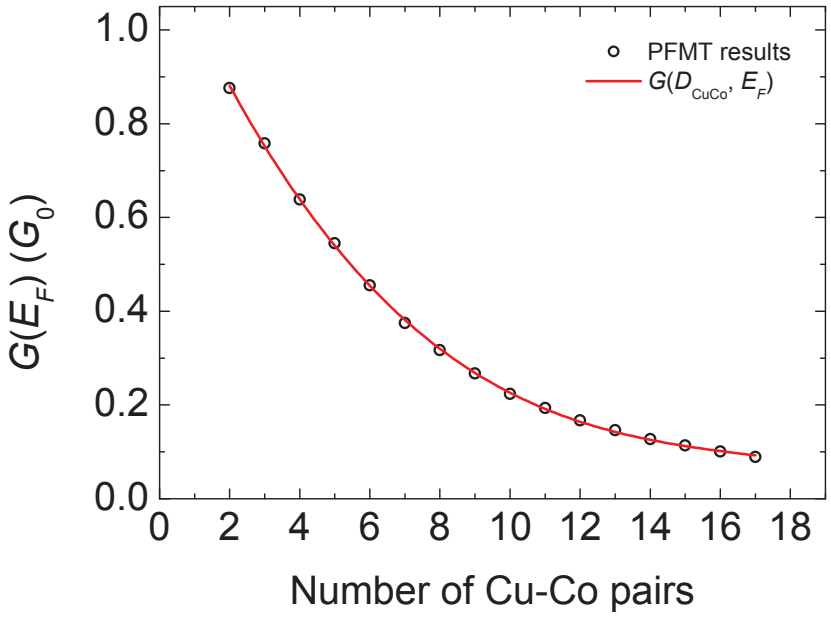

Figure 4.6: The total electronic conductance $G(D_{\mathrm{CuCo}}, E_F)$ in units of G_0, read at the Fermi level E_F as a function of the number of Cu-Co pairs on the DLCuCoW nanojunction wire. The PFMT results are represented by open circles, and the fitting function by the red curve.

exponential function

$$G(D_{\mathrm{CuCo}}, E_F) = G(2, E_F)\exp[-\alpha(D_{\mathrm{CuCo}} - 2)]$$
$$\text{for } D_{\mathrm{CuCo}} \geq 2. \tag{4.1}$$

Figure 4.4 resumes the transmission spectra at the Fermi energy, it shows the strong monotonic decay of the electronic conductance with the increase of the number of Cu-Co pairs of the nanojunction.

In the corresponding equation (4.1), $G(2, E_F) = 0.8760G_0$ is the conductance of a wire made up of two Cu-Co pairs, and $\alpha = 0.1630$ denotes the decay constant. equation (4.1) allows one hence to read the numerical values of the conductance $G(D_{\mathrm{CuCo}}, E_F)$ of the DLCuCoW wires for $D_{\mathrm{CuCo}} \geq 2$ using a simple formula which is useful in the analysis of potential applications of corresponding nanocircuits. This behavior is fundamentally different from the typical conductance oscillations observed for odd- and even-number monoatomic wires.

To understand the decrease of the conductance in Figure 4.6, one has to take a closer look at the band structure of the infinite -Cu-Co- diatomic chain which is the infinite limit of the DLCuCoW nanojunction. We have calculated the band structure for such an infinite diatomic wire as in Figure 4.7. This presents a band gap of Δ=0.35 eV and renders the system theoretically insulating. This band gap, which corresponds

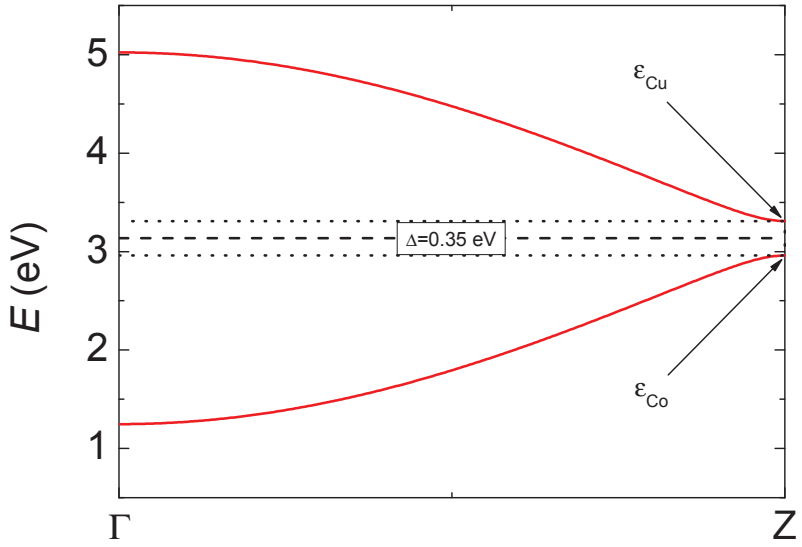

Figure 4.7: Band structure of the infinite variant of the DLCuCoW wire nanojunction over the first Brillouin zone. The band gap (Δ=0.35 eV) is marked by two dotted lines, between the copper (ε_{Cu}) and the cobalt (ε_{Co}) binding energies. The Fermi energy for the half-filled bands is represented by the dashed line.

directly to the difference of the binding energies for cobalt and copper atoms, presents a differential $\sim 10^{-1}$ with respect to the Cu binding energy. It is an effective potential barrier for electrons between successive Cu and Co sites, and results in a small but cumulative decrease of the conductance as the DLCuCoW wire nanojunction increases in length, when comparing to the theoretical maximum of G_0 for the pure atomic Cu wire. This direct interpretation is confirmed by the exponential form of equation (4.1), where $\exp[-\alpha(D_{CuCo}-2)] = \exp(-\alpha)^{D_{CuCo}-2}$, expressing the monotonic decay of the electronic conductance with the increasing length of the DLCuCoW nanojunction.

Chapter 5

Quantum electronic transport in multi-valence nanosystems

5.1 Diatomic silicon-carbide nanojunctions

Carbon exists in nature under a wide range of allotropic forms, as the two-dimensional graphene [Geim & Novoselov 2007], the cage fullerenes [Kroto *et al.* 1985], and the quasi-one-dimensional carbon nanotubes [Iijima & Ichihashi 1993]. These forms exhibit exceptional physical properties and can be considered as promising components for future nanodevices [Euen 1998]. The discovery of monatomic linear carbon wires (MLCW), [Jin *et al.* 2009], [Yuzvinsky *et al.* 2006], [Zhao *et al.* 2003], [Troiani *et al.* 2003], [Derycke *et al.* 1998], [Lagow *et al.* 1995], [Heath *et al.* 1987], turns the attention to another intriguing carbon allotropic form. In the experiment conducted recently by Jin *et al.* [Jin *et al.* 2009] the MLCW was produced by directly removing carbon atoms row by row from the graphene sheets, leading to a relatively stable freestanding nanostructure. The monatomic *linear* carbon wire (MLCW) systems are expected in the context of the development of nanoelectronic devices [Agraït *et al.* 2003] to have potentially interesting technological applications, in particular as connecting junction elements between the larger device components [Nitzan & Ratner 2003]. In this respect the electronic quantum transport properties are the key features of such wire nanojunctions [Wan *et al.* 1997].

At present the available experimental data do not provide essential knowledge about the electronic properties of the MLCW systems, and only theoretical studies shed some light on these properties. Furthermore, although the MLCW systems were investigated for a long time from the theoretical point of view [Fuentealba 1998], [Jones & Seifert 1997], [Lou & Nordlander 1996], [Xu *et al.* 1992], [Springborg *et al.* 1990], [Rice *et al.* 1986], [Springborg 1986], [Teramae *et al.* 1983], [Karpfen 1979], [Kértesz *et al.* 1979], [Kértesz *et al.* 1978], their interest was not highlighted until recently due to the open

attention paid to other carbon allotropic forms. It has been shown in particular that from the structural point of view the MLCW can form either as cumulene wires (interatomic double bonds) or polyyne wires (alternating interatomic single and triple bonds) [Cahangirov *et al.* 2010], [Jin *et al.* 2009], [Abdurahman *et al.* 2002], [Springborg 1986], [Karpfen 1979]. However, there is no straightforward answer which of these two structures is the favorable one; experimental studies do not give a satisfactory answer, and the theoretical calculations yield provisions which depend on the applied computational methods. The density functional theory (DFT) calculations predict double bond structures [Tongay *et al.* 2004], [Bylaska *et al.* 1998], whereas the *ab-initio* Hartree-Fock (HF) results favor the alternating bond systems [Kértesz *et al.* 1978], [Kértesz *et al.* 1979], [Karpfen 1979], [Teramae *et al.* 1983], [Abdurahman *et al.* 2002]. This situation arises from the fact that the DFT tends to underestimate bond alternation (second order Jahn-Teller effect), while the HF overestimates it [Abdurahman *et al.* 2002].

More recently, first-principle calculations have indicated [Zhang *et al.* 2011b], that both structures are stable and present mechanical characteristics of one-dimensional nanomaterial. Moreover, on the basis of the first-principle calculations, [Zhang *et al.* 2011a], [Zhang *et al.* 2011b], [Song *et al.* 2010], [Chen *et al.* 2009], [Wang *et al.* 2009], [Crljen & Baranović 2007], [Okano & Tománek 2007], [Tongay *et al.* 2005], [Senger *et al.* 2005], [Larade *et al.* 2001], [Lang & Avouris 2000], [Lang & Avouris 1998], the cumulene MLCW wires are expected to be almost perfect conductors, even better than linear gold wires [Tongay *et al.* 2004], while the corresponding polyyne wires are semiconducting [Song *et al.* 2010]. It is also worth noting that the MLCW cumulene system may exhibit conductance oscillations with the even and odd numbers of the wire atoms [Cahangirov *et al.* 2010], [Zhang *et al.* 2011a].

In the present sub-section we consider in particular the problem of the electronic quantum transport across molecular nanojunctions made up of silicon-doped carbon wires, prepared in ordered or substitutionally disordered configurations as in the schematic representation of Figure 5.1, where the nanojunctions are between pure MLCW wire leads. This problem has not been considered previously and is still unsolved to our knowledge. The interest in the quantum transport of such nanojunctions arises from the fact that the chemical defects or substitutional disorder may have a significant impact on their transport properties [Ke *et al.* 2008]. Chemical impurities doping the nanojunction may even allow the control of the transport for such nanostructures [Nozaki *et al.* 2010]. The properties of the nanoelectronic device and its functionality may hence be greatly affected or even built on such ordered and disordered configurations. The interest in silicon carbide, furthermore, stems from the fact that it is considered a good substrate material for the growth of graphene [Strupiński *et al.* 2011], and may produce interesting effects

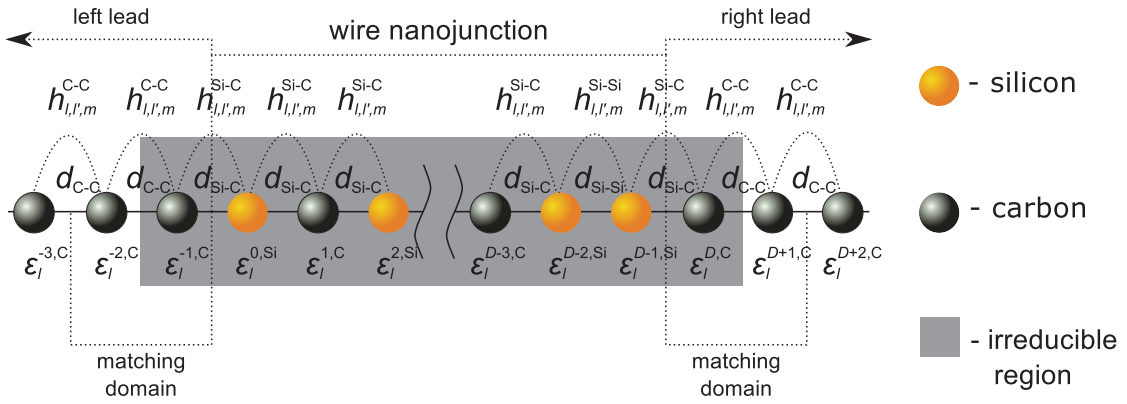

Figure 5.1: Schematic representation of the finite silicon-doped carbon wire nanojunction between two semi-infinite quasi one-dimensional carbon leads. The irreducible region and matching domains are distinguished (please see section 3.2 for more details). The binding energies for a given atomic site and the coupling terms between neighbor atoms with corresponding interatomic distances are depicted. The n and n' indices for the coupling parameters are dropped for simplicity.

in its interactions with Si or C [Wang *et al.* 2012].

5.1.1 The tight-binding model and basic electronic properties

In subsection 5.1.1 we present the results of our model calculations for the electronic structure of the carbon, silicon and silicon carbide wires under study. Our results are validated by comparison with the DFT calculations [Tongay *et al.* 2004], [Bekaroglu *et al.* 2010], which allows us to establish unambiguously our choice of the tight-binding parameters for these systems.

In principle, we can develop our model calculations for the nanojunctions and their leads using any adequate type of orbitals; even a single orbital suffices to calculate the electronic quantum transport for carbon nanojunctions, Nozaki *et al.* [Nozaki *et al.* 2010]. However, this approximation is inadequate for the silicon atoms. To treat both types of atoms on the same footing, we characterize hence the atoms by the electronic states $2s$ and $2p$ for carbon, and by the $3s$ and $3p$ for silicon. Such a scheme gives us four different orbitals, namely s, p_x, p_y and p_z, for both types of atoms.

In the present work our TB parameters are effectively rescaled from the Harrison's data in order to match our model calculations for the electronic structure with those given by the DFT. The utilized TB parameters are presented in Table 5.1, in comparison with the values given by Harrison. Note that the values of the on-site Hamiltonian matrix

Table 5.1: The values of the tight-binding parameters, $\varepsilon_l^{n,\alpha}$ and $h_{l,l',m}^{n,n',\beta}$ (in eV), and Harrison's dimensionless coefficients, $\eta_{l,l',m}$, as proposed in this work, and compared with the original values by Harrison [Harrison 2004]. Please note that the distance dependent $h_{l,l',\sigma}^{n,n',\beta}$ parameters are computed for the appropriate interatomic spacings d_β (in Å), tabulated below and assumed after [Tongay *et al.* 2004] and [Bekaroglu *et al.* 2010]. In order to keep table transparent indices n and n' for $\varepsilon_l^{n,\alpha}$ and $h_{l,l',m}^{n,n',\beta}$ are ommited.

	Harrison TB parameters			Present TB parameters		
α		C	Si		C	Si
ε_s		-19.38	-14.79		-18.89	-13.5
ε_p		-11.07	-7.59		-10.94	-8.38
β	C-C	Si-Si	Si-C	C-C	Si-Si	Si-C
$\eta_{s,s,\sigma}$	-1.32	-1.32	-1.32	-0.93	-1.48	-1.11
$\eta_{s,p,\sigma}$	1.42	1.42	1.42	0.94	1.19	0.95
$\eta_{p,p,\sigma}$	2.22	2.22	2.22	1.03	1.18	0.99
$\eta_{p,p,\pi}$	-0.63	-0.63	-0.63	-0.59	-0.41	-0.62
β	C-C	Si-Si	Si-C	C-C	Si-Si	Si-C
$h_{s,s,\sigma}$	-5.95	-2.08	-3.70	-4.19	-2.33	-3.11
$h_{s,p,\sigma}$	6.40	2.24	3.98	4.23	1.87	2.66
$h_{p,p,\sigma}$	10.01	3.50	6.22	4.64	1.86	2.77
$h_{p,p,\pi}$	-2.84	-0.99	-1.77	-2.66	-0.65	-1.74
β	C-C		Si-Si		Si-C	
d_β	1.3		2.2		1.649	

elements $\varepsilon_p^{n,\alpha}$ are identical for states p_x, p_y and p_z. The off-diagonal distance dependent $h_{l,l',m}^{n,n',\beta}$ elements are calculated on the basis of the HTBT approach. For symmetry considerations, these latter are positive or negative, also $h_{s,p,\sigma} = \eta_{s,p,\sigma} = 0$ and $h_{p,p,\sigma} = \eta_{p,p,\sigma} = 0$, for p_y and p_z, and $h_{p,p,\pi} = h_{p_y,p_y,\pi} = h_{p_z,p_z,\pi} = h_{p_x,p_x,\pi} = 0$ [Kaxiras 2003]. Table 5.1 is supplemented for the reader by Figures 2 which give the dependence of the hopping integrals with distance as calculated in the present paper (continuous curves), in comparison with the Harrison's data (open symbols).

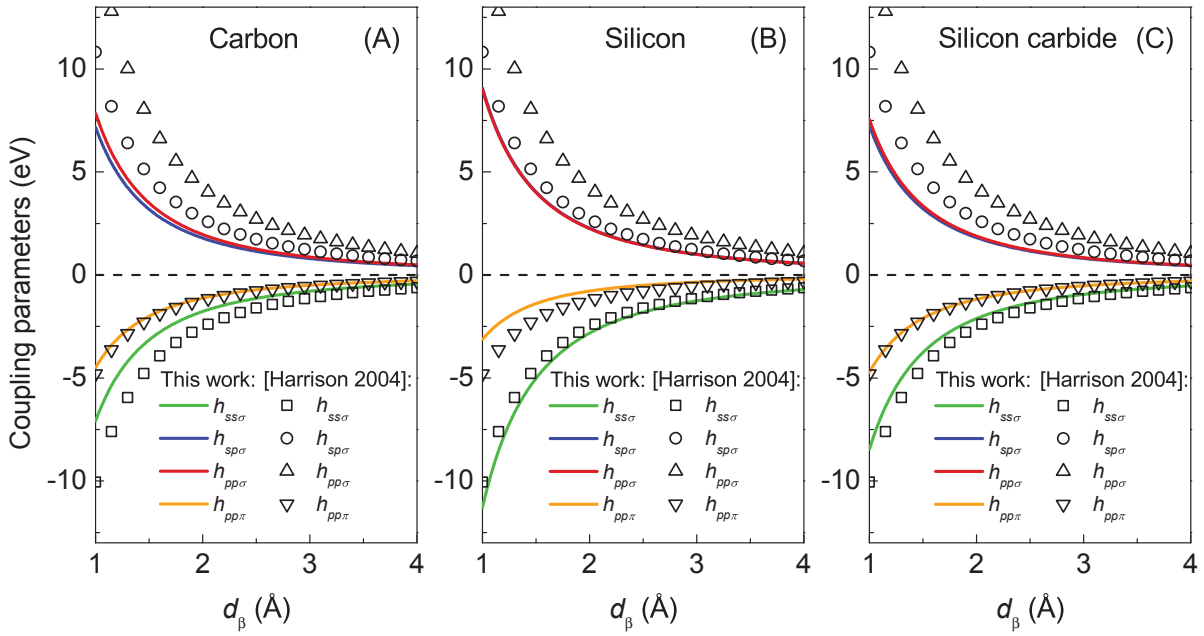

Figure 5.2: The nearest-neighbor tight-binding coupling parameters with the interatomic distance. The curves represent our calculated TB results in comparison with those calculated using the Harrison parameters (squares, triangles, circles).

Figure 5.2 clearly indicates the fact that qualitatively both Harrison's and our rescaled coupling parameters for silicon, carbon and diatomic silicon carbide wires, present the same functional behavior, confirming the desired conservation of their physical character. However, most of the rescaled coupling parameters have somehow smaller values then those initially proposed by Harrison; this trend can be also traced in Table 5.1 for the on-site parameters. This difference stems from the influence of the low-coordinated systems considered here, whereas the initial Harrison values are given to match tetrahedral phases [Harrison 2004]. Another general observation can be made for the tight-binding parameters of the σ-type interactions (the $h_{s,p,\sigma}$ and $h_{p,p,\sigma}$ ones), which present much closer values over the considered interatomic distance range then in the case of the Harrison data.

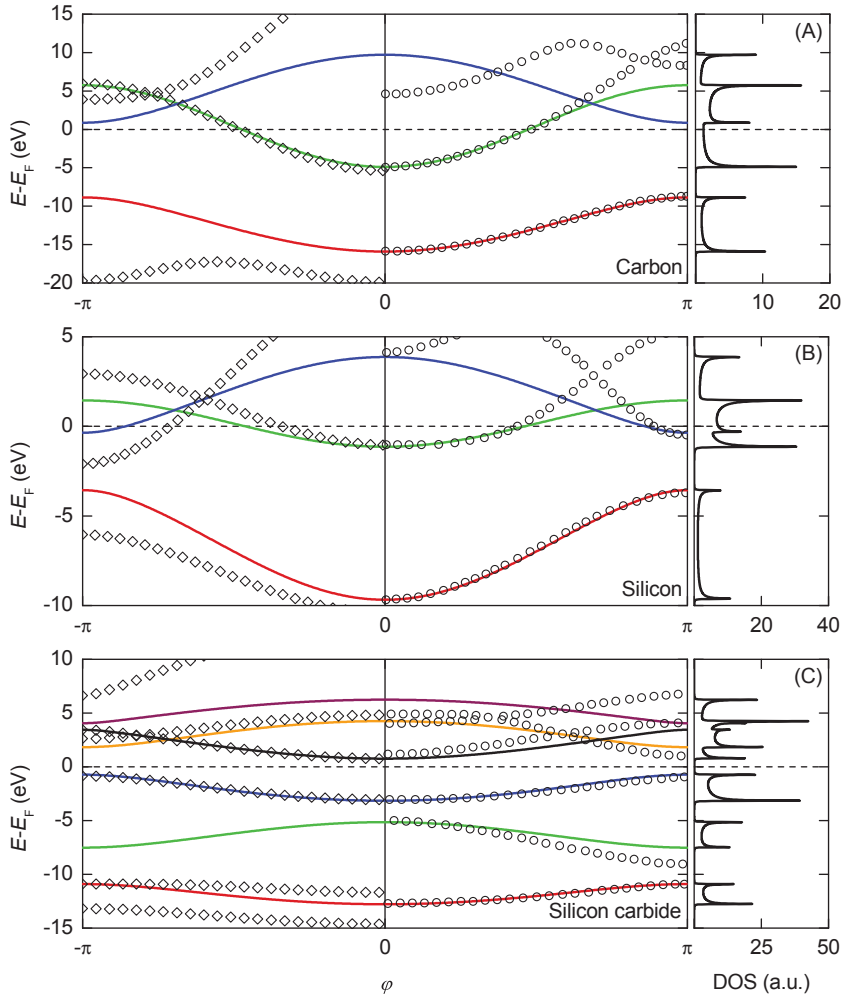

Figure 5.3: Electronic structures of carbon (A), silicon (B) and diatomic silicon carbide (C) for infinite linear atomic wires, are presented over the first Brillouin zone $\varphi = kd \in [-\pi, \pi]$. Our calculated results (*continuous curves*), represented by a color scheme (details in the text), are compared on the right hand side with the first-principle results (closed circles, $\varphi \in [0, \pi]$) [Tongay *et al.* 2004], [Bekaroglu *et al.* 2010], and on the left hand side with results calculated using Harrison TB parameters, [Harrison 2004] (diamonds, $\varphi \in [-\pi, 0]$). Our calculated Fermi levels are given as the zero reference energies, and the calculated electronic DOS in arbitrary units are presented in the right hand column.

Our calculated electronic band structures for silicon, carbon and diatomic silicon carbide infinite wires (continuous curves) are presented in Figures 5.3, in comparison with the DFT results, [Tongay *et al.* 2004], [Bekaroglu *et al.* 2010], as in the *right hand* side of the figures. We note for the carbon and silicon structures that our TB parameters correctly reproduce the DFT results up to energies slightly above the Fermi level. Electronic branches in the regions of high-energies are in qualitative agreement. In the case of the diatomic silicon carbide structure some of the electronic states perfectly match the DFT results even for the high-energy domains. The *left hand* side of Figures 5.3 compare our

results (continuous curves) with those from the older TB values given by Harrison (open symbols); as is seen our TB parameters constitute the most optimal set for the electronic transport calculations, since their corresponding electronic band structures conform to the appropriate energy ranges highlighted by the DFT results, and what is even more important, correctly reproduce the Fermi level.

In Figures 5.3 (A) and (B) for silicon and carbon, the red and blue colors correspond respectively to the σ and σ^* bands. These arise from the sp_x orbital hybrids, where the lowest lying bands are always occupied by two electrons. Bands marked by the red color have the π character and are degenerate. Their origin in the p_y and p_z orbitals allows them to hold up to four electrons. In Figure 5.3 (C) for the diatomic silicon carbide, starting from the band structure minimum, consecutive bands have their origin in the following orbitals: carbon $3s$ (red band), silicon $3s$ (green band), carbon $3p$ (blue and black bands), and silicon $3p$ (orange and violet bands). The blue and orange colors for the silicon carbide electronic structure indicate two doubly degenerate π-type bands.

The metallic or insulating character of the considered atomic wires, following the Fermi level, is appropriate only when the wires are infinite. It is well known that this character can change for the case of finite size wires with a limited number of atoms, or due to the type and quality of the leads.

5.1.2 Numerical characteristics for the carbon leads

In general, the infinite carbon wires which are considered as the leads in our work, present electronic band structure characteristics which incorporate not only propagating, see Figure 5.3 (A), but also evanescent states. Both of these types of states, which are derivable from the generalized eigenvalue problem as presented in equation (3.22), constitute a complete set over the allowed energies for the electrons incident along the leads, which can be further scattered at the considered nanojunction. This complete set of eigenstates is used as the basis for the numerical calculations of the quantum conductance presented in subsection 5.1.3.

Figure 5.4 (A) presents the three-dimensional representation of the solutions of equation (3.22) as a set of generalized functionals $z(E)$ for the σ, σ^* and π electronic states of the carbon leads. As described by Eqs.5, 8 and 9, the eigenstates in Figure 5.4 (A) characterized by $|z| = 1$, correspond to the propagating electronic waves described by the real wave vectors, whereas those by $|z| < 1$ to the evanescent and divergent eigenstates for the complex wave vectors. Furthermore, for convenience the corresponding moduli of the complex z factors are presented in Figure 5.4 (B). Note that the $|z| = 1$ solutions may be grouped into pairs for the two directions of propagation linked by the time-reversal symmetry. Due to the fact that each of these two solutions provides the

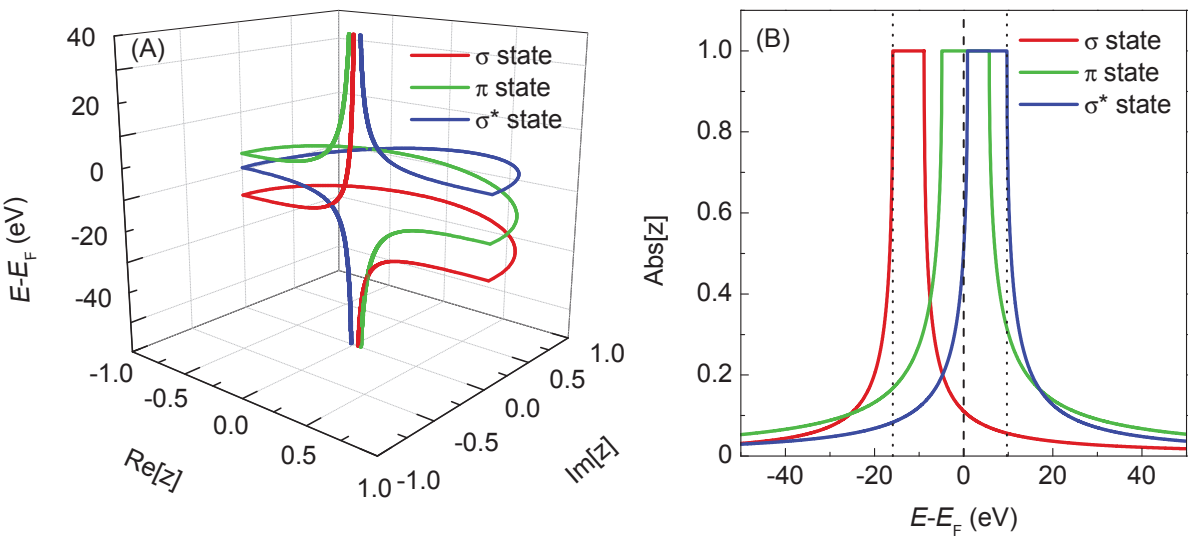

Figure 5.4: Three-dimensional representation of the functionals $z(E)$ on a complex plane in (A), and the evolution of their absolute values as a function of energy in (B), for carbon leads. The color scheme here is the same as that for carbon in figure 3 (A).

same information, we consider waves propagating only from left to right. However, this is not true for the $|z| < 1$ solutions which are always considered for both left and right as spatially evanescent. As can be seen in Figures 5.4, the generalized results for σ, σ^* and π states are represented by the same colors as the corresponding states in Figure 5.3 (A), following their propagating character for $|z| = 1$, and further extended to the physically $|z| < 1$ evanescent solutions.

Figures 5.4 provide then a more complete description for the electronic states of a given system compared to a typical band structure representation as in Figure 5.3, since both the propagating and evanescent states are shown. Such a general representation clearly indicates the importance of the evanescent eigenstates for a full description of the scattering problem presented in subsection 5.1.3. The energies considered in our calculations correspond to the range within the band structure boundaries, marked by two vertical dotted lines in Figure 5.4 (B). As a consequence not only the propagating states but also evanescent solutions are included in the quantum conductance calculations in subsection 5.1.3.

5.1.3 Transport properties

In this subsection the electronic transport properties of nanojunction systems composed of silicon-doped carbon wires between carbon leads, are calculated using the PFMT method. Figure 5.5 (A) presents a number of these systems, where we indicate the irreducible

domains by the shaded grey areas. Note that these systems are always composed of finite nanojunction regions of silicon and carbon atoms, coupled to two carbon semi-infinite leads. The first three systems of Figures 5.5, correspond to periodic diatomic silicon carbide nanojunctions composed of respectively 1, 2, and 3 Si-C atomic pairs. The next system corresponds to a nanojunction with a substitutional disorder, composed of 3 carbon and 3 silicon atoms. The last is a symmetric nanojunction of 5 silicon atoms and only one carbon atom in the middle. Figure 5.5 (B) presents the group velocities of electrons in the carbon leads.

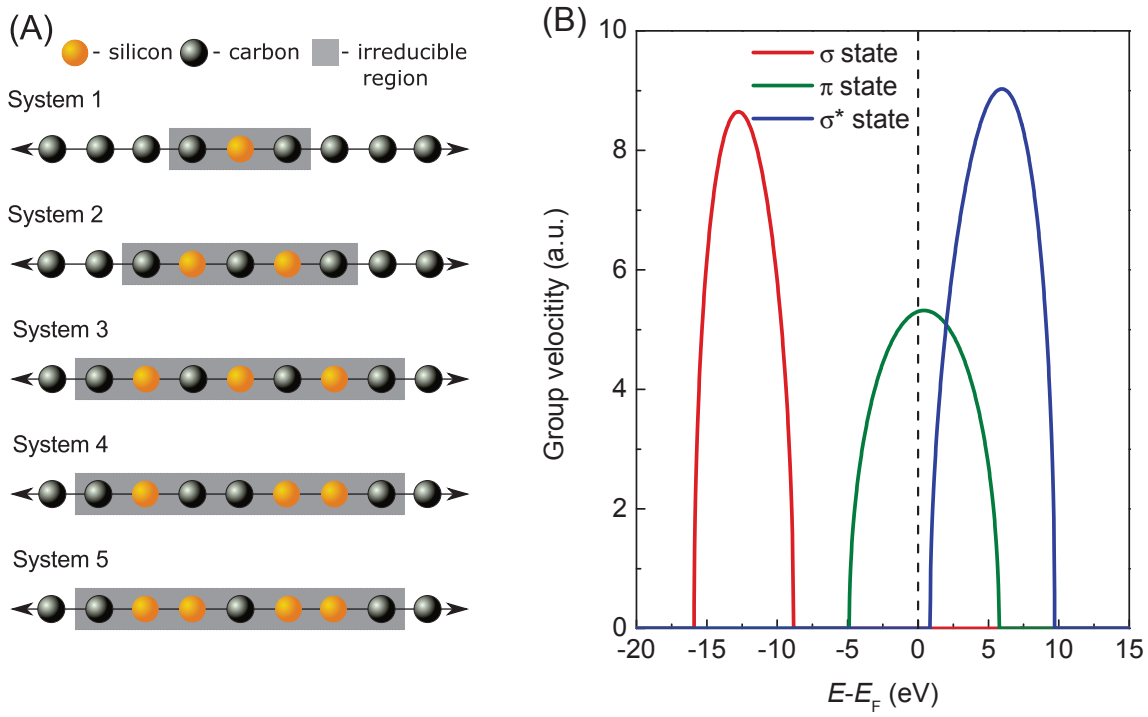

Figure 5.5: (A) Schematic representation of the five nanojunction systems, composed of silicon and carbon atoms between one-dimensional carbon leads, considered in the present work. The irreducible domains are marked by the shaded grey areas, whereas for the other cases only the irreducible domains are shown. (B) The group velocities for the propagating band structure modes on the carbon leads.

The calculated transmission and reflection scattering cross sections for each of the four available transport channels are presented in Figures 5.6. Each row of the figures corresponds to a nanojunction system as follows: (A)-(C) for 1,(D)-(F) for 2, (G)-(I) for 3, (J)-(L) for 4, (M)-(O) for 5. The red and green continuous curves represent the transmission and reflection spectra, respectively. The blue histograms correspond to the free electronic transport on the carbon leads, *i.e.* to the electronic transport on the prefect infinite quasi one-dimensional carbon wire over the different propagating states. These histograms constitute the reference to the unitarity condition which is used systematically

as a check on the numerical results. The leads Fermi level is marked by a dashed line and set as a zero energy reference. Under the zero bias limit, the total conductance is calculated at this Fermi level.

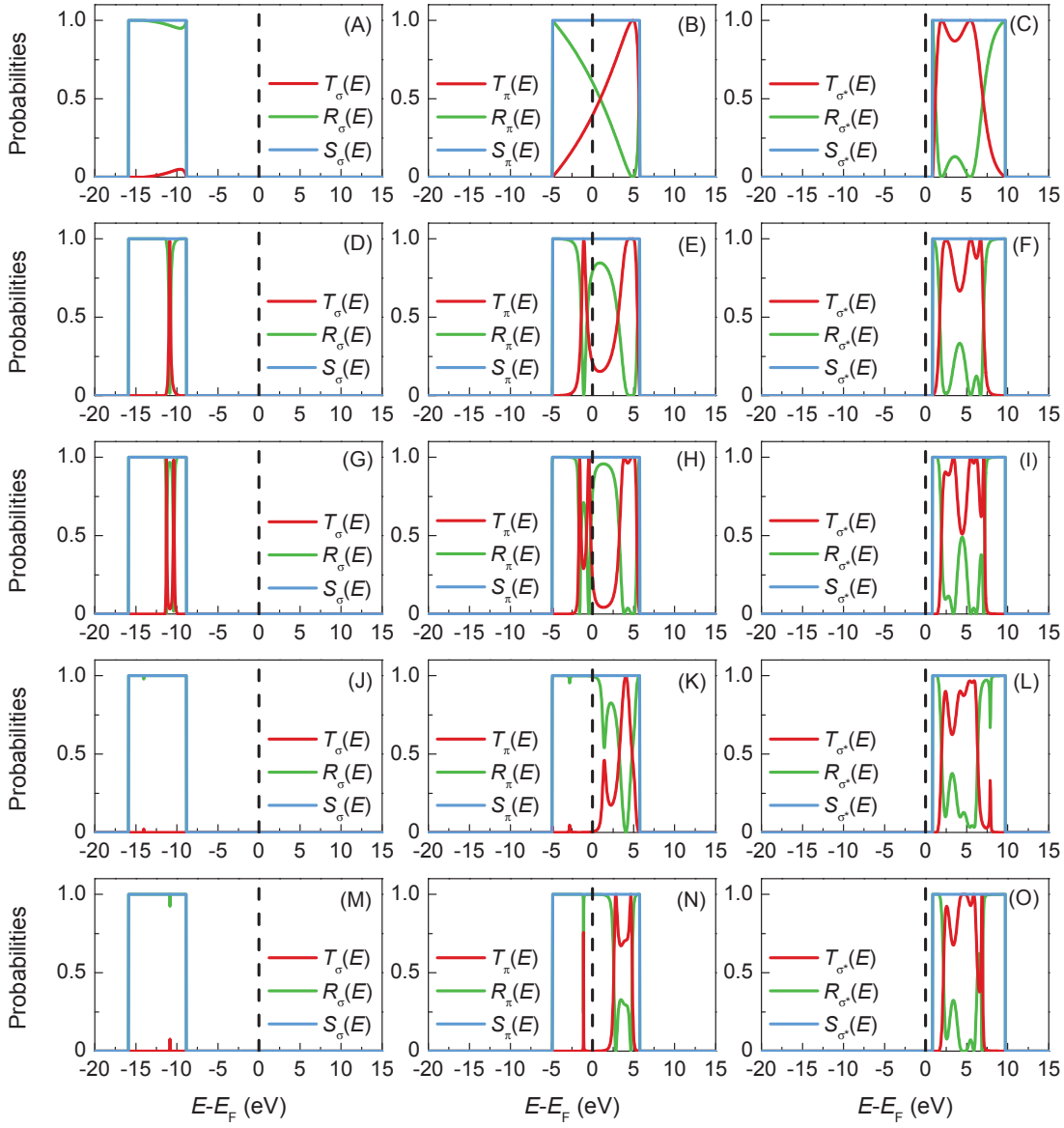

Figure 5.6: The transmission and reflection probabilities arcross five considered types of the silicon-doped carbon wires between two semi-infinite one-dimensional carbon leads. The arrangement of the subfigures is: (A)-(C) for case 1, (D)-(F) for case 2, (G)-(I) for case 3, (J)-(L) for case 4, and (M)-(O) for case 5. The Fermi level is set at the zero energy reference position.

In Figures 5.6, the transmission spectra present strong scattering resonances, showing increasing complexity with the increasing size and configurational order of the nanojunctions. The valence σ-state exhibits negligible transmission for all of the considered nanojunctions. The degenerate π-states and the σ^*-state present in contrast finite trans-

mission spectra. However, it is only the π-states which cross the Fermi level giving rise to electronic conductance across the nanojunction within the zero bias limit.

In particular, the first three considered systems represent increasing lengths of the diatomic silicon carbide nanojunction with the increasing number of ordered Si-C atomic pairs. The transmission at the Fermi level for these systems is non-zero, see Figure 5.3 (C), which contrasts with the insulating character of the infinite silicon carbide wire. One can connect this finite transmission to the indirect band gap (Δ) around the Fermi level for the diatomic silicon-carbide infinite wire (for more details please see Figure 5.3 (C)). This gap $\Delta \sim 1.5$ eV is indeed related to the difference between the binding energies of the silicon and carbon atoms, and corresponds to an effective potential barrier for the propagating π-state electrons. As the wire length increases by adding Si-C atomic pairs, as for the systems 1 to 3 of Figure 5.5 (B), the transmission decreases due to the cumulative barrier effects. We note that a similar effect for the monovalence diatomic copper-cobalt wire nanojunctions has been observed in a previous work.

Furthermore, it is instructive to compare the scattering spectra for the degenerate π-states, for the nanojunction systems 3 and 4. These two systems contain identical numbers of silicon and carbon atoms, however system 3 is an ordered configuration of Si-C pairs whereas 4 presents substitutional disorder of the atoms. It is seen that the disorder suppresses the conductance of the π-state electrons at the Fermi level within the zero bias limit. Another general observation can be made from the results for the nanojunction system 5 which contains more silicon than carbon atoms. Despite the finite size of this system, comparable to system 4, and despite the structural symmetry of its atomic configuration, the electronic transmission is suppressed at the Fermi level within the zero bias limit. This implies that one of the main observations of our paper is that structural symmetry on the nanojunction is not a guarantee for finite transmission in the case of the multivalence diatomic wire nanojunctions.

Figures 5.6 also show that the transmission spectra for the σ^*-state are close to unity over a significant range of energies from ~ 1 to ~ 7 eV, for all of the five nanojunction systems. This result may prove useful for the electronic conductance across the silicon-doped carbon nanojunctions under finite bias voltages.

In Figures 5.7, we present the total electronic conductance $G(E)$ as a function of energy E and in units of $G_0 = 2e^2/h$, for the considered nanojunction systems of a given length as depicted in Figure 5.5 (red). Moreover, the perfect electronic conductance on the carbon leads (blue) is given in comparison, and constitutes effectively the conductance of the infinite and perfect quasi one-dimensional carbon wire. In Figures 5.7, the Fermi level is indicated by the dashed line as a zero reference energy, and $G(E)$ is calculated from all the contributing eigenstates of Figures 5.6, including the two degenerate π-states.

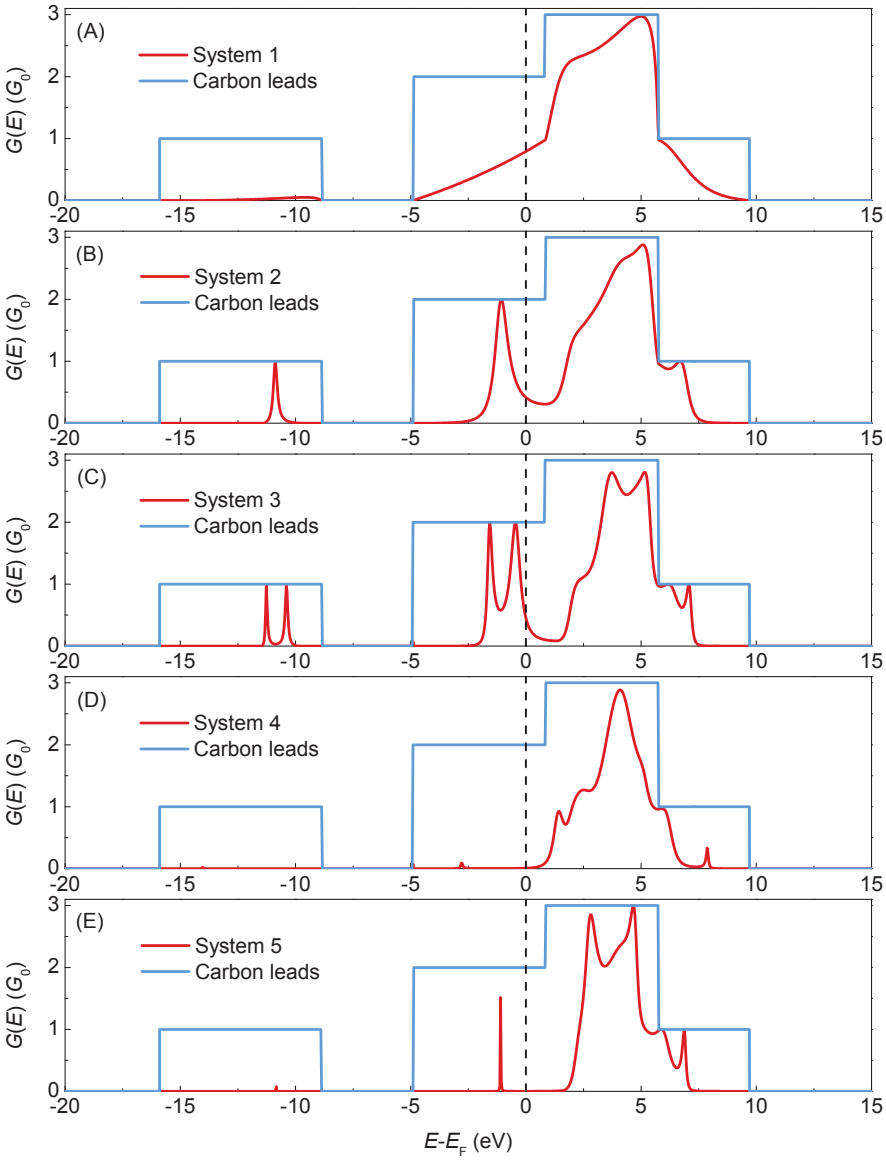

Figure 5.7: Total electronic conductance $G(E)$, as a function of energy E in units of $G_0 = 2e^2/h$, for silicon doped carbon wires. See text for details.

We note that the conclusions given for the results presented in Figures 5.6 are also followed by the more general representation of the electronic transport depicted in Figures 5.7. Furthermore, the results presented in Figures 5.7 confirm that only the electrons incident from the leads in the π states are responsible for the electronic conductance at the zero bias limit, readable from the Fermi level position. However, for all considered systems, the conductance at the Fermi level is theoretically limited to the value of 2 G_0 and the biggest conductance maxima close to the perfect infinite carbon wire value of 3 G_0 can be observed only in the energy interval from $\sim$ 1 to $\sim$ 7 eV, hence for energies above the Fermi level. Once again, this follows our previous observations for the transmission results for the π states, concluded from Figures 5.6. Nonetheless, only on the basis of the

results presented in Figures 5.7 can we note that due to the summation over all possible state contributions which constitute the $G(E)$ spectra, not only the σ^* state electrons but also some of those in the degenerate π states, contribute to the high conductance values in the cited energy intervals. This important observation proves that the σ^* and π states electrons are of crucial importance for both the zero-bias quantum conductance of the silicon-doped carbon wires, and the possible finite bias ones. This implies that the use of only a single orbital for the description of the carbon atoms will result in an inadequate description of the transport processes across low-coordinated systems containing these atoms.

5.2 Diatomic gallium-arsenite nanojunctions

As a supplementary results for section 5.1, we consider the quantum electronic transport characteristics across finite diatomic linear gallium-arsenite nanojunction wires (MLGW) held between two gallium leads. In particular three systems of consisting of one (case 1), two (case 2) and three (case 3) pairs of gallium-arsenite pairs are considered.

Table 5.2: The values of the tight-binding parameters, $\varepsilon_l^{n,\alpha}$ and $h_{l,l',m}^{n,n',\beta}$ (in eV), and Harrison's dimensionless coefficients, $\eta_{l,l',m}$, as proposed in Harrison [Harrison 2004]. Please note that the distance dependent $h_{l,l',\sigma}^{n,n',\beta}$ parameters are computed for the appropriate interatomic spacings d_β (in Å), tabulated below and assumed after [Durgun *et al.* 2004] and [Tongay *et al.* 2004]. In order to keep table transparent indices n and n' for $\varepsilon_l^{n,\alpha}$ and $h_{l,l',m}^{n,n',\beta}$ are ommited.

α	Ga	As	β	Ga-Ga	Ga-As
ε_s	-11.55	-18.92	d_β	2.6	2.3
ε_p	5.67	-8.98			
β	Ga-Ga	Ga-As	β	Ga-Ga	Ga-As
$\eta_{s,s,\sigma}$	-1.32	-1.32	$h_{s,s,\sigma}$	-1.49	-1.90
$\eta_{s,p,\sigma}$	1.42	1.42	$h_{s,p,\sigma}$	1.60	2.05
$\eta_{p,p,\sigma}$	2.22	2.22	$h_{p,p,\sigma}$	2.50	3.20
$\eta_{p,p,\pi}$	-0.63	-0.63	$h_{p,p,\pi}$	-0.71	-0.91

In the first step the electronic band structures within the tight-binding approximation are calculated for the gallium and gallium-arsenite infinite wire nanojunctions as presented in figures 5.8. Both systems are described by the minimal basis consisting of s, p_x, p_y, and p_z orbitals. The values of the TBA parameters are the same as in [Harrison 2004], assuming the appropriate Ga-Ga and Ga-As interatomic spacings after

[Durgun *et al.* 2004] and [Tongay *et al.* 2004] (please see Table 5.2, for the details).

Obtained results indicate that both systems are metallic due to the fact that Fermi level crosses their conduction bands as it can be seen on figures 5.8.

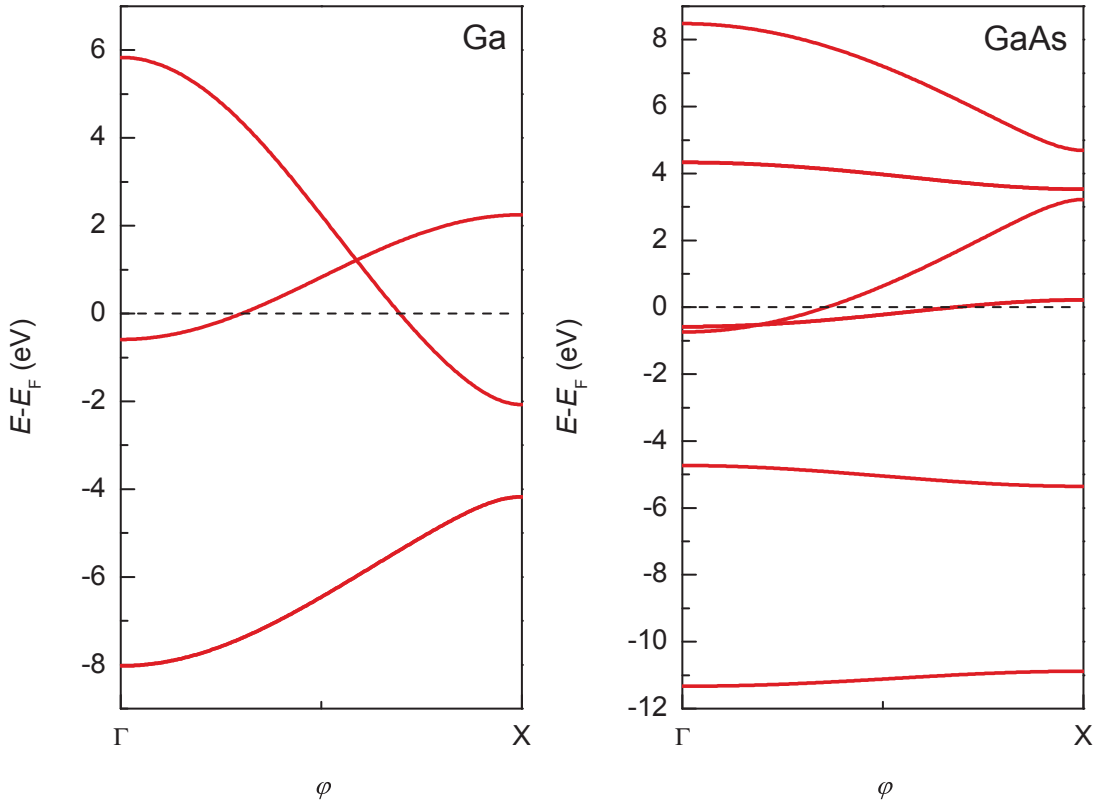

Figure 5.8: Electronic structures of gallium (Ga) and gllium-arsenite (Ga-As) infinite linear atomic wires, presented over the first Brillouin zone $\varphi = kd \in [-\pi, \pi]$. Our calculated Fermi levels are given as the zero reference energies..

Next, the PFMT method is applied to the considered systems. The final results presenting overall conductance across these wire nanojunctions are depicted in figure 5.9. Again strong conductance maxima can be observed, in particular in the energy ranges from $\sim$ 8 eV to $\sim$ 7.5 eV, and from $\sim$ 1 eV to $\sim$ 2 eV, where the conductance value reaches its theoretical maximum of 1 and 3 G_0, respectively.

The most important observation is made for quantum electronic conductance at the Fermi level. In similar fashion as it has been shown for silicon-doped carbon wire nanojunctions, the diatomic gallium-arsenite ones exhibit conductance decay when the number of Ga-As atomic pairs increases. However, the band structure of the Ga-As infinite system as presented in one of the figures 5.8, does not present any band gap at the Fermi energy. Due to this fact, decay of the conductance value at this level can not be explained within such band gap, as it was done for the silicon-doped carbon wire nanojunctions. I what follows, the surprising conductance behavior of the Ga-As diatomic systems must

be, in our opinion, directly related to the increasing number of atomic pairs, suggesting the fact that each pair generates the potential strong enough to lower the value of the conductance.

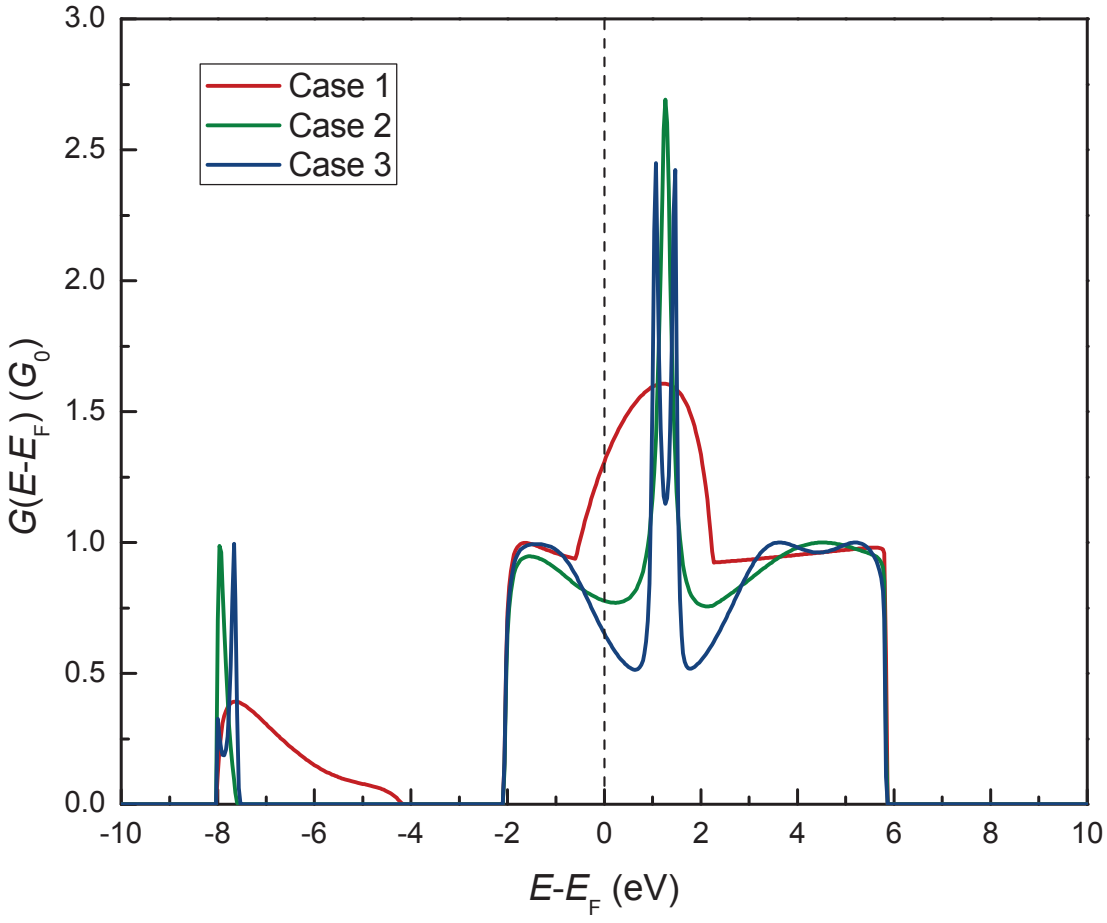

Figure 5.9: Total electronic conductance $G(E)$, as a function of energy E in units of $G_0 = 2e^2/h$, for diatomic gallium-arsenite nanojunction wires.

By arguing the fact that electric leads assumed for our calculation are made of gallium atoms, each gallium-arsenite pair acts as a strong chemical defect, even when the pairs are arrangement in periodic structure as in this sub-section.

Chapter 6

Summary and perspectives

6.1 Summary

In this work we have presented a general method based on the algebraic phase field matching theory (PFMT), to calculate the electronic quantum transport across nanosystems of arbitrary form between material leads of any possible dimensions. Furthermore, integrated tight-binding approximation allows us to discretize the entire model calculation in the real-space, and equally important, to make time economies in the numerical computations. The presented PFMT approach, a transparent and time-saving method, should be especially interesting for the treatment of complex systems presenting multichannel conductance, and can serve as a alternative technique to the wide range of Green's functions based methods.

In particular, the PFMT method is applied in this thesis to calculate the quantum electronic conductance across wire nanojunctions held between one-dimensional electric leads.

First, the model calculations are carried out for nanojunctions made up of sodium atomic wires (MLNaW) between leads of the same element. Our calculated results for the electronic quantum transport are shown to be a function of the physical parameters of the wires, and exhibit the well known oscillation behavior for even- and odd-number wire lenghts. They are also in agreement with the first-principle results [Egami *et al.* 2010], [Lee *et al.* 2008], [Egami *et al.* 2005]. This clearly confirms the validity of the presented PFMT model.

Our model calculations are also carried out for the diatomic copper-cobalt wires (DLCuCoW) held between copper leads. This system is selected for its mechanical and thermodynamical stability at low temperatures, which is one of the important features required for future nanoelectronic devices. In contrast to the MLNaW system, the electronic quantum transport of the DLCuCoW wire nanojunction, at the Fermi energy,

exhibits exponential decay with increasing wire length. This behavior is explained notably in terms of the band gap of the infinite variant of the DLCuCoW nanojunction wire. A relation, depicting analytically the numerical values of the conductance $G(N_{\mathrm{CuCo}}, E_F)$ of the DLCuCoW wires for any length $N_{\mathrm{CuCo}} \geq 2$, is given and may help to simplify the analysis of potential applications for corresponding nanocircuits.

Next, the unknown properties of the quantum electronic conductance for nanojunctions made of silicon-doped carbon wires between carbon leads and the gallium-arsenite diatomic nannojunctions between gallium leads, are studied in depth. The local basis for the electronic wave functions is assumed to be composed of four different atomic orbitals for silicon and carbon, namely the s, p_x, p_y, and p_z states.

We calculate the electronic band structures for three nanomaterials, namely the one-dimensional infinite wires of silicon, carbon. This permits a matching comparison with the available corresponding DFT results, with the objective to select the optimal TB parameters for the three nanomaterials.

This optimal set of the tight-binding parameters is then used to calculate the electronic conductance across the silicon-doped carbon wire nanojunctions. In the case of diatomic gallium-arsenite wires the initial tight-binding parameters values as given by [Harrison 2004] are used.

Various nanojunction cases are analyzed to sample their behavior under different atomic configurations. We show that despite the non conducting character of the infinite silicon carbide wires, its finite implementation as nanojunctions exhibit a finite conductance. This outcome is explained by the energy difference between the binding energies of the silicon and carbon atoms, which corresponds to an effective potential barrier for the degenerate π-state electrons transmitted across the nanojunction under zero bias field. Similar effect is observed in the diatomic gallium-arsenite nanojunction wires, however it is explained only on the basis of the chemical defect influence.

The conductance effects that may arise due to minimal substitutional disorder and to artificially organized symmetry considerations on the silicon carbide wire nanojunction are also investigated. By exchanging the positions of two silicon and carbon atoms on an initial nanojunction to generate a substitutional disordered, we show that the total quantum conductance is suppressed at the Fermi level. This is in sharp contrast with the finite and significant conductance for the initial atomically ordered nanojunction with periodic configurations of the silicon and carbon atoms. Also, the analysis of a silicon carbide nanojunction of a comparable size as the one above, presenting symmetry properties, shows that the quantum conductance is suppressed at the Fermi level. We note also that the biggest maxima of the conductance spectra for the zero bias limit can be observed for high energies for all of the considered systems. This conclusion reveals

the fact that electrons incident from the leads in both σ^* and π states are crucial for the considerations of the electronic transport properties of the silicon-doped carbon wire nanojunctions.

6.2 Perspectives

In novel nanotechnology and nanoscience the carbon nanomaterials and their properties constitute one of the most intriguing domains for the scientists [Guisinger & Arnold 2010], [Avouris *et al.* 2007]. These materials presenting rich polymorphism and corresponding wide range of extraordinary physical and chemical properties are considered as great theoretical playground for many interesting phenomena, and also as possible new basic building blocks for future nanodevices [Guisinger & Arnold 2010].

The one atom thick graphitic sheets, known as graphene [Novoselov *et al.* 2004], represents particular allotropic form of carbon materials, constituting fundamental theoretical and structural concepts for these. On itself, graphene structure based on the hexagonally arranged carbon atoms (the so-called *honeycomb* pattern), which are connected by strong in-plane σ-type bonds and constitute two interpenetrating sublattices denoted as A and B (please see figure 6.1 (A) where all structural details are presented). Such hexagonal structure of carbon is well known from a long time *i.e.* graphite is build on the basis of stacked graphene-like layers, rolled up graphene sheets constitute nanotubes [Iijima & Ichihashi 1993], whereas the graphene-based spheres are known as fullerenes [Kroto *et al.* 1985]. However, until recently thin carbon sheets where theoretically expected to be thermodynamically unstable [Peierls 1935], [Landau 1937]. In 2004, simple at the first sight, experiment of repeated peeling of graphite (the so-called *exfoliation* or *cleavage technique*) led to monocrystalline graphitic films of few atoms thickness [Novoselov *et al.* 2004]. The earlier difficulties in experimental realization of two-dimensional layers steamed mainly from the lack of clear signatures in transmission electron microscopy of such materials, as well as its complete transparency to the visible light which makes them invisible on most substrates (*e.g.* glass or metals) in an optical microscopes [Novoselov *et al.* 2005]. During next few years, systematic experimental studies on initially *rough* new carbon structure led to purely monolayer graphene of one atom thickness. At present one of the most promising experimental methods to obtain monolayer graphene is its epitaxial growth on the SiC substrates [Strupiński *et al.* 2011].

The described above discovery was important due to the fact that physicists were interested in the physical properties of purely two-dimensional structures for a decades. Indeed, graphene reveled large number of peculiar features. First, due to the mentioned above in-plane σ-type bonds between carbon atoms, graphene is a material with a ex-

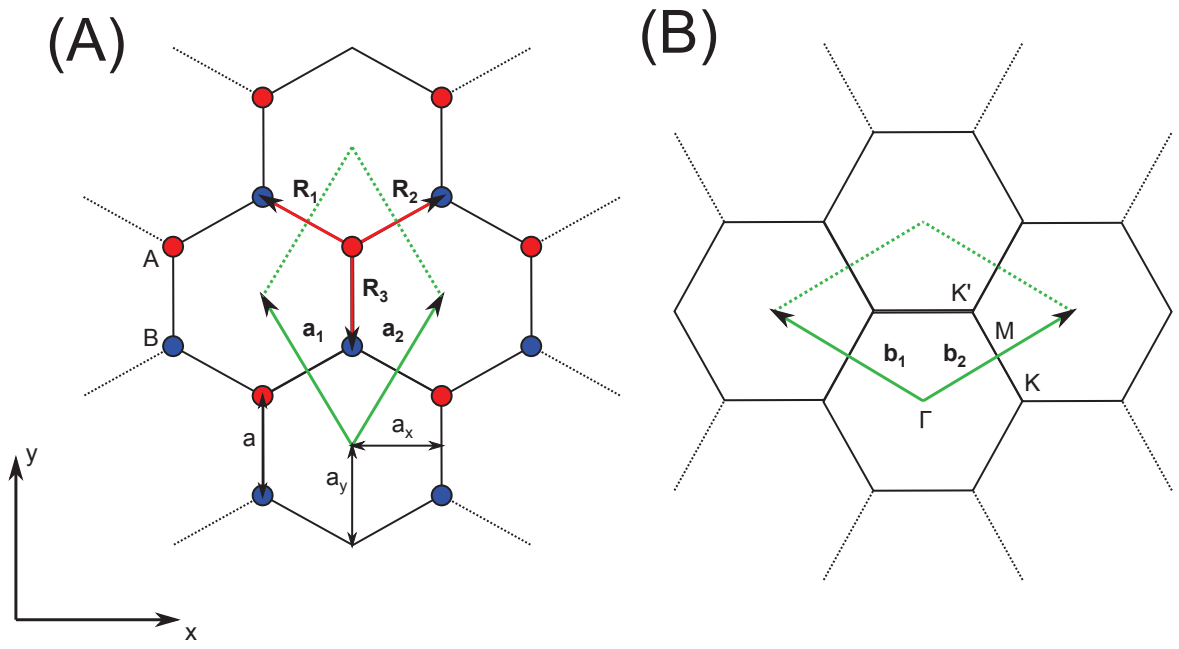

Figure 6.1: (A) Unit cell of pristine graphene in the real space, as described by the lattice basis vectors: $\mathbf{a}_1 = (-\sqrt{3}a/2)\mathbf{x} + (3a/2)\mathbf{y}$ and $\mathbf{a}_2 = (\sqrt{3}a/2)\mathbf{x} + (3a/2)\mathbf{y}$ with magnitude $|\mathbf{a}_1| = |\mathbf{a}_2| = \sqrt{3}a$, and nearest-neighbour vectors: $\mathbf{R}_1 = (-\sqrt{3}a/2)\mathbf{x} + (a/2)\mathbf{y}$, $\mathbf{R}_2 = (\sqrt{3}a/2)\mathbf{x} + (a/2)\mathbf{y}$ and $\mathbf{R}_3 = -a\mathbf{y}$; where $a = 1.42$Å, $a_x = \frac{\sqrt{3}a}{2}$, and $a_y = a$. (B) Unit cell of the pristine graphene in the reciprocal lattice, as described by the reciprocal lattice basis vectors: $\mathbf{b}_1 = (-2\pi/\sqrt{3}a)\mathbf{x} + (2\pi/3a)\mathbf{y}$ and $\mathbf{b}_2 = (2\pi/\sqrt{3}a)\mathbf{x} + (2\pi/3a)\mathbf{y}$, and the high-symmetry points: $\Gamma = (0, 0)$, $K = \big(4\pi/3\sqrt{3}a, 0\big)$, $K' = \big(2\pi/3\sqrt{3}a, 2\pi/3a\big)$, and $M = \big(2\pi/3\sqrt{3}a, \pi/3a\big)$.

ceptionally high in-plane strength and stiffness on the order of 130 GPa and 1 TPa, respectively [Lee *et al.* 2008]. Furthermore, graphene exhibits excellent thermal conductivity on the order of 3-5 kW/mK [Balandin *et al.* 2008], [Hu *et al.* 2009]. Nonetheless, the most intriguing are the electronic properties of graphene, arising from the confinement of the electrons in the two-dimensions and characteristic *honeycomb* structure, making this material one of the most promising candidates for the future nanodevices.

In particular, graphene sheets presents extremely high electron mobility (about 10^3 $\mathrm{cm}^2/\mathrm{Vs}$) which is far greater than that in silicon [Novoselov *et al.* 2004], a material which is fundamental in present electronics. This happens due to the peculiar zero-bandgap electronic band structure with characteristic conical shapes in the spectrum (the so-called *Dirac cones*), which has been predicted theoretically long time ago during investigations on the electronic properties of graphite [Wallace 1947], [Slonczewski & Weiss 1958] (please see figure 6.2). We note that band structure presented on figure is obtained within orthonormal π-type dispersion relation with two atoms per unit cell and only nearest-

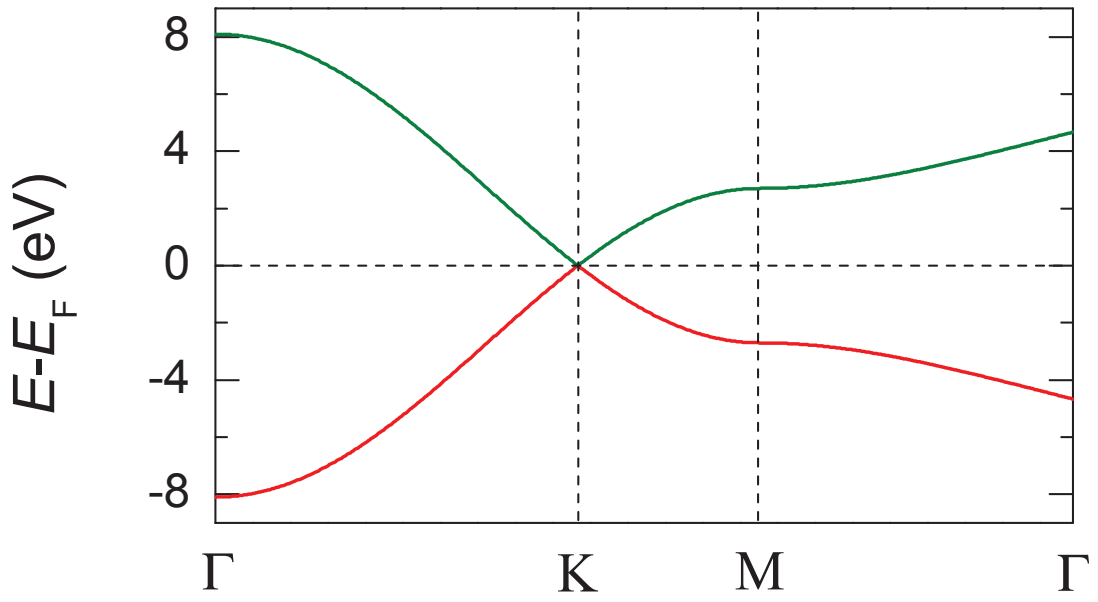

Figure 6.2: Band structure of graphene obtained on the basis of orthonormal π-type tight-binding model with only nearest-neighbor interations included. The red and green colors are used in order to distinct two individual π-type bands. The characteristic *Dirac cones* are visible at the K point of the two-dimensional Brillouin zone. The Fermi level is set at zero energy reference.

neighbour interactions, apart of the fact that carbon has the sp^2 hybridization. However, the core 1s or semi-core 2s electrons couple with the $2p_x$ and $2p_y$ ones creating the parallel to the plane and already mentioned strong σ-type bonds, which correspond to the branches in the electronic spectra away from the Fermi level. Only the highest energy electrons of the p_z states form the perpendicular to the plane π-type bonds which give the only contribution to the electronic branches around the Fermi level.

From the electronic point of view, it has been also shown that low-energy particles in graphene can be formally described by the Dirac-like Hamiltonian and the linear dispersion relation suggest that they behave as massless relativistic particles leading to the mentioned high electron mobility and phenomena like Klein paradox, an unimpeded penetration of relativistic particles through high and wide potential barriers [Katsnelson *et al.* 2006] [Katsnelson & Novoselov 2007].

Nevertheless, usefulness of pristine graphene as a material which can be used for conventional semiconductor device operations is highly limited due to the zero-bandgap in its electronic spectrum. One of the major research domains on graphene at present, concerns controlled generation of such bandgap [Shimizu *et al.* 2010]. This can be done by forma-

tion of few layers graphene nanostructures, when the inversion symmetry of single sheet of graphene is broken [Zhao *et al.* 2010], [Zhang *et al.* 2009], [Craciun *et al.* 2009]. As one may expect such attempt has a disadvantage in difficulty of correct control of the exact number of layers in resulting systems, what may leads to the suppression of the initial interesting properties of graphene. Alternative to this approach is the process of carving out from pristine graphene variously oriented nanoribbons. This method is especially popular at present, since by varying the length of the given graphene nanoribbon the size of the bandgap varies, and even more by passivation of the graphene nanoribbons with hydrogen, the indirect bandgap can be converted into the direct one as a result of enhanced interactions between electrons and nuclei at the edges of the ribbon [Ma *et al.* 2012]. However, experimental realization of defect-free nanoribbon systems using popular lithographic methods is rather hard, inducing the defect related undiserable phenomena such as hopping conductance or the stochastic single-electron charging effects [Han 2010], [Stampfe 2009], [Han 2007]. An interesting attempt to overcome this problems is preparation process of the graphene nanoribbons using high-temperature hydrogen-annealing of unzipped carbon nanotubes presented by [Shimizu *et al.* 2010]. Obtained within this process nanoribbons with the width $\sim$ 100 nm have low-density of defects and presents bandgaps on the order of $\sim$ 50 meV. The third approach which is worth consideration is the doping process of the graphene with foreign atoms. This allows one to theoretically open the band gap over entire Brillouin zone, *e.g.* by boron-nitride [Ci *et al.* 2010], [Shinde & Kumar 2011], [Fan *et al.* 2012] or lithium doping [Profeta *et al.* 2012], or just at given crystallographic high-symmetry points, *e.g.* by out of-plane metallic atoms doping [Aktürk *et al.* 2010], [Ataca *et al.* 2011]. Since the traditional doping techniques are well established, the last band gap engineering method is expected to be the most effective at the present. Furthermore, it allows one to overcome difficulties in controlling the edges of the material as in the case of graphene nanoribbons, or the complexity of electrically gated multi-layer graphene structures.

Due to the above intrinsic electronic features as well as the presence of the long coherence length, graphene and its modifications are perfect subject for nanodevices presenting room-temperature ballistic electronic transport. Indeed, the electronic transport properties of pristine and modified graphene has been of crucial interest for the scientists in recent years. One can list here investigations on the pristine graphene [Du *et al.* 2008], a disordered one [Ostrovsky *et al.* 2006], the considerations of the electronic transport across graphene nanoribbons in its perfect and modified forms [Wakabayashi *et al.* 2009], [Wu & Childs 2011].

In my future work I would like to concentrate on the electronic transport properties of the graphene-based nanodevices which still need attention. Of the most intriguing are the

in- or out of-plane doped graphene materials, which can lead to the higher conductance values as nanojunctions or engineering new graphene-based semiconducting devices. In this case the two general aspects should be analyzed, namely the scattering at the ordered or weakly disordered graphene-based nanojunctions. The latter one will however need a proper extension to the method presented in this thesis, by iterating in its approach the novel *coherent potential approximation* (CPA), recently developed for the magnetic case [Ghader & Khater 2012]. Furthermore, due to the structural modifications the π-type tight-binding model discussed in this section will not be valid anymore for all new structural cases. For example, doping graphene with low-lying periodic table elements will lead to the change from the sp^2 to sp^3 hybridization, which will require use of the additional orbitals within the minimal basis of atomic wave functions assumed for calculations *e.g.* as in the case of the hydrogen deposition [Boykin *et al.* 2011]. It will be also of crucial interest to consider interaction beyond the nearest-neighbour regime in order to allow the influence on the electronic structure of the chemical elements which can be described by the π-type Hamiltonian but are at the out of-plane positions.

Another important extension should concerns influence of the electron-electron, electron-phonon or electron-magnon coupling on the electronic transport properties of the discussed structures. In my opinion above plans should constitute a major contribution to the developing nanoelectronic domain allowing me to continue my investigations on the fundamental aspects of the quantum electronic transport in nanostrucutres.

Appendix A - Explicit forms of the $\mathbf{E}_{i,j}$ and $\mathbf{H}_{i,j}$ matrices

The explicit forms of the submatrices of equation (3.14) are given in the following manner

$$\mathbf{E}_{i,j} = \begin{bmatrix} \boldsymbol{\varepsilon}_1 & \mathbf{h}_{2,1}^{\dagger} & \cdots & \cdots & \mathbf{h}_{n,1}^{\dagger} \\ \mathbf{h}_{2,1} & \boldsymbol{\varepsilon}_2 & \ddots & & \vdots \\ \vdots & \ddots & \ddots & \ddots & \vdots \\ \vdots & & \ddots & \boldsymbol{\varepsilon}_{n-1} & \mathbf{h}_{n,n-1}^{\dagger} \\ \mathbf{h}_{n,1} & \cdots & \cdots & \mathbf{h}_{n,n-1} & \boldsymbol{\varepsilon}_n \end{bmatrix}, \tag{6.1}$$

and

$$\mathbf{H}_{i,j} = \begin{bmatrix} 0 & \cdots & \mathbf{h}_{1,2} & \cdots & \mathbf{h}_{1,n-1} & \mathbf{h}_{1,n} \\ \vdots & \ddots & \ddots & \ddots & \mathbf{h}_{2,n-1} & \mathbf{h}_{2,n} \\ 0 & \ddots & \ddots & \ddots & \ddots & \vdots \\ \vdots & \ddots & \ddots & \ddots & \ddots & \mathbf{h}_{n,n} \\ 0 & 0 & \ddots & \ddots & \ddots & \vdots \\ 0 & 0 & \cdots & 0 & \cdots & 0 \end{bmatrix}, \tag{6.2}$$

where

$$\boldsymbol{\varepsilon}_{i',j'} = \begin{bmatrix} \varepsilon_s^{n,\alpha} & 0 & \cdots & \cdots & 0 \\ 0 & \varepsilon_{p_x}^{n,\alpha} & \ddots & & \vdots \\ \vdots & \ddots & \ddots & \ddots & \vdots \\ \vdots & & \ddots & \varepsilon_{l-1}^{n,\alpha} & 0 \\ 0 & \cdots & \cdots & 0 & \varepsilon_l^{n,\alpha} \end{bmatrix}, \tag{6.3}$$

and

$$\mathbf{h}_{i',j'} = \begin{bmatrix} h_{s,s,\sigma}^{n,n',\beta} & h_{s,p_x,\sigma}^{n,n',\beta} & \cdots & \cdots & h_{s,l',m}^{n,n',\beta} \\ h_{p_x,s,\sigma}^{n,n',\beta} & h_{p_x,p_x,\sigma}^{n,n',\beta} & \ddots & & \vdots \\ \vdots & \ddots & \ddots & \ddots & \vdots \\ \vdots & & \ddots & h_{l-1,l'-1,m}^{n,n',\beta} & h_{l-1,l',m}^{n,n',\beta} \\ h_{l,s,m}^{n,n',\beta} & \cdots & \cdots & h_{l,l'-1,m}^{n,n',\beta} & h_{l,l',m}^{n,n',\beta} \end{bmatrix}. \tag{6.4}$$

Equations (6.1) and (6.2) denote $N_x N_l$ square matrices, where matrix (6.2) is upper triangular. In this manner component matrices (6.3) and (6.4) are of the dimension $N_l \times N_l$. Additionally, matrix $\boldsymbol{\varepsilon}_{i',j'}$ always denotes diagonal matrix, while $\mathbf{h}_{i',j'}$ matrix is much more complex, with possible non-zero elements at every position. Please note, that some of the $h^{n,n',\beta}_{l,l',m}$ elements can vanish due to the symmetry conditions and simplifies the notation of the $\mathbf{h}_{i',j'}$ matrix.

Appendix B - Partitioning technique

The partitioning technique is suitable method which allows to avoid singularity problem of the $\mathbf{H}_{N,N-1}$ and $\mathbf{H}^{\dagger}_{N,N-1}$ matrices and calculate only non-trivial solutions of equation (3.22). This section gives only our short remarks on the partitioning technique, and the detailed discussion of this method can be found in [Khomyakov & Brocks 2004].

Following studies from [Khomyakov & Brocks 2004] equation (3.22) is partitioned into two parts, of respectively $D_1 - D_2$ and D_2 sizes, where

$$D_1 = N_x N_l, \tag{6.5}$$

and

$$D_2 = N_n N_l. \tag{6.6}$$

In equation (6.6), parameter N_n stands for the order of nearest-neighbour interactions assumed in calculations *e.g.* $N_n = 1$ for the first nearest-neighbour interactions. on the basis of equations (6.5) and (6.6), reduced $2N_l$ eigenvalue problem is written as

$$\left[\begin{bmatrix} \mathbf{A}_{1,1} & \mathbf{A}_{1,2} \\ \mathbf{I}_{2,2} & 0 \end{bmatrix} - z \begin{bmatrix} \mathbf{B}_{1,1} & \mathbf{B}_{1,2} \\ 0 & \mathbf{I}_{2,2} \end{bmatrix}\right] \times \begin{bmatrix} \mathbf{c}_2(x_N, \mathbf{k}) \\ \mathbf{c}_2(x_{N-1}, \mathbf{k}) \end{bmatrix} = 0. \tag{6.7}$$

At this point we correct the misprint from [Khomyakov & Brocks 2004] and write the submatrices of equation (6.7) in the following form

$$\mathbf{A}_{1,1} = E\mathbf{I}_{2,2} - \mathbf{E}_{2,2} - \mathbf{E}_{2,1}\left[E\mathbf{I}_{1,1} - \mathbf{E}_{1,1}\right]^{-1}\mathbf{E}_{1,2}, \tag{6.8}$$

$$\mathbf{A}_{1,2} = -\mathbf{H}_{2,2} - \mathbf{E}_{2,1}\left[E\mathbf{I}_{1,1} - \mathbf{E}_{1,1}\right]^{-1}\mathbf{H}_{1,2}, \tag{6.9}$$

$$\mathbf{B}_{1,1} = \mathbf{H}^{\dagger}_{2,2} + \mathbf{H}^{\dagger}_{1,2}\left[E\mathbf{I}_{1,1} - \mathbf{E}_{1,1}\right]^{-1}\mathbf{E}_{1,2}, \tag{6.10}$$

$$\mathbf{B}_{1,2} = \mathbf{H}_{1,2}\left[E\mathbf{I}_{1,1} - \mathbf{E}_{1,1}\right]^{-1}\mathbf{H}_{1,2} \tag{6.11}$$

Please note, that reduced problem of equation (6.7) gives $2N_l$ eigenvalues with $2N_l$ corresponding eigenvectors, what is N_x times less then can be expect from the physical point of view. Nevertheless, those solutions can be easily separated into $N_x N_l$ eigenvalues and $N_x N_l$ eigenvectors of a purely physical character.

Appendix C - Explicit forms of the $\mathbf{M}_{i,j}$, $\mathbf{M}_1^{in}$, and $\mathbf{M}_2^{in}$ components

The submatrices of the *matched* $(D+2)\times(D+2)$ square matrix $\mathbf{M}$ in equation (3.28), for a given i and j indices, are given as

$$\mathbf{M}_{i,j} = E\mathbf{I} - \mathbf{E}_{i,i} \text{ for } \begin{cases} i = j \\ D > i > 1 \\ D > j > 1 \end{cases}, \tag{6.12}$$

$$\mathbf{M}_{i,j} = -\mathbf{H}_{i,i-1} \text{ for } \begin{cases} i \neq j \\ i > 2 \\ j = i-1 \end{cases}, \tag{6.13}$$

$$\mathbf{M}_{i,j} = -\mathbf{H}^{\dagger}_{i,i-1} \text{ for } \begin{cases} i \neq j \\ i < D+1 \\ j = i+1 \end{cases}, \tag{6.14}$$

except of the submatrices which describe the boundary atoms of the system and are expressed in the following manner

$$\begin{aligned} &\mathbf{M}_{1,1} = -\mathbf{H}_{-1,-2}\mathbf{c}_l(\mathbf{r}_n, z_{\gamma'}, E_\gamma)z_{\gamma'}^2 \\ &+ (E\mathbf{I} - \mathbf{E}_{-1,-1})\,\mathbf{c}_l(\mathbf{r}_n, z_{\gamma'}, E_\gamma)z_{\gamma'}, \\ &\mathbf{M}_{2,1} = -\mathbf{H}_{0,-1}\mathbf{c}_l(\mathbf{r}_n, z_{\gamma'}, E_\gamma)z_{\gamma'}, \\ &\mathbf{M}_{D+1,D+2} = -\mathbf{H}^{\dagger}_{D-1,D}\mathbf{c}_l(\mathbf{r}_n, z_{\gamma'}, E_\gamma)z_{\gamma'}^D, \\ &\mathbf{M}_{D+2,D+2} = -\mathbf{H}_{D,D+1}\mathbf{c}_l(\mathbf{r}_n, z_{\gamma'}, E_\gamma)z_{\gamma'}^{D+1} \\ &+ (E\mathbf{I} - \mathbf{E}_{D,D})\,\mathbf{c}_l(\mathbf{r}_n, z_{\gamma'}, E_\gamma)z_{\gamma'}^D, . \end{aligned} \tag{6.15}$$

Finally, the $\mathbf{M}_1^{in}$ and $\mathbf{M}_2^{in}$ of equation (3.28) vector components are written as

$$\begin{aligned} \mathbf{M}_1^{in} &= \mathbf{H}_{-1,-2}\mathbf{c}_l(\mathbf{r}_n, z_\gamma, E_\gamma)z_\gamma^{-2} \\ &+ (E\mathbf{I} - \mathbf{E}_{-1,-1})\,\mathbf{c}_l(\mathbf{r}_n, z_\gamma, E_\gamma)z_\gamma^{-1}, \end{aligned} \tag{6.16}$$

and

$$\mathbf{M}_2^{in} = -\mathbf{H}_{0,-1}\mathbf{c}_l(\mathbf{r}_n, z_\gamma, E_\gamma)z^{-1}. \tag{6.17}$$

Appendix D - Group velocities

As specified in section 3.2, the group velocities for individual states, can be calculated on the basis of equation (3.18) rewritten in the following manner

$$[v\mathbf{I} - \mathbf{V}]\,\mathbf{v}(\mathbf{k}, E) = 0, \tag{6.18}$$

where v denotes the eigenvalues of equation (6.18) which yields all required electron group velocities for each propagating state. Further $\mathbf{V}$ is the $N_x \times N_l$ size matrix of the form

$$\mathbf{V} = \frac{\partial \mathbf{M}_d}{\partial \mathbf{k}}. \tag{6.19}$$

Finally $\mathbf{v}(\mathbf{R}_N, \mathbf{k})$ stands for eigenvectors of the problem of equation (6.18). We note that usually equation (6.19) includes the constant part d_β/h, where h is the Planck constant. However, for the purpose of electronic conductance calculations within the PFMT approach, this term can be omitted due to the fact that only the ratios of the given group velocities are important (please see equations (3.29) and (3.30)).

Appendix E - Remarks on the numerical procedures

The numerical code applied for numerical calculations across chapters 4, and 5 based on the *phase field matching theory* presented in chapter 3. It has been entirely written in the *Wolfram Mathematica*® software (version 8.0.4.0) by the author of this thesis, under common coordination of both supervisors.

To make the numerical procedures transparent, the entire code has been divided into three main modules namely: *electronic band structure module* (EBSM), *general secular equation module* (GSEM) and the *phase field matching module* (PFMM). All modules based on the integrated within *Wolfram Mathematica*® software linear algebra methods. The operational principle of each module as well as their interaction are presented in schematic diagram 6.3.

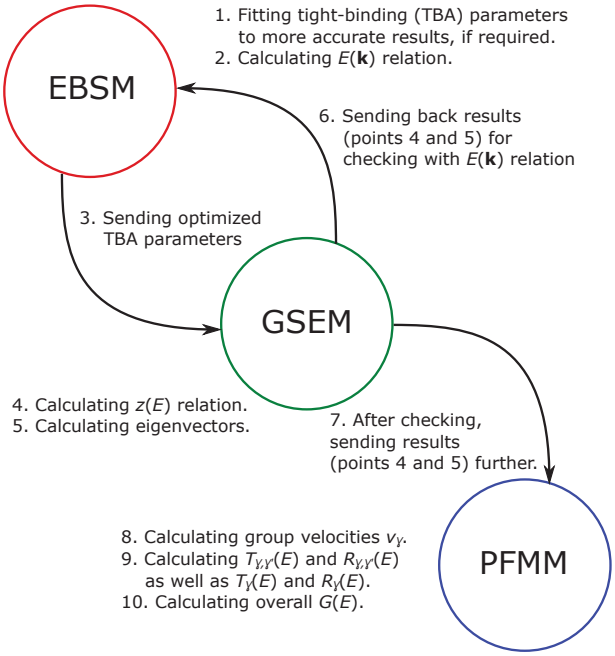

Figure 6.3: Schematic diagram of the operational principle (please follow points form 1 to 10) and their interactions of all modules used for numerical calculations in the presented thesis.

Bibliography

[Abdurahman *et al.* 2002] A. Abdurahman, A. Shukla and M. Dolg. *Ab initio many-body calculations of static dipole polarizabilities of linear carbon chains and chainlike boron clusters.* Phys Rev B, vol. 65, page 115106, 2002.

[Agraït *et al.* 2003] N. Agraït, A. Levy-Yeyati and J. M. van Ruitenbeek. *Quantum properties of atomic-sized conductors.* Phys Rep, vol. 377, pages 81–279, 2003.

[Aktürk *et al.* 2010] E. Aktürk, C. Ataca, and S. Ciraci. *Effects of silicon and germanium adsorbed on graphene.* Appl Phys Lett, vol. 96, page 123112, 2010.

[Ando 1991] T. Ando. *Quantum point contacts in magnetic fields.* Phys Rev B, vol. 44, pages 8017–8027, 1991.

[Ataca *et al.* 2011] C. Ataca, E. Aktürk, H. Şahin and S. Ciraci. *Adsorption of carbon adatoms to graphene and its nanoribbons.* J Appl Phys, vol. 109, page 013704, 2011.

[Avouris *et al.* 2007] P. Avouris, Z. Chen and V. Perebeinos. *Carbon-based electronics.* Nat Nanotechnol, vol. 2, pages 60–615, 2007.

[Balandin *et al.* 2008] A. A. Balandin, S. Ghosh, W. Z. Bao, I. Calizo, D. Teweldebrhan, F. Miao and C. N. Lau. *Superior Thermal Conductivity of Single-Layer Graphene.* Nano Lett, vol. 8, pages 902–907, 2008.

[Bekaroglu *et al.* 2010] E. Bekaroglu, M. Topsakal, S. Cahangirov and S. Ciraci. *First-principles study of defects and adatoms in silicon carbide honeycomb structures.* Phys Rev B, vol. 81, page 075433, 2010.

[Bettini *et al.* 2006] J. Bettini, F. Sato, P.Z. Coura, S.O. Dantas, D.S. Galv ao and D. Ugarte. *Experimental realization of suspended atomic chains composed of different atomic species.* Nature Nanotechnol, vol. 1, pages 182–185, 2006.

[Bloch 1929] F. Bloch. *Über die Quantenmechanik der elektronen in kristallgittern.* Z Phys, vol. 52, pages 555–600, 1929.

[Borisenko & Ossicini 2008] V.E. Borisenko and S. Ossicini. What is what in the nanoworld. John Wiley & Sons Inc., Weinheim, 2008.

[Boykin & Klimeck 2004] T. B. Boykin and G. Klimeck. *The discretized Schrödinger equation and simple models for semiconductor quantum wells.* Eur J Phys, vol. 25, pages 503–514, 2004.

[Boykin & Klimeck 2005] T. B. Boykin and G. Klimeck. *The discretized Schrödinger equation for the finite square well and its relationship to solid-state physics.* Eur J Phys, vol. 26, pages 865–881, 2005.

[Boykin *et al.* 2011] T. B. Boykin, M. Luisier, G. Klimeck, X. Jiang, N. Kharche, Y. Zhou and S. K. Nayak. *Accurate six-band nearest-neighbor tight-binding model for the π-bands of bulk graphene and graphene nanoribbons.* J Appl Phys, vol. 109, page 104304, 2011.

[Brovko *et al.* 2011] O. Brovko, P.A. Ignatiev and V.S. Stepanyuk. *Confined bulk states as a long-range sense for impurities and a transfer channel for quantum information.* Phys Rev B, vol. 83, page 125415, 2011.

[Büttiker 1986] M. Büttiker. *Four-Terminal Phase-Coherent Conductance.* Phys Rev Lett, vol. 57, pages 1761–1764, 1986.

[Bylaska *et al.* 1998] E. J. Bylaska, J. H. Weare and R. Kawai. *Development of bond-length alternation in very large carbon rings: LDA pseudopotential results.* Phys Rev B, vol. 58, pages R7488–R7491, 1998.

[Cahangirov *et al.* 2010] S. Cahangirov, M. Topsakal and S. Ciraci. *Long-range interactions in carbon atomic chains.* Phys Rev B, vol. 82, page 195444, 2010.

[Chen *et al.* 2009] W. Chen, A. V. Andreev and G. F. Bertsch. *Conductance of a single-atom carbon chain with graphene leads.* Phys Rev B, vol. 80, page 085410, 2009.

[Ci *et al.* 2010] L. Ci, L. Song, C. Jin, D. Jariwala, D. Wu, Y. Li, A. Srivastava, Z.F. Wang, K. Storr, L . Balicas, F. Liu and P. M. Ajayan. *Atomic layers of hybridized boron nitride and graphene domains.* Nature Mater, vol. 9, pages 430–435, 2010.

[Cohen *et al.* 1994] R.E. Cohen, M.J. Mehl and D.A. Papaconstantopoulos. *Tight-binding total-energy method for transition and noble metals.* Phys Rev B, vol. 50, pages 14694–14697, 1994.

[Craciun *et al.* 2009] M. F. Craciun, S. Russo, M. Yamamoto, J. B. Oostinga, A. F. Morpurgo and S. Tarucha. *Trilayer graphene is a semimetal with a gate-tunable band overlap.* Nat Nanotechnol, vol. 4, pages 383–388, 2009.

[Crljen & Baranović 2007] Ž. Crljen and G. Baranović. *Unusual Conductance of Polyyne-Based Molecular Wires.* Phys Rev Lett, vol. 98, page 116801, 2007.

[Datta 1995] S. Datta. Electronic transport in mesoscopic systems. Cambridge University Press, Cambridge, 1995.

[de la Vega *et al.* 2004] L. de la Vega, A. Martín-Rodero, A. Levy Yeyati and A. Saúl. *Different wavelength oscillations in the conductance of 5d metal atomic chains.* Phys Rev B, vol. 70, page 113107, 2004.

[Delga *et al.* 2011] A. Delga, J. Lagoute, V. Repain, C. Chacon, Y. Girard, M. Marathe, S. Narasimhan and S. Rousset. *Electronic properties of Fe clusters on a Au(111) surface.* Phys Rev B, vol. 84, page 035416, 2011.

[Deretzis & Magna 2011] I. Deretzis and A. La Magna. *Coherent electron transport in quasi one-dimensional carbon-based systems.* Eur Phys J B, vol. 81, page 15, 2011.

[Derycke *et al.* 1998] V. Derycke, P. Soukiassian, A. Mayne, D. Dujardin and J. Gautier. *Carbon Atomic Chain Formation on the β-SiC(100) Surface by Controlled $sp \rightarrow sp^3$ Transformation.* Phys Rev Lett, vol. 81, pages 5868–5871, 1998.

[Du *et al.* 2008] X. Du, I. Skachko, A. Barker and E.Y. Andrei. *Approaching ballistic transport in suspended graphene.* Nature Nanotechnol, vol. 3, pages 491–495, 2008.

[Dupas *et al.* 2007] C. Dupas, P. Houdy and M. Lahmani. Nanoscience - nanotechnologies and nanophysics. Springer, Berlin, 2007.

[Durgun *et al.* 2004] E. Durgun, S. Dag and S. Ciraci. *Theoretical study of Ga-based nanowires and the interaction of Ga with single-wall carbon nanotubes.* Phys Rev B, vol. 70, page 155305, 2004.

[Egami *et al.* 2005] Y. Egami, T. Ono and K. Hirose. *Even-odd oscillation in conductance of single-row sodium nanowire.* Phys Rev B, vol. 72, page 125318, 2005.

[Egami *et al.* 2010] Y. Egami, K. Hirose and T. Ono. *Time-saving first-principles calculation method for electronic transport between jellium electrodes.* Phys Rev E, vol. 82, page 056706, 2010.

[Euen 1998] P. L. Euen. *Nanotechnology: Carbon-based electronics.* Nature, vol. 393, pages 15–16, 1998.

[Fan *et al.* 2012] X. Fan, Z. Shen, A. Q. Liu and J. L. Kuo. *Band gap opening of graphene by doping small boron nitride domains.* Nanoscale, vol. 4, pages 2157–2165, 2012.

[Fellay *et al.* 1997] A. Fellay, F. Gagel, K. Maschke, A. Virlouvet and A. Khater. *Scattering of vibrational waves in perturbed quasi-one-dimensional multichannel waveguides.* Phys Rev B, vol. 55, pages 1707–1717, 1997.

[Fölsch *et al.* 2004] S. Fölsch, P. Hyldgaard, R. Koch and K.H. Ploog. *Quantum confinement in monatomic Cu chains on Cu(111).* Phys Rev Lett, vol. 92, page 056803, 2004.

[Fuentealba 1998] P. Fuentealba. *Static dipole polarizabilities of small neutral carbon clusters C_n ($n \leqslant 8$).* Phys Rev A, vol. 58, pages 4232–4234, 1998.

[Geim & Novoselov 2007] A. K. Geim and K. S. Novoselov. *The rise of graphene.* Nature Mater, vol. 6, pages 183–191, 2007.

[Ghader & Khater 2012] D. Ghader and A. Khater. *to be published.* 2012.

[Guisinger & Arnold 2010] N. P. Guisinger and M. S. Arnold. *Beyond Silicon: Carbon-Based Nanotechnology.* MRS Bull, vol. 4, pages 273–279, 2010.

[Han 2007] M. Y. Han. *Energy band-gap engineering of graphene nanoribbons.* Phys Rev Lett, vol. 98, page 206805, 2007.

[Han 2010] M. Y. Han. *Electron transport in disordered graphene nanoribbons.* Phys Rev Lett, vol. 104, page 056801, 2010.

[Hands *et al.* 2010] I. D. Hands, J. L. Dunn and C. A. Bates. *Visualization of static Jahn-Teller effects in the fullerene anion C_{60}^{-}.* Phys Rev B, vol. 82, page 155425, 2010.

[Harrison 2002] W.A. Harrison. *Why tight-binding theory?* Solid State Commun, vol. 124, pages 443–447, 2002.

[Harrison 2004] W. A. Harrison. Elementary electronic structure. World Scientific, Singapore, 2004.

[Havu *et al.* 2006] P. Havu, V. Havu, M.J. Puska, M.H. Hakala, A.S. Foster and R.M. Nieminen. *Finite-element implementation for electron transport in nanostructures.* J Chem Phys, vol. 124, page 054707, 2006.

[Heath *et al.* 1987] J. R. Heath, Q. Zhang, S. C. O'Brien, R. F. Curl, H. W. Kroto and R. E. Smalley. *The formation of long carbon chain molecules during laser vaporization of graphite.* J Am Chem Soc, vol. 109, pages 359–363, 1987.

[Hu *et al.* 2009] J. N. Hu, X. L. Ruan and Y. P. Chen. *Thermal Conductivity and Thermal Rectification in Graphene Nanoribbons: A Molecular Dynamics Study.* Nano Lett, vol. 9, pages 2730–2735, 2009.

[Hückel 1931] E. Hückel. *Quantentheoretische beiträge zum benzolproblem.* Z Phys, vol. 70, pages 204–286, 1931.

[Iijima & Ichihashi 1993] S. Iijima and T. Ichihashi. *Single-shell carbon nanotubes of 1-nm diameter.* Nature, vol. 363, pages 603–605, 1993.

[Jin *et al.* 2009] C. Jin, H. Lan, L. Peng, K. Suenaga and S Iijima. *Deriving Carbon Atomic Chains from Graphene.* Phys Rev Lett, vol. 102, page 205501, 2009.

[Jones & Seifert 1997] R. O. Jones and G. Seifert. *Density functional study of carbon clusters and their ions.* Phys Rev Lett, vol. 79, pages 443–446, 1997.

[Karpfen 1979] A. Karpfen. *Ab initio studies on polymers. I. The linear infinite polyyne.* J Phys C Solid State Phys, vol. 12, pages 3227–3237, 1979.

[Katsnelson & Novoselov 2007] M. I. Katsnelson and K.S. Novoselov. *Graphene: New bridge between condensed matter physics and quantum electrodynamics.* Solid State Commun, vol. 143, pages 3–13, 2007.

[Katsnelson *et al.* 2006] M. I. Katsnelson, K.S. Novoselov and A. K. Geim. *Chiral tunnelling and the Klein paradox in graphene.* Nature Phys, vol. 2, pages 620–625, 2006.

[Kaxiras 2003] E. Kaxiras. Atomic and electronic structure of solid. Cambridge University Press, New York, 2003.

[Ke *et al.* 2008] Y. Ke, K. Xia and H. Guo. *Disorder Scattering in Magnetic Tunnel Junctions: Theory of Nonequilibrium Vertex Correction.* Phys Rev Lett, vol. 100, page 166805, 2008.

[Keldysh 1965] L.V. Keldysh. *Quantum point contacts in magnetic fields.* Sov. Phys. JETP, vol. 20, pages 1018–1026, 1965.

[Kértesz *et al.* 1978] M. Kértesz, J. Koller and A. Ažman. *Ab initio Hartree-Fock crystal orbital studies. II. Energy bands of an infinite carbon chain.* J Chem Phys, vol. 68, pages 2779–2782, 1978.

[Kértesz *et al.* 1979] M. Kértesz, J. Koller and A. Ažman. *Different orbitals for different spins for solids: Fully variational ab initio studies on hydrogen and carbon atomic chains, polyene, and poly(sulphur nitride).* Phys Rev B, vol. 19, pages 2034–2040, 1979.

[Khater & Szczęśniak 2011] A. Khater and D. Szczęśniak. *A simple analytical model for electronic conductance in a one dimensional atomic chain across a defect.* J Phys Conf Ser, vol. 289, page 012013, 2011.

[Khater *et al.* 2011a] A. Khater, M. Belhadi and M. Abou Ghantous. *Phonons heat transport at an atomic well boundary in ultrathin solid films.* Eur Phys J B, vol. 80, pages 363–369, 2011.

[Khater *et al.* 2011b] A. Khater, B. Bourahla, M. Abou Ghantous, R. Tigrine and R. Chadli. *Magnons coherent transmission and heat transport at ultrathin insulating ferromagnetic nanojunctions.* Eur Phys J B, vol. 82, pages 53–61, 2011.

[Khomyakov & Brocks 2004] P. A. Khomyakov and G. Brocks. *Real-space finite-difference method for conductance calculations.* Phys Rev B, vol. 70, page 195402, 2004.

[Khomyakov & Brocks 2006] P. A. Khomyakov and G. Brocks. *Stability of conductance oscillations in monatomic sodium wires.* Phys Rev B, vol. 74, page 165416, 2006.

[Kobayashi 2011] K. Kobayashi. *Electron transmission through atomic steps of Bi_2Se_3 and Bi_2Te_3 surfaces.* Phys Rev B, vol. 84, page 205424, 2011.

[Koskinen & Mäkinen 2009] P. Koskinen and V. Mäkinen. *Density-functional tight-binding for beginners.* Comput Mater Sci, vol. 47, pages 237–253, 2009.

[Kröger *et al.* 2009] J. Kröger, A. Sperl, N. Néel and R. Berndt. *Scanning tunneling microscopic investigations into the conductance of single-atom junctions.* J Scann Probe Microsc, vol. 4, pages 49–65, 2009.

[Kroto *et al.* 1985] H. W. Kroto, J. R. Heath, S. C. O'Brien, R. F. Curl and R. E. Smalley. *C_{60}: Buckminsterfullerene.* Nature, vol. 318, pages 162–163, 1985.

[Krstić *et al.* 2002] P.S. Krstić, X.G. Zhang and W.H. Butler. *Generalized conductance formula for the multiband tight-binding model.* Phys Rev B, vol. 66, page 205319, 2002.

[Lagoute *et al.* 2007] J. Lagoute, C. Nacci and S. Fölsch. *Doping of monatomic Cu chains with single Co atoms.* Phys Rev Lett, vol. 98, page 146804, 2007.

[Lagow *et al.* 1995] R. J. Lagow, J. J. Kampa, H. C. Wei, S. L. Battle, J. W. Genge, D. A. Laude, C. J. Harper, R. Bau, R. C. Stevens, J. F. Haw and E. Munson. *Synthesis of Linear Acetylenic Carbon: The "sp" Carbon Allotrope.* Science, vol. 267, pages 362–367, 1995.

[Lamba 2009] V. Lamba. *Modelling of molecular/nano devices.* Proc IMechE Part N J Nanoengineering and Nanosystems, vol. 223, pages 57–62, 2009.

[Landau 1937] L. D. Landau. *Zur Theorie der phasenumwandlungen II.* Phys Z Sowjetunion, vol. 11, pages 26–35, 1937.

[Landauer 1957] R. Landauer. *Spatial Variation of Currents and Fields Due to Localized Scatterers in Metallic Conduction.* IBM J Res Dev, vol. 1, pages 223–231, 1957.

[Lang & Avouris 1998] N. D. Lang and Ph. Avouris. *Oscillatory Conductance of Carbon-Atom Wires.* Phys Rev Lett, vol. 81, pages 3515–3518, 1998.

[Lang & Avouris 2000] N. D. Lang and Ph. Avouris. *Carbon-Atom Wires: Charge-Transfer Doping, Voltage Drop, and the Effect of Distortions.* Phys Rev Lett, vol. 84, pages 358–361, 2000.

[Lang 1997] N. D. Lang. *Anomalous dependence of resistance on length in atomic wires.* Phys Rev Lett, vol. 79, pages 1357–1360, 1997.

[Larade *et al.* 2001] B. Larade, J. Taylor, H. Mehrez and H. Guo. *Conductance, I-V curves, and negative differential resistance of carbon atomic wires.* Phys Rev B, vol. 64, page 075420, 2001.

[Lee *et al.* 2004] Y.J. Lee, M. Brandbyge, M.J. Puska, J. Taylor, K. Stokbro and R.M. Nieminen. *Electron transport through monovalent atomic wires.* Phys Rev B, vol. 69, page 125409, 2004.

[Lee *et al.* 2008] C. Lee, X. Wei, J. W. Kysar and J. Hone. *Measurement of the elastic properties and intrinsic strength of monolayer graphene.* Science, vol. 321, pages 385–388, 2008.

[Li & Kosov 2006] Z. Li and D.S. Kosov. *First-principles calculations of conductance within a plane wave basis set via non-orthogonal Wannier-type atomic orbitals.* J Phys Condens Matter, vol. 18, pages 1347–1358, 2006.

[Lödwin 1950] P.-O. Lödwin. *On the non-orthogonality problem connected with the use of atomic wave functions in the theory of molecules and crystals.* J Chem Phys, vol. 18, pages 365–375, 1950.

[Lou & Nordlander 1996] L. Lou and P. Nordlander. *Carbon atomic chains in strong electric fields*. Phys Rev B, vol. 54, pages 16659–16662, 1996.

[Ma *et al.* 2012] F. Ma, Z. Guo, K. Xu and P. K. Chu. *First-principle study of energy band structure of armchair graphene nanoribbons*. Solid State Commun, vol. 152, pages 1089–1093, 2012.

[Mattheiss 1972a] L. F. Mattheiss. *Electronic structure of the 3d transition-metal monoxides. I. Energy-band results*. Phys Rev B, vol. 5, pages 290–306, 1972.

[Mattheiss 1972b] L. F. Mattheiss. *Electronic structure of the 3d transition-metal monoxides. II. Interpretation*. Phys Rev B, vol. 5, pages 306–315, 1972.

[Mitin *et al.* 2008] V.V. Mitin, V.A. Kochelap and M.A. Stroscio. Introduction to nanoelectronics. Cambridge University Press, New York, 2008.

[Mozos *et al.* 1997] J. L. Mozos, C.C. Wan, G. Tarashi, J. Wang and H. Guo. *Quantized conductance of Si atomic wires*. Phys Rev B, vol. 56, pages R4351–R4354, 1997.

[Mozos *et al.* 1998] J. L. Mozos, C.C. Wan, G. Tarashi, J. Wang and H. Guo. *Transport through a single-atom junction*. J Phys Condens Matter, vol. 10, pages 2663–2671, 1998.

[Néel *et al.* 2011] N. Néel, R. Berndt, J. Kröger, T.O. Wehling, A.I. Lichtenstein and M.I. Katsnelson. *Two-site Kondo effect in atomic chains*. Phys Rev Lett, vol. 107, page 106804, 2011.

[Newton 2002] R.G. Newton. Scattering theory of waves and particles. Dover Publications, New York, 2002.

[Nilius *et al.* 2002] N. Nilius, T.M. Wallis and W. Ho. *Development of one-dimensional band structure in artificial gold chains*. Science, vol. 297, pages 1853–1856, 2002.

[Nitzan & Ratner 2003] A. Nitzan and M.A. Ratner. *Electron Transport in Molecular Wire Junctions*. Science, vol. 300, pages 1384–1389, 2003.

[Novoselov *et al.* 2004] K. S. Novoselov, A. K. Geim, S. V. Morozov, D. Jiang, Y. Zhang, S. V. Dubonos, I. V. Grigorieva and A. A. Firsov. *Electric Field Effect in Atomically Thin Carbon Films*. Science, vol. 306, pages 666–669, 2004.

[Novoselov *et al.* 2005] K. S. Novoselov, F. Schedin D. Jiang, T. J. Booth, V. V. Khotkevich, S. V. Morozov and A. K. Geim. *Two-dimensional atomic crystals*. Proc Natl Acad Sci, vol. 102, pages 10451–10453, 2005.

[Nozaki *et al.* 2010] D. Nozaki, H. M. Pastawski and G. Cuniberti. *Controlling the conductance of molecular wires by defect engineering.* New J Phys, vol. 12, page 063004, 2010.

[Okano & Tománek 2007] S. Okano and D. Tománek. *Effect of electron and hole doping on the structure of C, Si, and S nanowires.* Phys Rev B, vol. 75, page 195409, 2007.

[Oncel 2008] N. Oncel. *Atomic chains on surfaces.* J Phys Condens Matter, vol. 20, page 393001, 2008.

[Ostrovsky *et al.* 2006] P. M. Ostrovsky, I. V. Gornyi and A. F. Mirlin. *Electronic transport in disordered graphene.* Phys Rev B, vol. 74, page 235443, 2006.

[Papaconstantopoulos & Mehl 2003] D.A. Papaconstantopoulos and M.J. Mehl. *The Slater-Koster tight-binding method: a computationally efficient and accurate approach.* J Phys Condens Matter, vol. 15, pages R413–R440, 2003.

[Peierls 1935] R. E. Peierls. *Quelques proprietes typiques des corpses solides.* Ann I H Poincare, vol. 5, pages 177–222, 1935.

[Porezag *et al.* 1995] D. Porezag, Th. Frauenheim, Th. Köhler, G. Seifert and R. Kaschner. *Construction of tight-binding-like potentials on the basis of density-functional theory: application to carbon.* Phys Rev B, vol. 51, pages 12947–12957, 1995.

[Profeta *et al.* 2012] G. Profeta, M. Calandra and F. Mauri. *Phonon-mediated superconductivity in graphene by lithium deposition.* Nature Phys, vol. 8, pages 131–134, 2012.

[Rice *et al.* 1986] M. J. Rice, S. R. Phillpot, A. R. Bishop and D. K. Campbell. *Solitons, polarons, and phonons in the infinite polyyne chain.* Phys Rev B, vol. 34, pages 4139–4149, 1986.

[Saubanère *et al.* 2010] M. Saubanère, J.L. Ricardo-Chávez and G.M. Pastor. *Electronic and magnetic properties of Co and Ni impurities in Cu wires: first-principles investigation of local moment formation in one dimension.* Phys Rev B, vol. 82, page 054436, 2010.

[Scott *et al.* 2002] L.T. Scott, M.M. Boorum, B.J. McMahon, S. Hagen, M. Mack, J. Blank, H. Wagner and A. de Meijere. *A rational chemical synthesis of C_60.* Science, vol. 295, pages 1500–1503, 2002.

[Senger *et al.* 2005] R. T. Senger, S. Tongay, E. Durgun and S. Ciraci. *Atomic chains of group-IV elements and III-V and II-VI binary compounds studied by a first-principles pseudopotential method.* Phys Rev B, vol. 72, page 075419, 2005.

[Shen *et al.* 2010] L. Shen, M. Zeng, S.-W. Yang, C. Zhang, X. Wang and Y. Feng. *Electron transport properties of atomic carbon nanowires between graphene electrodes.* J Am Chem Soc, vol. 132, pages 11481–11486, 2010.

[Shi & Papaconstantopoulos 2004] L. Shi and A. Papaconstantopoulos. *Modifications and extensions to Harrison?s tight-binding theory.* Phys Rev B, vol. 70, page 205101, 2004.

[Shimizu *et al.* 2010] T. Shimizu, J. Haruyama, D. C. Marcano, D. V. Kosinkin, J. M. Tour, K. Hirose and K. Suenaga. *Large intrinsic energy bandgaps in annealed nanotube-derived graphene nanoribbons.* Nat Nanotechnol, vol. 6, pages 45–50, 2010.

[Shinde & Kumar 2011] P. P. Shinde and V. Kumar. *Direct band gap opening in graphene by BN doping: Ab ignition calculations.* Phys Rev B, vol. 84, page 125401, 2011.

[Slater & Koster 1954] J. C. Slater and G. F. Koster. *Simplified LCAO Method for the Periodic Potential Problem.* Phys Rev, vol. 94, pages 1498–1524, 1954.

[Slonczewski & Weiss 1958] J. C. Slonczewski and P. R. Weiss. *Band structure of graphite.* Phys Rev, vol. 109, pages 272–279, 1958.

[Smit *et al.* 2003] R.H.M. Smit, C. Untiedt, G. Rubio-Bollinger, R.C. Segers and J.M. van Ruitenbeek. *Observation of a parity oscillation in the conductance of atomic wires.* Phys Rev Lett, vol. 91, page 076805, 2003.

[Smith *et al.* 2010] D.T. Smith, J.R. Pratt, F. Tavazza, L.E. Levine and A.M. Chaka. *An ultrastable platform for the study of single-atom chains.* Rev Sci Instrum, vol. 107, page 084307, 2010.

[Song *et al.* 2010] B. Song, S. Sanvito and H. Fang. *Anomalous I-V curve for monoatomic carbon chains.* New J Phys, vol. 12, page 103017, 2010.

[Springborg *et al.* 1990] M. Springborg, S. L. Dreschel and J. Málek. *Anharmonic model for polyyne.* Phys Rev B, vol. 41, pages 11954–11966, 1990.

[Springborg 1986] M. Springborg. *Self-consistent, first principles calculations of the electronic structures of a linear, infinite carbon chain.* J Phys C, vol. 19, pages 4473–4482, 1986.

[Stampfe 2009] C. Stampfe. *Energy gaps in etched graphene nanoribbons.* Phys Rev Lett, vol. 102, page 056403, 2009.

[Strupiński *et al.* 2011] W. Strupiński, K. Grodecki, A. Wysmołek, R. Stępniewski, T. Szkopek, P. E. Gaskell, A. Grüneis, D. Haberer, R. Bożek, J. Krupka and J. M. Baranowski. *Graphene epitaxy by chemical vapor deposition on SiC.* Nano Lett, vol. 11, pages 1786–1791, 2011.

[Szczęśniak & Khater 2012] D. Szczęśniak and A. Khater. *Electronic conductance via atomic wires: a phase field matching theory approach.* Eur Phys J B, vol. 85, page 174, 2012.

[Szczęśniak *et al.* 2012] D. Szczęśniak, A. Khater, Z. Bąk, R. Szczęśniak and M. Abou-Ghantous. *Quantum conductance of silicon-doped carbon wire nanojunctions.* Nanoscale Res Lett, vol. 7, page 616, 2012.

[Teramae *et al.* 1983] M. Teramae, T. Yamabe and A. Imamura. *Ab initio effective core potential studies on polymers.* Theor Chim Acta, vol. 64, pages 1–12, 1983.

[Thygesen & Jacobsen 2003] K.S. Thygesen and K.W. Jacobsen. *Four-atom period in the conductance of monatomic Al wires.* Phys Rev Lett, vol. 91, page 146801, 2003.

[Tigrine *et al.* 2008] R. Tigrine, A. Khater, B. Bourahla, M. Abou Ghantous and O. Rafli. *Magnon scattering by a symmetric atomic well in free standing very thin magnetic films.* Eur Phys J B, vol. 62, pages 59–64, 2008.

[Tongay *et al.* 2004] S. Tongay, E. Durgun and S. Ciraci. *Atomic strings of group IV, III-V, and II-VI elements.* Appl Phys Lett, vol. 85, pages 6179–6181, 2004.

[Tongay *et al.* 2005] S. Tongay, S. Dag, E. Durgun, R. T. Senger and S. Ciraci. *Atomic and electronic structure of carbon strings.* J Phys Cond Matter, vol. 17, pages 3823–3836, 2005.

[Troiani *et al.* 2003] H. E. Troiani, M. Miki-Yoshida, G. A. Camacho-Bragado, M. A. L. Marques, A. Rubio, J. A. Ascencio and M. Jose-Yacaman. *Direct Observation of the Mechanical Properties of Single-Walled Carbon Nanotubes and Their Junctions at the Atomic Level.* Nano Lett, vol. 3, pages 751–755, 2003.

[Tsukamoto *et al.* 2009] S. Tsukamoto, Y. Egami and T. Ono. *Ballistic electron transport through atomic nanowires.* J Comput Theor Nanosci, vol. 6, pages 2521–2544, 2009.

[Valkering *et al.* 2005] A.M.C. Valkering, A.I. Mares, C. Untiedt, K. Babaei Gavan, T.H. Oosterkamp and J.M. van Ruitenbeek. *A force sensor for atomic point contacts.* Rev Sci Instrum, vol. 76, page 103903, 2005.

[Ventra 2008] M. Di Ventra. Electrical transport in nanoscale systems. Cambridge University Press, New York, 2008.

[Virlouvet *et al.* 1999] A. Virlouvet, A. Khater, H. Aouchiche, O. Rafli and K. Maschke. *Scattering of vibrational waves in perturbed two-dimensional multichannel asymmetric waveguides as on an isolated step.* Phys Rev B, vol. 59, pages 4933–4942, 1999.

[Wakabayashi *et al.* 2009] K. Wakabayashi, Y. Takane, M. Yamamoto and M. Sigrist. *Electronic transport properties of graphene nanoribbons.* New J Phys, vol. 11, page 095016, 2009.

[Wallace 1947] P.R. Wallace. *The band theory of graphite.* Phys Rev, vol. 71, pages 622–634, 1947.

[Wallis *et al.* 2005] T.M. Wallis, N. Nilius, G. Mikaelian and W. Ho. *Electronic properties of artificial Au chains with individual Pd impurities.* J Chem Phys, vol. 122, page 011101, 2005.

[Wan *et al.* 1997] C. C. Wan, J. L. Mozos, G. Taraschi, J. Wang and H. Guo. *Quantum transport through atomic wires.* Appl Phys Lett, vol. 71, pages 419–421, 1997.

[Wang *et al.* 2009] Y. Wang, Z. Z. Lin, W. Zhang, J. Zhuang and X. J. Ning. *Pulling long linear atomic chains from graphene: Molecular dynamics simulations.* Phys Rev B, vol. 80, page 233403, 2009.

[Wang *et al.* 2012] F. Wang, K. Shepperd, J. Hicks, M. S. Nevius, H. Tinkey, A. Tejeda, A. Taleb-Ibrahimi, F. Bertran, P. Le Fèvre, D. B. Torrance, P. N. First, W. A. de Heer, A. A. Zakharov and E. H. Conrad. *Silicon intercalation into the graphene-SiC interface.* Phys Rev B, vol. 85, page 165449, 2012.

[Wolf 2003] E.L. Wolf. Nanophysics and nanotechnology. John Wiley & Sons Inc., Weinheim, 2003.

[Wu & Childs 2011] Y. Wu and P. A. Childs. *Conductance of Graphene Nanoribbon Junctions and the Tight Binding Model.* Nanoscale Res Lett, vol. 6, page 62, 2011.

[Xu *et al.* 1992] C. H. Xu, C. Z. Wang, C. T. Chan and K. M. Ho. *A transferable tight-binding potential for carbon.* J Phys Condens Matter, vol. 4, pages 6047–6054, 1992.

[Yamaguchi *et al.* 1997] F. Yamaguchi, T. Yamada and Y. Yamamoto. *Even-odd conductance oscillation in atomic wires.* Solid State Commun, vol. 102, pages 779–783, 1997.

[Yan *et al.* 2007] Q. Yan, B. Huang, J. Yu, F. Zheng, J. Zang, J. Wu, B.-L. Gu, F. Liu and W. Duan. *Intrinsic current-voltage characteristics of graphene nanoribbon transistors and effect of edge doping.* Nano Lett, vol. 7, pages 1469–1473, 2007.

[Yuzvinsky *et al.* 2006] T. D. Yuzvinsky, W. Mickelson, S. Aloni, G. E. Begtrup, A. Kis and A. Zettl. *Shrinking a Carbon Nanotube.* Nano Lett, vol. 6, pages 2718–2722, 2006.

[Zhang *et al.* 2008] L. Zhang, J. S. Wang and B. Li. *Ballistic magnetothermal transport in a Heisenberg spin chain at low temperatures.* Phys Rev B, vol. 78, page 144416, 2008.

[Zhang *et al.* 2009] Y. Zhang, T. Tang, C. Girit, Z. Hao, M. C. Martin, A. Zettl, M. F. Crommie, Y. R. Shen and F. Wang. *Direct observation of a widely tunable bandgap in bilayer graphene.* Nature, vol. 459, pages 820–823, 2009.

[Zhang *et al.* 2011a] G. P. Zhang, X. W. Fang, Y. X. Yao, C. Z. Wang, Z. J. Ding and K. M. Ho. *Electronic structure and transport of a carbon chain between graphene nanoribbon leads.* J Phys Cond Matter, vol. 23, page 025302, 2011.

[Zhang *et al.* 2011b] Y. Zhang, Y. Su, L. Wang, E. S. W. Kong, X. Chen and Y. Zhang. *A one-dimensional extremely covalent material: monatomic carbon linear chain.* Nanoscale Res Lett, vol. 6, page 577, 2011.

[Zhao *et al.* 2003] X. Zhao, Y. Ando, Y. Liu, M. Jinno and T. Suzuki. *Carbon Nanowire Made of a Long Linear Carbon Chain Inserted Inside a Multiwalled Carbon Nanotube.* Phys Rev Lett, vol. 90, page 187401, 2003.

[Zhao *et al.* 2010] Y. Zhao, P. Cadden-Zimansky, Z. Jiang and P. Kim. *Symmetry breaking of the zero-energy Landau level in bilayer graphene.* Phys Rev Lett, vol. 104, page 066801, 2010.

[Zhou *et al.* 2008] Y.-H. Zhou, X.-H. Zheng, Y. Xu and Z.Y. Zeng. *First-principles study on the differences between the equilibrium conductance of carbon and silicon atomic wires.* J Phys Condens Matter, vol. 20, page 045225, 2008.

[Zugarramurdi *et al.* 2011] A. Zugarramurdi, A.G. Borisov, N. Zabala, E.V. Chulkov and M.J. Puska. *Clustering and conductance in breakage of sodium nanowires.* Phys Rev B, vol. 83, page 035402, 2011.